Title
Tectonic Significance of the Chambers Well Dike Swarm

Author
Gentry, Beau James

Publication Date
2015

Peer reviewed|Thesis/dissertation

UNIVERSITY OF CALIFORNIA

Santa Barbara

Tectonic Significance of the Chambers Well Dike Swarm

Whipple Mountains Metamorphic Core Complex, CA

A Thesis submitted in partial satisfaction of the

requirements for the degree Master of Science

in Geological Sciences

by

Beau James Gentry

Committee in charge:

Professor Phillip B. Gans, Chair

Professor John M. Cottle

Professor Bradley R. Hacker

September 2015

The thesis of Beau James Gentry is approved.

John M. Cottle

Bradley R. Hacker

Phillip B. Gans, Committee Chair

July 2015

Tectonic Significance of the Chambers Well Dike Swarm

By

Beau James Gentry

ABSTRACT

Tectonic Significance of the Chambers Well Dike Swarm

by

Beau James Gentry

A suite of Miocene dikes, collectively termed the Chambers Well dike swarm are exposed the southwestern footwall of the Whipple Detachment fault (WDF) and provide key insight into the evolution of the Whipple Mountains metamorphic core complex. New geologic mapping, U-Pb zircon geochronology, and whole-rock geochemistry allow for the assessment of: 1.) The ages, compositions, and volume of the dikes in the context of the local volcanic and extensional history 2.) The magnitude and timing of footwall rotation. 3.) The amount of slip on the southwestern WDF. The dikes intruded an approximately 40 km^2 portion of the footwall of the WDF, comprised of an assemblage of Proterozoic gneisses and amphibolite bodies. Dikes can be broadly divided into two distinct groups; an andesite-rhyolite series (61-78 wt. % SiO_2) ranging in age from 18.75 to 20.1 Ma, and a subordinate group of younger diabase dikes (55 wt. % SiO_2). In the central portion of the dike swarm, dike-to-wall rock ratios range from 0.93 to 2.60 and imply ~100 to 250% WNW-ESE extension that was accommodated by intrusive dilation. Dike dips vary systematically from sub-vertical in the eastern portion of the swarm to gently east-dipping (~20-30˚) in the west, and take the form an inward-dipping fan. The combined field observations, geochronology, and geochemistry from the Chambers Well dikes and lava flows in the hanging wall of the WDF indicate that the western Whipple Mountains was a major Miocene eruptive center with local magmatic activity that

began ~20 Ma. Early stages of extension (20.2 and 18.75 Ma) were dominated by intrusive dilation, but transitioned to large scale extensional faulting and tilting at 19.0-18.5 Ma, and may have been the result of thermal weakening of the crust. The asymmetric, fan-shaped geometry of the Chambers Well dike swarm can be explained by the combination of emplacement from an elongate, compositionally-zoned pluton at depth followed by ~40˚ of SW rotation about a horizontal axis, parallel to strike of upper plate strata (310˚). Restoring this rotation brings the mean dike orientations to sub-vertical, with strikes ranging from 310˚ to 002˚, and suggests an extension direction between 040˚ and 090˚. This interpretation also implies that the WDF initiated with a much steeper dip (~40-50˚), in agreement with classical Andersonian fault mechanics. Similarities in compositions and ages between the Chambers Well dikes and upper plate lava flows suggest that the dikes are the feeders to the thick volcanic sequence exposed in the western Whipple Mountains and Mopah Range. This correlation implies that there has been little-to-no NW-directed slip on the southwestern potion of the WDF since ~20 Ma.

INTRODUCTION

Metamorphic core complexes (MCC's) are characteristic of highly extended terranes and occur ubiquitously throughout the North American Cordillera. These "core complexes" share a common architecture; a gently-dipping detachment fault separates faulted and tilted upper-crustal rocks from structurally deeper, autochthonous rocks which are locally mylonitic and show a markedly different deformational style and degree of metamorphism. The detachment faults that are hosted in MCC's are thought to be regional slip surfaces which have accommodated tens of kilometers of displacement. These faults commonly have a dome-like geometry, which is interpreted to be the result of the isostatic rebound of the lower plate.

While MCC's and their characteristic low-angle detachment faults are well documented, factors which affect how they form and evolve remain a topic of debate. Many core complexes provide clear evidence for synextensional magmatism, however, this is not true of all MCC's and the causal relationship between extension and magmatism remains ambiguous (Leeman and Harry, 1993; Spencer *et al*., 1995; Coney and Harms, 1984; Wernicke *et al*. 1987).

Additionally, Anderson's model for faulting, which has been supported by innumerable experiments and seismic data from active normal faults, fails to predict the formation of gently-dipping normal faults and points to a clear lack of understanding of these structures (Anderson, 1905; Jackson, 1987; Jackson and McKenzie 1983; Jackson and White, 1989; Abers et al., 1997).

The Whipple Mountains, CA, which host the Whipple detachment fault (WDF), are generally viewed as an archetypical example of a cordilleran MCC. This study characterizes a suite of dikes, termed the Chambers Well dike swarm, which lies in the footwall of the WDF, in order to shed light on the formation and evolution of the Whipple Mountains MCC. Field relationships, geochronology, and whole-rock chemistry presented here help to establish relationships between the Chambers Well dike swarm and the evolution of the WDF.

GEOLOGY OF THE WHIPPLE MOUNTAINS

The Whipple Mountains MCC lies in southeastern California, in a region termed the Colorado River Extensional Corridor (CREC) (Howard and John, 1987) (Fig. 1). The CREC is part of a larger belt of metamorphic core complexes stretching from Canada to Mexico (Coney, 1980) (Fig. 2), and has undergone more than 100% northeast-directed, Miocene crustal extension in the vicinity of the Whipple Mountains (Davis et al., 1980; Howard and John 1987; Reynolds and Spencer, 1985; Nielson and Beratan, 1990).

The gently northeast-dipping Whipple Detachment Fault crops out in the Whipple Mountains MCC and separates an "upper plate" of internally faulted and tilted section of Miocene volcanic and sedimentary rocks and their underlying basement, from a lower plate pf Proterozoic gneisses and amphibolites and a suite of younger (Mesozoic-Miocene) intrusions (Davis et al. 1980). Rocks in the lower plate of the WDF are exposed in the core of the range, and are bounded by exposures of the WDF and upper plate rocks (Fig. 3). The assemblage of crystalline rocks in the footwall of the WDF locally contains a penetrative Miocene (?), mylonitic foliation and lineation which overprints older fabrics in the Proterozoic gneisses, and generally suggests a top-to-the-northeast sense of shear (Davis et al. 1986). Mylonitic fabrics are restricted to the eastern half of the footwall, and end abruptly at a west-dipping "mylonitic front", which is thought to be the upper limit of footwall mylonitization.

In the non-mylonitic, western portion of the lower plate, an extensive swarm of mafic to silicic dikes, termed the Chambers Well dike swarm, intruded the crystalline basement (Davis et al. 1982). The dikes are exposed in a window into the lower plate of the WDF, and upper plate rocks crop out to the south and west of the dike swarm. The WDF projects into the air above the Chambers Well dike swarm, but likely lies within several hundred meters of the present day ground surface (Fig. 4). The dikes were originally interpreted to have been emplaced late-to-post tectonic, with respect to mylonitization and detachment faulting, and were thought to be the youngest magmatic activity in the footwall of the WDF (Davis *et al.*, 1982).

While some reconnaissance work has been done on the Chambers Well dike swarm (Davis et al. 1982, DeWitt et al., 1982, Anderson and Cullers, 1990), the ages of dikes, their compositions,

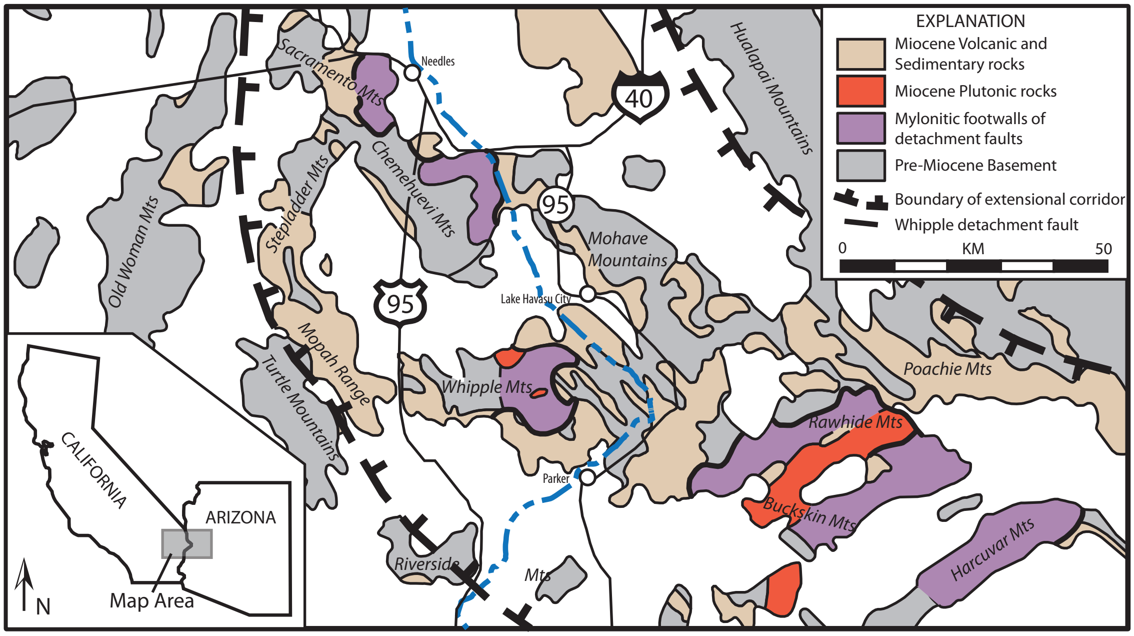

Figure 1. Simplified geologic map of the lower Colorado River extensional corridor (LCREC), highlighting the location of several metamorphic core complexes. (Gans, unpublished).

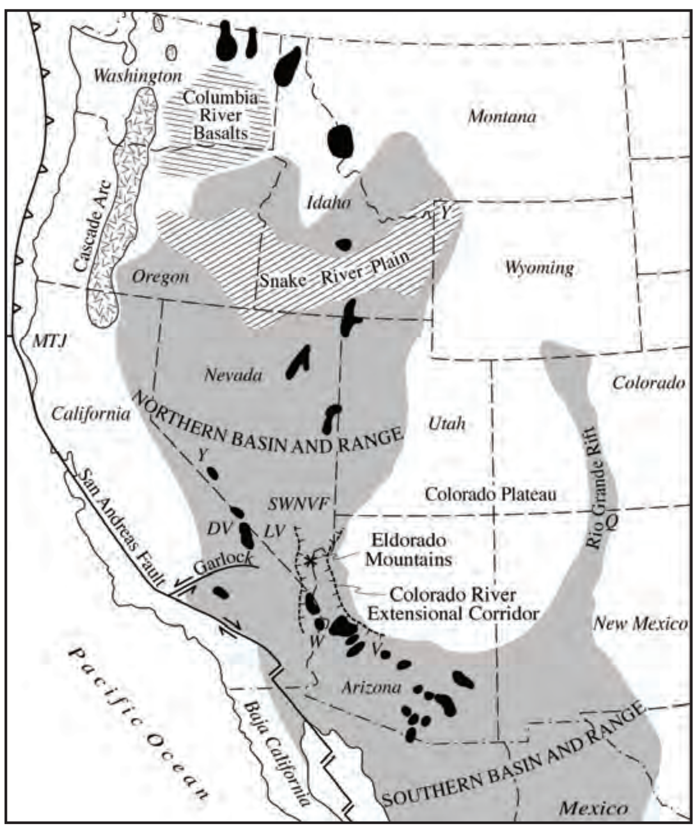

Figure 2. Map showing the location of metamorphic core complexes (black shapes) throughout the basin and range province, western US. (Gans and Bohrson, 1998)

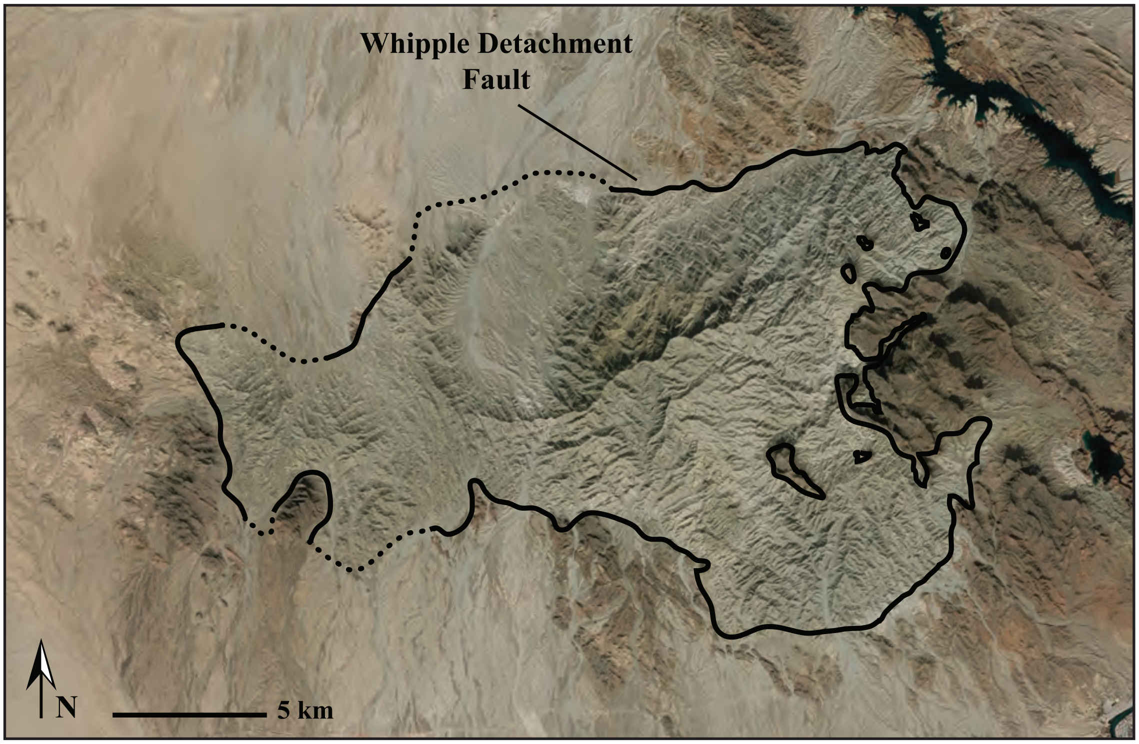

Figure 3. Satellite image of the Whipple Mountains, CA. Dark brown rocks, flanking the range, lie in the hanging wall of the WDF, while light gray-green rocks, in the core of the range, lie in the footwall (modified from Google Earth).

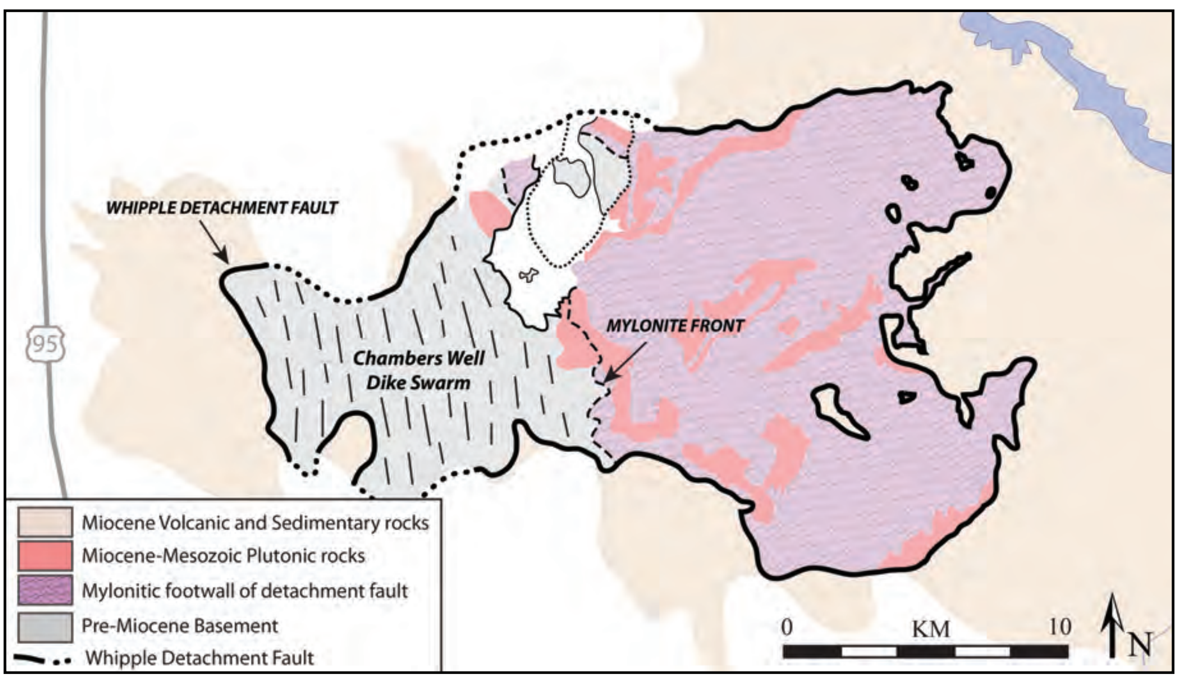

Figure 4. Simplified geologic map of the Whipple Mounatins MCC. Key features inlcude the WDF, mylonite front, and Chambers Well dike swarm (modified from Anderson and Cullers, 1990).

orientations, and distributions have not been well documented. Furthermore, the relationship between the dikes and slip on the WDF and upper plate faulting, and correlations between distinct suites of dikes and hanging wall volcanic rocks have not been examined.

METHODS

Geologic Mapping and Structural Data Collection

Geologic mapping of an approximately $15km^2$ area of the dike swarm was conducted at a scale of 1:5,000 and compiled at 1:10,000. Dikes were divided into eight lithologic units based on color and mineralogy, with particular attention given to the composition and modal percentages of phenocrysts.

Dike orientations and basement foliations were measured across the map area, and are crucial for documenting the geometry of the dike swarm and assessing the amount of rotation that has affected this portion of the footwall of the WDF. The exposed quenched margins of dikes were measured directly, however, dike margins are often concealed by talus from more resistant, ridge-forming dikes. In these cases, the internal flow banding, and partings that paralleled flow banding, were collected as the dike orientation. Sighting the strike and dip of well exposed dikes crossing large gullies with sufficient topographic relief was used to confirm the average orientation.

Five, 100 m long transects were measured, perpendicular to the strike of dikes in order to quantify the relative proportions of dike-to-host rock. Transects were conducted in areas with subdued topography, where the bedrock was entirely exposed, and where dikes had similar orientations. A 100 m tape was laid out, and the widths of country rock versus dike rock were recorded. In areas where there was a significant incline (> 5°), the slope angle was measured and the horizontal thicknesses of dikes were calculated.

Whole-Rock Geochemical Analyses

Samples were collected from a suite of dike compositions for geochemistry (Table 1). Major elements were measured by x-ray fluorescence (XRF) at Pomona College. Data was collected using a PanAlytical Axios wavelength-dispersive system equipped with a standard set of crystals and a duplex detector for increased accuracy and precision of the transition metals. Instrument calibration and sample preparation methods are the same as those used by Johnson et al. (1999).

Whole-rock trace and rare earth elements were measured by laser-ablation quadrupole ICP-MS at UCSB. The system consists of a Photon Machines 193 nm wavelength ArF excimer laser attached to an Agilent 7700S quadrupole ICP-MS. Samples were ablated using a 50 µm beam along a 250 µm long transect, at a rate of 4 µm/sec. Three line scans were performed on each sample. USGS whole-rock reference materials Atho-G, BHVO-2, AGV-2, ML3B, StHs 6/80, BCR-2, GOR132, and T-1 were measured at the beginning and end of the analytical session, with Atho-G and AGV-2 measured between every 9 unknowns. Atho-G was used as the primary reference material and AGV-2 as the secondary reference material to assess precision and accuracy of the measurements of each element. All Data were processed using Igor Pro, the plugin Iolite v. 2.1.3 (Paton et al., 2011), and Ca, measured by XRF, was used as an internal standard.

Geochronology

Twelve samples for zircon geochronology were collected from the coarse-grained interiors of dikes across the southwestern footwall (Table 2). Additionally, two samples were collected from dikes which intrude a package of Proterozoic gneisses which may lie in the hanging wall of the WDF, to the west of the map area (Fig. 5). Samples were crushed and sieved to 90-250 µm, and then panned to concentrate "heavy" minerals. This concentrate was repeatedly passed through a Frantz magnetic separator, until a non-magetic (< 55V) separate was achieved. The non-magnetic fraction was stirred into methylene iodine (ρ =3.3), and minerals which sank (ρ >3.3) were recovered. Zircons were hand-picked from this high-purity separate, and mounted in epoxy pucks. Generally, zircons that were euhedral, 50-100µm long, and free of inclusions were targeted, however, a number of

Sample ID	Map Unit	Rock Type	Sample Location (UTM)		
CW-11	Tkfr	K-Feldspar rhyolite	11 S	730419	3797680
CW-12	Tqchr	Quartz-rich chlortized hornblence rhyolite	11 S	729712	3798011
CW-13	N/A	K-altered rhyolite	11 S	731061	3797488
CW-14	Tar	Aphryic rhyolite	11 S	731580	3795037
CW-15	Tfbr	Fresh biotite rhyolite	11 S	731314	3795580
CW-16	Tchr	cholitized hornblende rhyolite	11 S	731150	3795647
CW-17	Tpa	Plag-phyric andesite	11 S	731058	3796776
CW-18	Tmd	Diabase/Microdiorite	11 S	731576	3797115

Table 1. Descriptions of samples collected for whole-rock geochemistry.

Sample ID	Map Unit	Rock Type	Sample Location	Sample Location (UTM)		
CW-01	Tfbr	Fresh biotite rhyolite	Chambers Well map area	11 S	731571	3795029
CW-02	Tpa	Plag-phyric andesite	Chambers Well map area	11 S	731571	3795029
CW-04	Tar	Aphyric Rhyolite	Chambers Well map area	11 S	731571	3795029
CW-05	Tchr	Chloritized hornblende rhyolite	Chambers Well map area	11 S	731530	3796092
CW-07	Tkfr	K-feldspar rhyolite	Chambers Well map area	11 S	730971	3796729
CW-21	Tchr	Chloritized hornblende rhyolite	Chambers Well map area	11 S	729728	3793948
KFC-02	Tppd	Porphyritic plag dacite	Chambers Well map area	11 S	730528	3795111
KFC-03	Tfbr	Fresh biotite rhyolite	Chambers Well map area	11 S	730613	3795071
KFC-05	Tfbr	Fresh biotite rhyolite	Chambers Well map area	11 S	730748	3795092
KFC-06	Tpa	Plag-phyric andesite	Chambers Well map area	11 S	730814	3795072
KFC-07	Tpa	Plag-phyric andesite	Chambers Well map area	11 S	730960	3795003
WFW-03	Tchr	Chloritized hornblende rhyolite	"Upper plate" dike	11 S	718855	3799199
WFW-04	Tchr	Chloritized hornblende rhyolite	"Upper plate" dike	11 S	718342	3799194
WFW-06	Tchr	Chloritized hornblende rhyolite	Western footwall	11 S	725686	3797100

Table 2. Descriptions of samples collected for U-Pb zircon Geochronology.

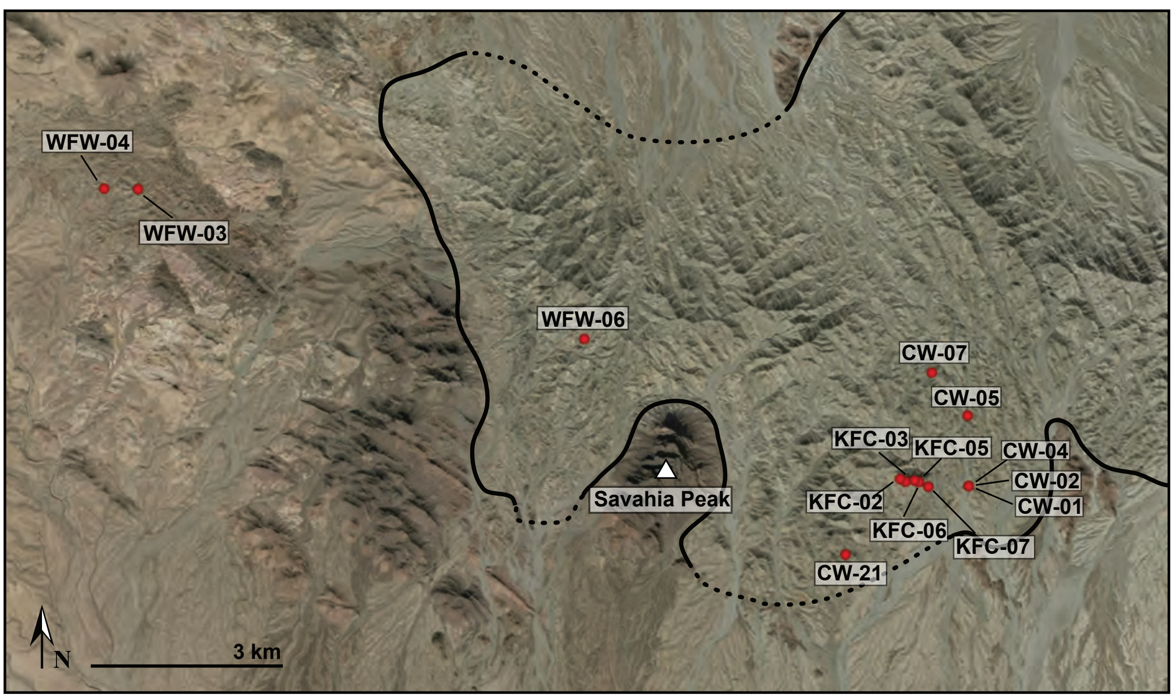

Figure 5. Satellite image of the SW Whipple Mountains, showing the locations of samples collected for U-Pb zircon geochronology. Location of Savahia Peak and the approximate trace of the WDF are shown for reference (modified from Google Earth).

larger, rounded zircons were also sampled when present (Fig. 6). Zircon yield varied by rock type; felsic samples generally yielded ~100-200, dominantly euhedral grains, and several samples had well over 500 grains. Mafic samples had fewer zircons (0-30 grains), and were dominated by larger, rounded grains.

U-Pb data were collected using the LA-ICP-MS facility at UCSB (Cottle *et al.*, 2012, 2013). Instrumentation consisted of a Photon Machines 4-ns-pulse duration, 193-nm-wavelength ArF excimer laser attached to a Nu Plasma HR multicollector (MC) ICPMS set up to measure U, Th, and Pb isotope ratios. Analytical conditions used are as follows: Spot diameter of 24 μm, laser energy of 3–4 mJ, firing frequency of 4 Hz, and 75–100 shots per analysis. Data reduction, including corrections for baseline, instrumental drift, mass bias, and down-hole fractionation was carried out using Igor Pro and the plugin Iolite v. 2.1.3 (Paton et al., 2010). The primary reference material used was zircon "91500" (Wiedenbeck *et al*., 1995). This reference material was used to monitor and correct for instrumental drift, mass bias, and down-hole interelement fractionation.

Secondary zircon reference materials, "GJ-1" (Jackson *et al.*, 2004), "Plešovice" (Sláma *et al*., 2008), and "Peixe" (Dickinson and Gehrels, 2003) were analyzed at the beginning and end of each run and treated as unknowns to assess accuracy and precision within each analytical session. For "unknown" zircons, spots locations were chosen to avoid large cracks, and cathodoluminescence (CL) images were used to place spots within single CL-domains. Multiple spots were placed on zircons which contained a visible core and rim, sampling each domain (Fig. 7).

All uncertainties are quoted at 2σ and include contributions from the reproducibility of the reference materials for 207Pb/206Pb, 206Pb/238U, and 207Pb/235U. A 207Pb/206Pb intercept of 0.837 (Stacey and Kramers, 1975) was used to calculate 207Pb-corrected intercept ages for analyses containing excess 'common lead'. All U-Pb data were plotted using the Isoplot Excel plugin, version 3.75 (Ludwig, 2012).

RESULTS

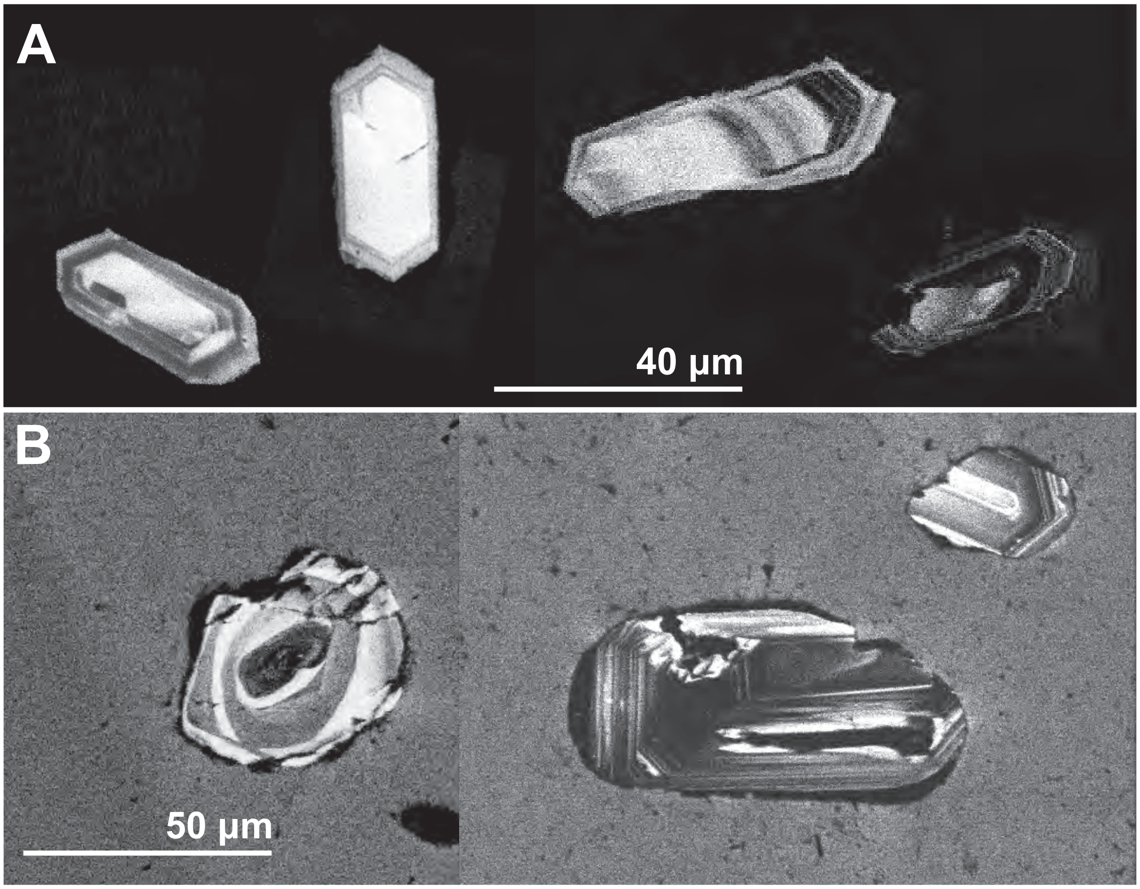

Figure 6. Cathodoluminescence (CL) images showing contrasts in zircon morphology that were observed within samples. A.) Euhedral zircons with well defined crystal faces and B.) rounded, irregular-shaped zircons. Effort was made to sample fresh, euhedral zircons that were free of cracks, however, many samples yielded abundant, large, rounded zircons.

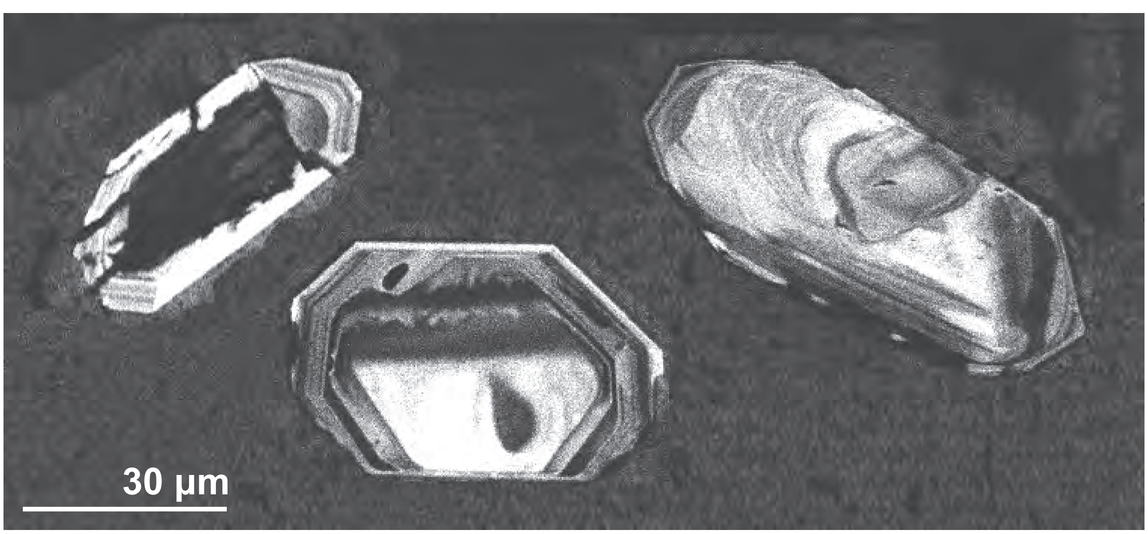

Figure 7. CL images showing several examples of zircons which contained a clear core and rim. Laser spot locations were chosen to sample zircon cores and rims separately.

Field Relationships

Geologic Mapping

While it is recognized that dikes occur throughout much of the SW footwall, this study focuses on the portion of the dike swarm between Chambers Well Rd. and Savahia Peak, where the dikes are best exposed and the spatial distribution, range of compositions, and relative ages of dikes can be assessed. Here we present a 1:10,000-scale geologic map and structural data from this representative portion of the dike swarm (Fig. 8).

Exposures in this area consist of Proterozoic basement composed of quartzo-feldspathic banded gneisses, irregular pods of leucogranite, and amphibolite bodies, which are cut by a dense swarm of generally NNW striking Miocene dikes. Dikes here can be broadly divided into a suite of rhyolite dikes and a subordinate group of younger diabase dikes. The eastern portion of the map area, near Chambers Well Road, has generally subdued topographic relief and dikes here form a series of resistant N-S trending ridges. To the west, the dikes have less of a topographic expression and are exposed in the walls of steep-sided hills and washes. Dike density is highest in the eastern portion of the map area, and the dikes span the widest compositional range in this area. In the western half of the map area, just east of Savahia Peak, dikes are less abundant and are less compositionally diverse.

Dikes range from 0.5 to 10 m in thickness, and some individual dikes can be traced out for more than a kilometer along strike. Although mapped at a detailed scale, many thin and discontinuous dikes are not represented on the map. Thus, the map grossly underrepresents the total number of dikes and fails to capture the proportions of dikes to wall rock. For this reason, geologic mapping was supplemented with a series of 100 m long transects, measured perpendicular to dike margins, to document the relative proportions of dike and wall rock across the map area.

Map Units

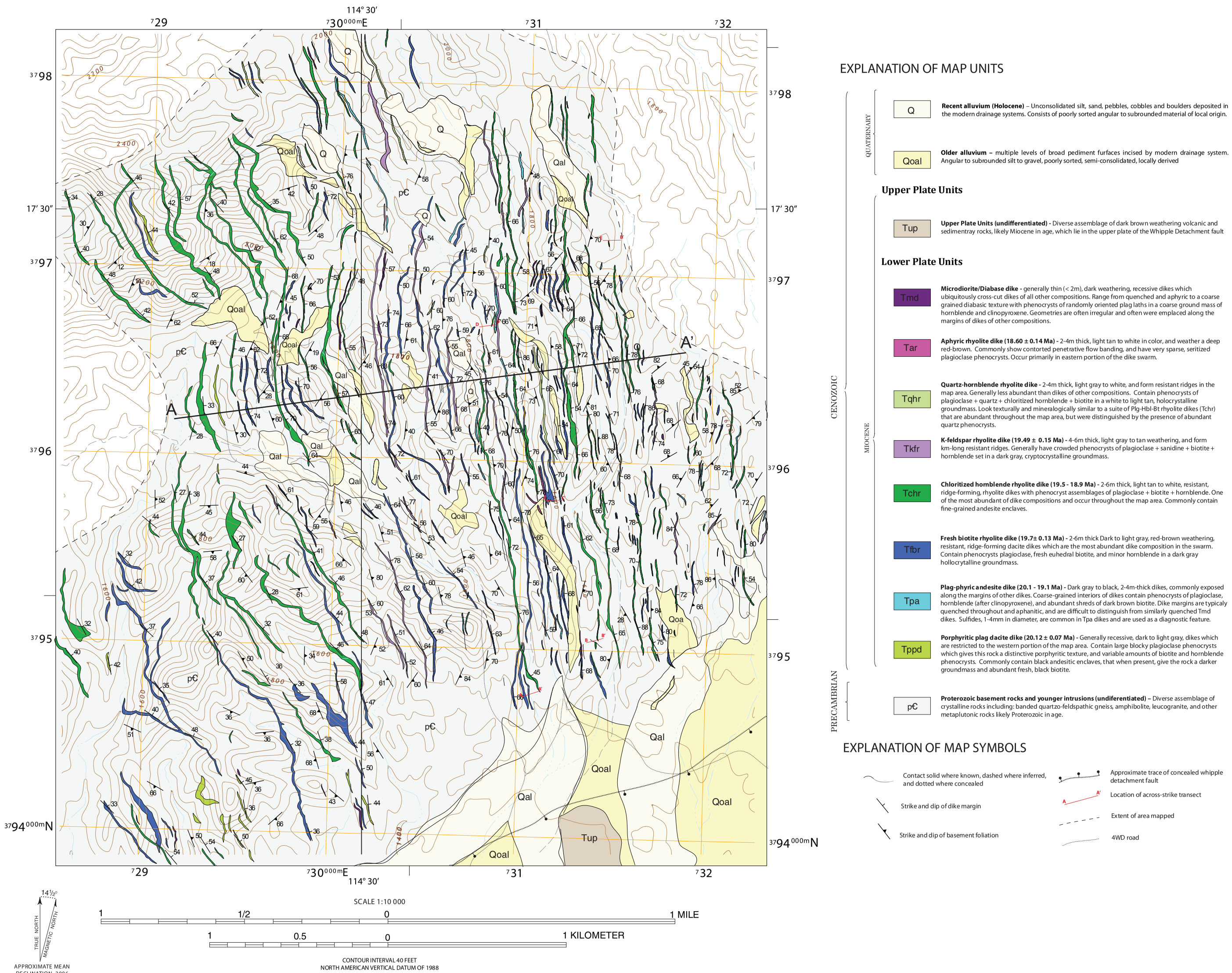

Figure 8. Geologic map of a portion of the Chambers Well dike swarm, between Savahia peak and Chambers Well Rd..

Most dikes can be easily be classified as belonging to one of the distinct map units, as there are clear contrasts in phenocryst assemblages and groundmass color between dikes. However, dikes with compositions that are transitional between groups were also observed. Additionally, two groups of more mafic dikes were identified; plag-phyric, sulfide-rich andesite and plg-hbl-cpx diabase. While these dikes are distinguishable in the coarse interiors of thicker dikes (>2m), thin, quenched, aphyric mafic dikes are common, and are difficult to confidently assign to either of the two groups (Fig. 9).

The host rock to the Chamber's Well dike swarm is dominantly comprised of Proterozoic, Quartzo-feldsoathic gneisses and numerous irregular amphibolite and leucogranite bodies. Because the focus of this study was the dike swarm itself, the basement rocks were left undifferentiated. The orientations of foliations within the Proterozoic basement were, however, recorded across the map area.

Miocene Dikes:

Diabase/Microdiorite (Tmd): Diabase dikes are generally thin (< 2m), dark weathering, and recessive, and ubiquitously cross-cut dikes of all other compositions within the map area. These dikes have more irregular geometries and are commonly exposed along the margins of dikes of other compositions. Tmd dikes range from nearly aphyric on the chilled margins to phaneritic in the coarse-grained centers of thicker dikes (> 1m); they contain phenocrysts of randomly oriented, milky white, euhedral plagioclase laths (30%) within a matrix of dark green/black anhedral, blocky hornblende (70%).

Aphyric Rhyolite (Tar): Tar dikes typically range from 2-4m thick, are light tan to white in color, and weather a deep red-brown. The dikes commonly show contorted, penetrative flow banding, and are nearly aphyric. Tar dike are generally sparse in the dike swarm, and crop out dominantly in the southeastern portion of the map area. There is an excellent exposure of a Tar dike cutting an older rhyolite dike on the east side of southern Chambers Well Road. Both dikes in this outcrop are, in turn, cut by a Tmd dike. Tar dikes have a holocrystalline groundmass (98%) that is composed of very fine grained quartz and plagioclase, with ubiquitous secondary sericite oriented parallel to flow banding. Plagioclase is the only phenocryst (2%), and the sparse grains, which are 3-4mm in diameter, are highly sericitized.

Quartz-Hornblende Rhyolite (Tqhr): T_{qhr} dikes are commonly 2-4m thick, light gray to white, and form resistant ridges in the map area. T_{qhr} dikes are generally less abundant than dikes of other compositions. T_{qhr} dikes have phenocrysts of blocky, milky white plagioclase (27%) which are 2-3mm in diameter; 4-5mm rounded, clear quartz grains (9%); and 1-2mm, acicular to blocky, dark green, chloritized hornblende (4%). Phenocrysts are supported in a white to light tan, holocrystalline groundmass (60%) of plagioclase and quartz. Tqhr dikes look texturally and mineralogically similar to a suite of Plg-Hbl-Bt dacite dikes (Tchr) that are abundant throughout the map area, however, T_{qhr} contain abundant, rounded quartz phenocrysts.

K-Feldspar Rhyolite (Tkfr): T_{kfr} dikes are more resistant than most other dike compositions, and form several continuous, N-S trending ridges. The dikes are light gray to tan weathering and commonly 4-6m thick. These dikes have phenocrysts, approximately 2-3mm in diameter, of milky white, blocky plagioclase (14%); blocky grains of pink sanidine which are surrounded by rims of milky white plagioclase (9%); fresh, platy, black biotite (4%); and black acicular to blocky hornblende (3%), all set in a dark gray, cryptocrystalline groundmass (70%). Tkf_r dikes look very similar to biotite-hornblende rhyolite dikes (Tfb_r) which are widespread throughout the dike swarm. The presence of pink sanidine phenocrysts was used as a distinguishing feature of Tkfr dikes.

Chloritized Hornblende Rhyolite (Tchr): A suite of light tan to white, resistant, ridge-forming, rhyolite dikes are ubiquitous throughout the Chambers Well dike swarm. These dikes have phenocryst assemblages of 3-4mm, milky white, blocky plagioclase (33%); 1-3mm, platy, dark green, shreds of chloritized biotite (7%); 2-4mm, acicular to prismatic, dark green, chloritized hornblende (4%), and minor, 1-3mm, rounded, clear quartz (0.5%). Opaque minerals (Fe and Ti oxides) account for 2% of the rock volume, and the white to light gray, holocrystalline groundmass constitutes 53%. Tchr dikes commonly contain fine-grained andesite enclaves, and therefore provide clear evidence for magma mingling.

Fresh Biotite Rhyolite (Tfbr): Dark to light gray, red-brown weathering, resistant, ridge-forming dacite dikes are one of the most abundant dike composition in the swarm and crop out throughout the entire map area. The dikes contain phenocrysts of milky-white, blocky, zoned plagioclase (23%); fresh, black euhedral biotite tabs (4%); and dark gray-green, acicular to blocky hornblende (3%). The dikes have a groundmass (70%) consisting of fine grained plagioclase laths and biotite shreds, which ranges from holocrystalline in the interior of dikes to cryptocrystalline/glassy on the chilled margins of dikes.

Plag-phyric Andesite (Tpa): Dark gray to black andesite dikes, 2-4m-thick, are commonly exposed along the margins of other dikes, dominantly in the eastern half of the map area. The coarse-grained interiors of T_{pa} dikes are composed of 0.25-3mm, fresh, translucent white, plagioclase (64%); 0.1-2mm, blocky, dark green to black, hornblende (19%); and abundant, 0.1mm, shreds of dark brown biotite (12%). In thin section, hornblende has partially replaced clinopyroxene. Thin Tpa dikes are commonly quenched throughout and aphanitic, and are difficult to distinguish from similarly quenched Tmd dikes. Sulfides, however, 1-4mm in diameter, are common in Tpa dikes and were used as a diagnostic feature.

Porphyritic Plag Dacite (Tppd): Tppd dikes are restricted to the western portion of the map area and are generally exposed in washes within areas of low relief. Tppd dikes range in color from dark gray to a weathered red brown and contain large (5mm), blocky, milky white plagioclase phenocrysts which gives this rock its distinctive porphyritic texture. Mafic phases in Tppd dikes include biotite and hornblende, but vary in modal abundances. Tppd dikes commonly contain black, nearly aphyric andesitic enclaves with crenulate margins. When these enclaves are present, the groundmass of Tppd dikes is generally darker gray, and the dikes contain abundant fresh, black biotite. Locally these dikes also contain sanidine which occurs replacing plagioclase.

Proterozoic Basement:

Proterozoic basement and younger intrusions (undifferentiated) (p€): Proterozoic quartzo-feldspathic gneisses, discontinuous amphibolite bodies, and several younger leucocratic intrusions compose the country rock to the Chambers Well dikes. The light to dark grey and green weathering quartzo-feldspathic gneisses have a steeply NE-dipping foliation that is locally mylonitic and defined by aligned biotite that is commonly replaced by chlorite. These relatively high temperature fabrics, evidenced by polygonal quartz grain boundaries, are interpreted to be Proterozoic in age and not a product of Miocene extension and detachment faulting. Dark gray to black weathering, discontinuous amphibolite bodies generally do not have a penetrative fabric, which is likely due to the lack of micas or other platy minerals.

Relative Ages of Dikes

The dikes in the Chambers Well Swarm share a common NNE-SSW strike, and examples where one dike clearly cuts across another are not common. Even so, there are a number of outcrops where clear cross-cutting relationships can be observed. The most prevalent and consistent examples of such are Tmd dikes which ubiquitously crosscut dikes of all other compositions. The thin diabase dikes are commonly exposed along the margins of other dikes, where both dikes appear mutually quenched against one another. However, in many locations Tmd dikes cut across older rhyolite dikes, and give an unambiguous relative age relationship (Fig. 10). This relationship was observed consistently throughout the map area, and a rhyolite dike was never observed cutting a Tmd dike.

An aphyric rhyolite (Tar) dike was observed cutting across a fresh biotite rhyolite (Tfbr) in an outcrop along the southern portion of Chambers Well Rd. Both dikes in this outcrop are in turn cut by a Tmd dike. In multiple locations, chloritized hornblende dacite dikes (Tchr) cut across Tfbr dikes. Plag-phyric andesite dikes (Tpa) were commonly observed with irregular, discontinuous map traces, as they were cut by numerous other dikes. In unambiguous cases, where the relative ages of dikes could be confidently assessed, Tmd dikes were always the youngest, followed by Tar, Tchr, Tfbr, and then Tpa. There were many instances, however, where these age relationships were called into question but the limited exposure prevented an adequate assessment of their relative ages. Additionally, age relationships between other dike compositions (Tkfs, Tqchr, and Tppd) were unable to be confidently established by field relationships.

Structural Data

Across the SW footwall of the WDF, dikes consistently strike NNW-SSE and dips range from 20°-90°, with a mean dike orientation of 343/53 (Fig. 11). There is no clear difference in the orientation of dikes by composition, instead dike dips vary by E-W position in the dike swarm (Fig. 12). Just east of CW road, dikes are generally near vertical and progressively grade to more gentle dips toward the west (Fig. 13). Outside of the map area, west of Savahia Peak, dikes have much less consistent orientations and, in general are gently dipping (Fig. 14). To the east of the map area, exposure is generally poor, however, from the limited data collected in this area, it appears that dikes dip steeply to the WSW.

Dike margins are generally poorly exposed throughout the entire map area, and their dips often vary 10-20˚ along an individual dike. It should be noted that while the dikes are relatively planar, measurements reflect only their local orientations. Additionally, steeply dipping, ridge forming dikes are preferentially exposed throughout the map area, as the margins of more gently

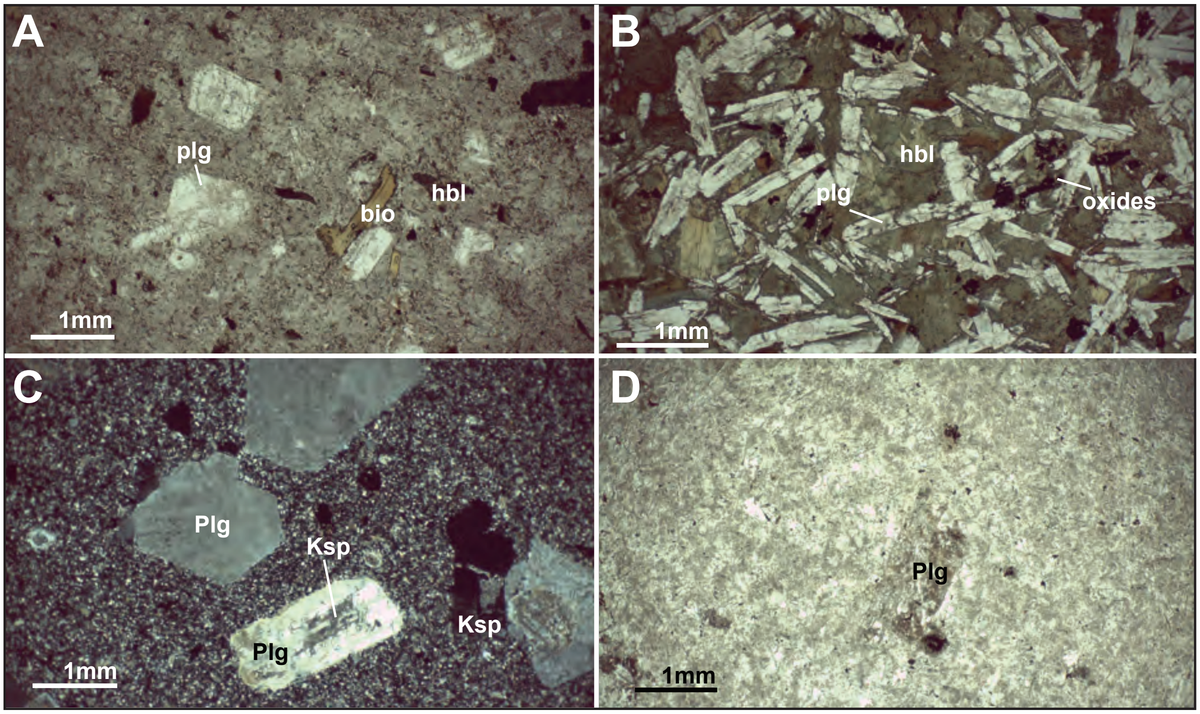

Figure 9. Photomicrographs of a range of textures obserevd in thin section. A.) Plane polarized light (PPL) photomicrograph of a Tfbr dike with distinctive "fresh" biotite and blocky plag phenocrysts. B.) Tmd dike with characteristic, randomly oriented plag laths and interstitial hornblende (PPL). C.) A cross-polarized light (XPL) image of a Tkfr dike with large phenocrysts of plag and K-feldspar set in a very fine grained groundmass. D.) Tar dike with a single, highly sericitized plag phenocryst (PPL). Abbreviations: Plg- Plagioclase, Bio- Biotite, Hbl- Hornblende, Ksp- K-feldpsar

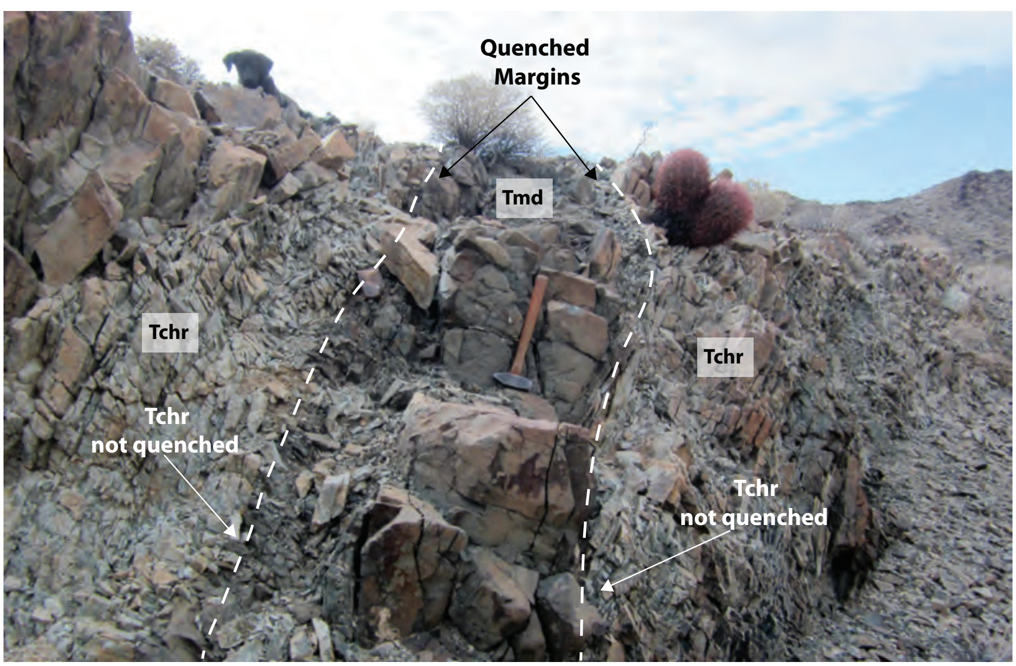

Figure 10. Field photograph showing a Tmd dike unambiguously cutting across a Tchr dike. The margins of the Tmd dike are quenched up against the coarse grained interior of the Tchr dike.

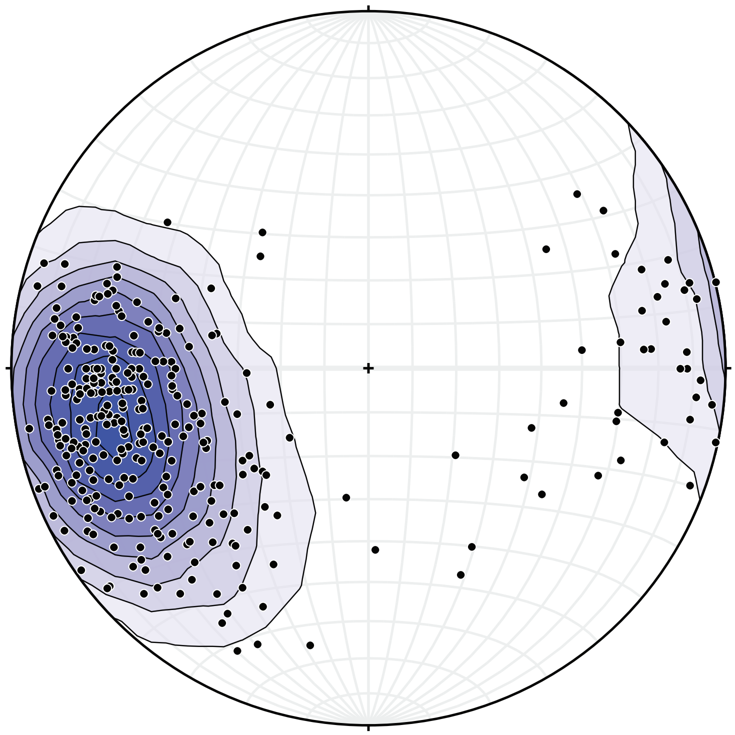

Figure 11. Lower hemisphere stereonet projection showing contoured poles to dikes (C.I.= 2σ, n= 315). Dikes dominantly dip 40-80˚ to the ENE, but a group of dikes dip steeply to the WSW.

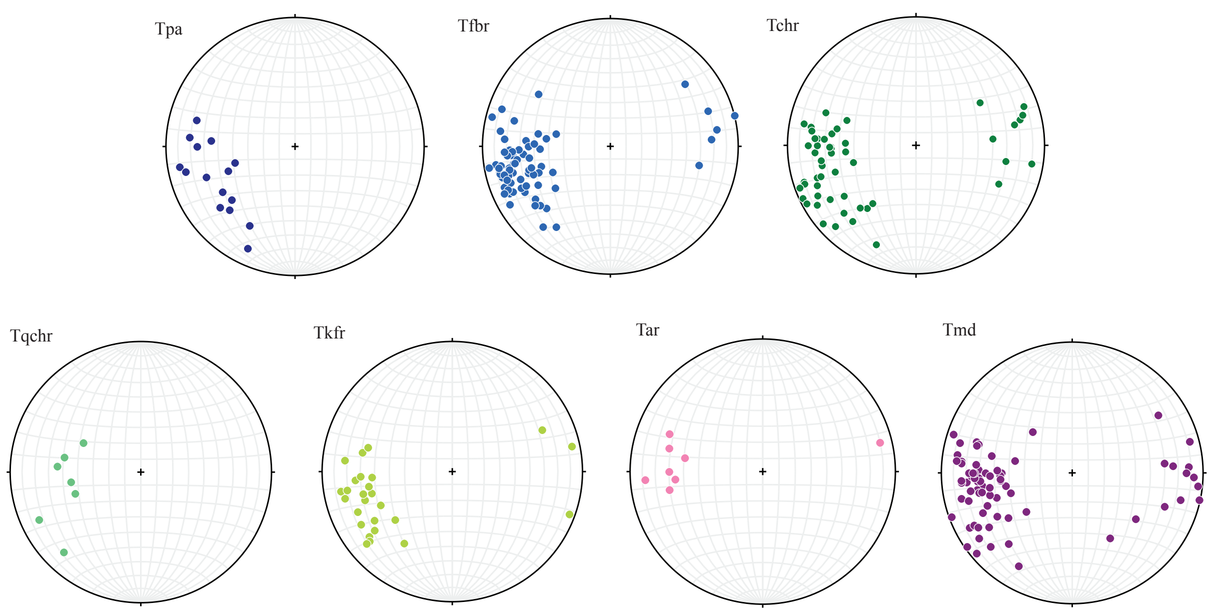

Figure 12. Lower hemisphere stereonet projection showing poles to dikes, separated by composition. There is no statistical difference between the mean orientation of dikes from each map unit.

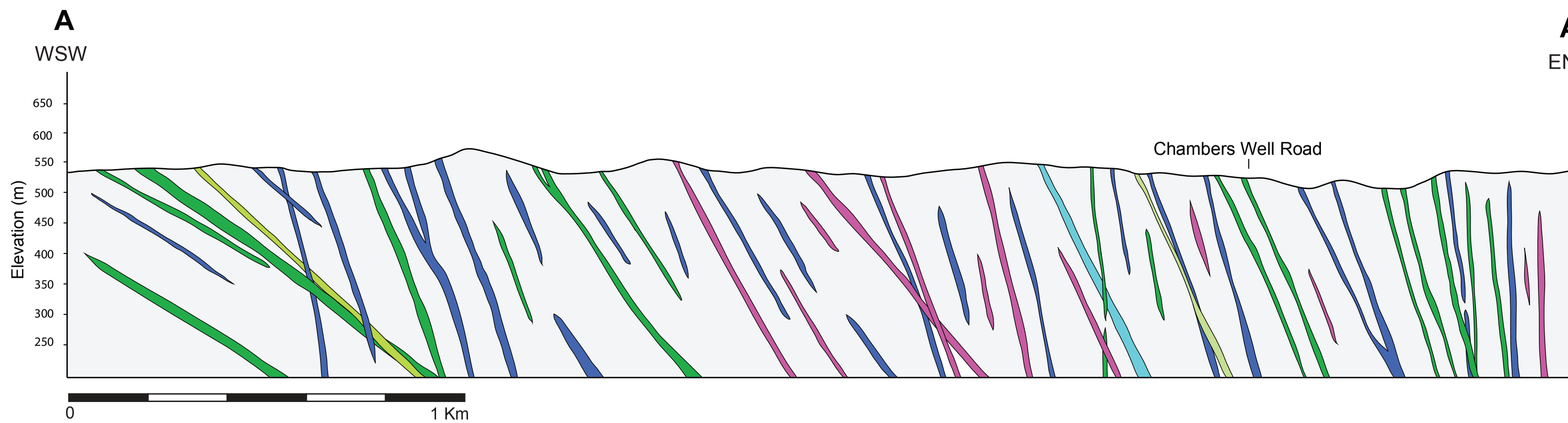

Figure 13. Cross section A-A’ showing the distribution of dike compositions and range of orientations across the Chambers Well dike swarm. The location of Chambers Well Road is shown for reference.

dipping dikes are commonly concealed by talus. This likely resulted in a bias toward more steeply dipping dikes that were measured.

Foliation attitudes in the Proterozoic basement vary locally, however, generally strike to the northeast and dip steeply to the southeast (Fig. 15). Dikes clearly cut sharply across the basement foliation throughout the map area.

Minor attention was given to dikes below the mylonitic front, which lies ~2 km east of the map area. Several dikes in this area contain a penetrative mylonitic fabric and have contacts which are concordant with the steeply west-dipping mylonitic foliation of the surrounding wall rock. While compositionally similar to the Chambers Well dikes, U-Pb zircon ages from these deformed intrusions were distinctly older than the rest of the dike swarm (75 Ma -1800 Ma), and therefore, their orientations are not addressed here.

Across-Strike Transects

Five, detailed, 100 m-long, across-strike transects were measured within the map area; results are summarized in figure 16. The transects show an impressive density of dikes, with dike-to-wall rock ratios ranging from 0.93 to 2.60, and account for many thin and discontinuous dikes which are unable to be represented on the 1:10,000-scale map. Assuming that the dikes were emplaced by the dilation of extensional fractures, this would imply an approximately 100-250% extension across the map area (β= 2-3.5). Tpba dikes represent the most abundant dike composition (39%), followed by Tfbd (30%), Tchd (18%), and Tmd (10%). Measured proportions of dike compositions in 100 m transects are consistent with the estimated relative abundances of dike composition based on field observations.

Geochemistry

In addition to classification of the dikes based on their phenocryst assemblages, major and trace elements were measured from each representative map unit, excluding Tppd. While there is

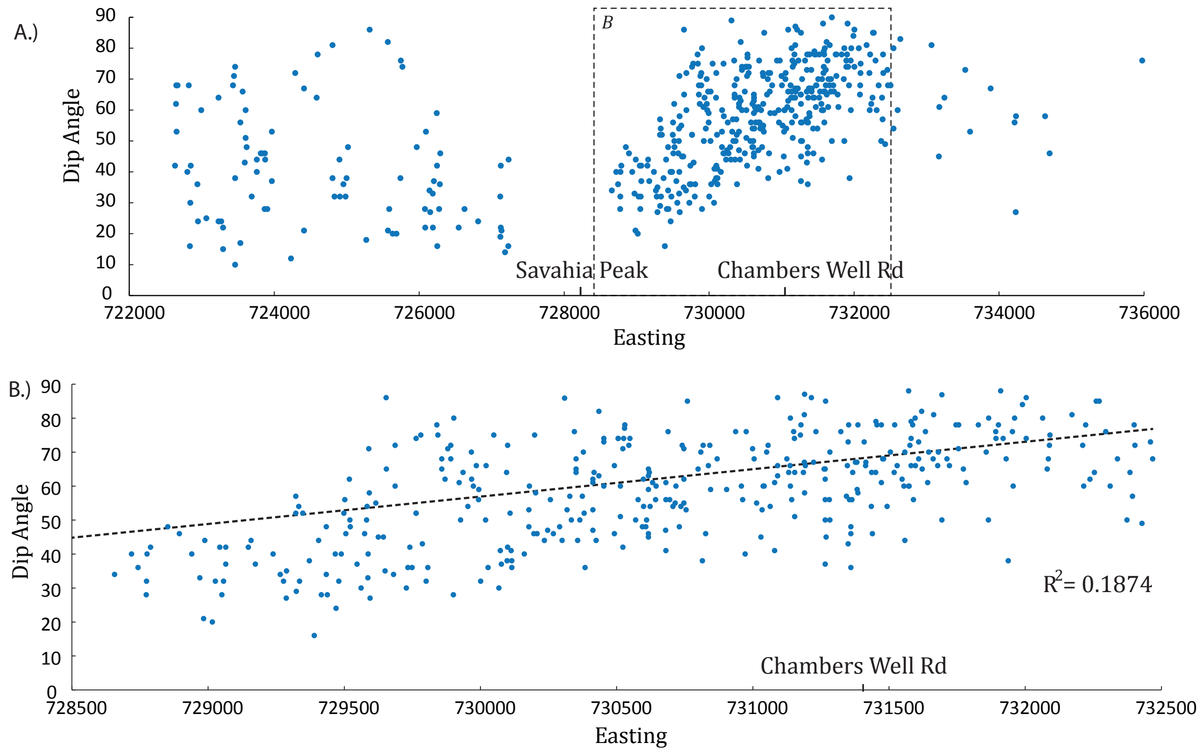

Figure 14. Plot of dip angle vs. E-W position in the dike swarm for A.) dike orientations collected across the entire footwall (n= 502) and B.) data collected within the map area (n= 315). Dikes which crop out between Savahia Peak and Chambers Well Rd. show a linear decrease in dip angle from east to west, while dikes west of Savahia Peak have more irregular orientations.

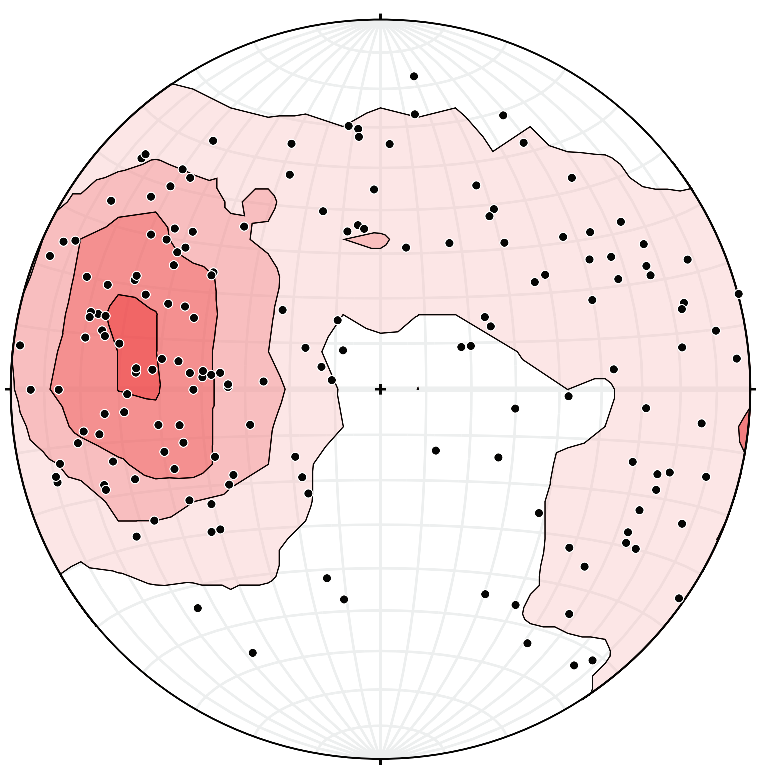

Figure 15. Lower hemisphere stereonet projection showing contoured poles to foliations in proterozoic basement rocks (C.I.= 2 σ, n= 169). Foliations are locally variable throughout the map area, but dominantly dip to the ENE. While the mean foliation orientation is similar to the mean dike orinetation, dikes clearly cut across foliations in the proterozoic host rock.

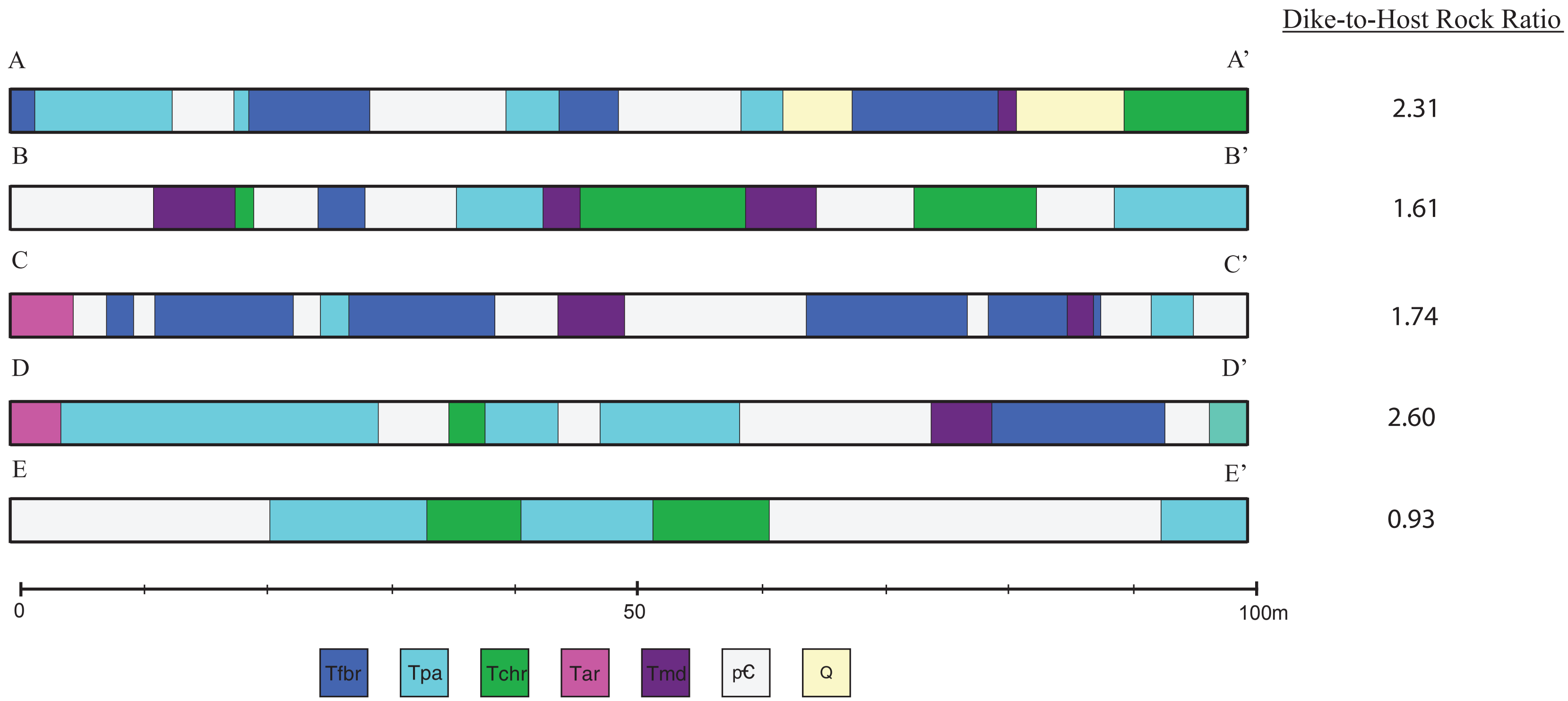

Figure 16. Schematic representation of five across-strike transects that were measured within the map area, perpendicular to dike margins. Bright colors represent various dike compositions, while proterozoic host rock is shown in white. Dike-to-host rock ratios, shown to the right of each transect, range from 0.93 to 2.60 and imply between ~200-350% extension that was accomodated by the emplacement of the dike swarm.

clear evidence of secondary k-feldpsar, sericite, chlorite, and epidote, whole rock compositions appear reasonable for the observed phenocryst assemblages and are taken to represent magmatic compositions.

The dikes have silica contents ranging from 54-77%, with most samples containing >70% SiO_2. Major oxides (Al2O3, CaO, P2O5, MgO, K2O, and Na2O) generally show linear correlations with silica content, and are broadly compatible with a petrogenesis involving significant mixing between a mafic (basaltic) and silicic (crustal?) end member (Fig. 17). On a total alkali vs. silica (TAS) plot, samples generally cluster near the dacite rhyolite boundary with the exception of Tpa and Tmd, which fall in the andesite and basaltic andesite fields, respectively (Fig. 18). The two mafic samples are distinctly separate from rhyolite samples, and there is a lack of samples that are transitional between the two groups.

Samples are generally enriched in the strongly incompatible, large-ion lithophile (LIL) elements by ~10-120x, relative to MORB (Pearce and Parkinson, 1993), and show less enrichment in the more compatible, high field strength (HFS) elements (Fig. 19). All samples have negative phosphorus and titanium anomalies, but are more pronounced in high-silica samples.

Samples are generally enriched in rare earth elements (REE) relative to chondritic values (McDonough and Sun, 1995), with light rare earth elements (LREE) enriched by ~50-200x, while light rare earths (HREE) are enriched by 5-12x. REE abundances generally decrease with increasing SiO2 content. REE patterns are characterized by a negative slope, with La/Yb ranging from 5 to 32, and a pronounced europium anomaly (Fig. 20). Enrichment factors and slopes of REE patterns are consistent with those reported by Anderson and Cullers (1990) for the Chambers Well dikes, however, we observe a clear europium anomaly that was not noted by previous studies.

Geochronology

Samples commonly contain a small proportion of zircons that are Mesozoic though Proterozoic in age, which are interpreted to be inherited from the surrounding wall rock. The dikes

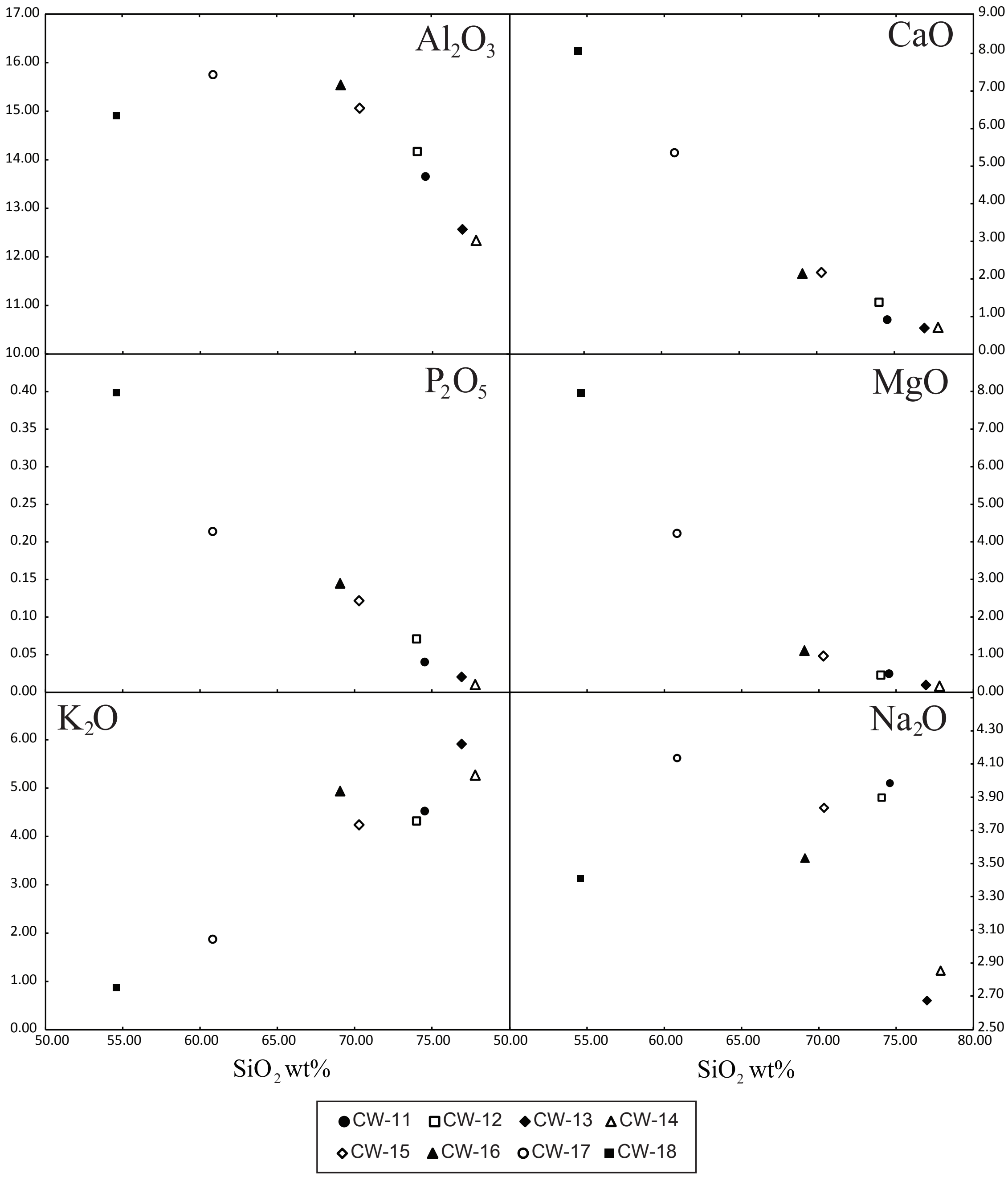

Figure 17. Harker diagrams of weight percent of six major oxides vs. SiO2 in a suite of samples from the Chambers Well dike swarm. Samples generally form linear trends, compatible with a cogenetic history. No correlation exists between wt. % Na2O and SiO2 which may be the result of Na mobility during secondary hydrothermal alteration. The graph of Al2O3 contains an inflection at an SiO2 content of approximately 70%, and likely reflects crystallization of biotite.

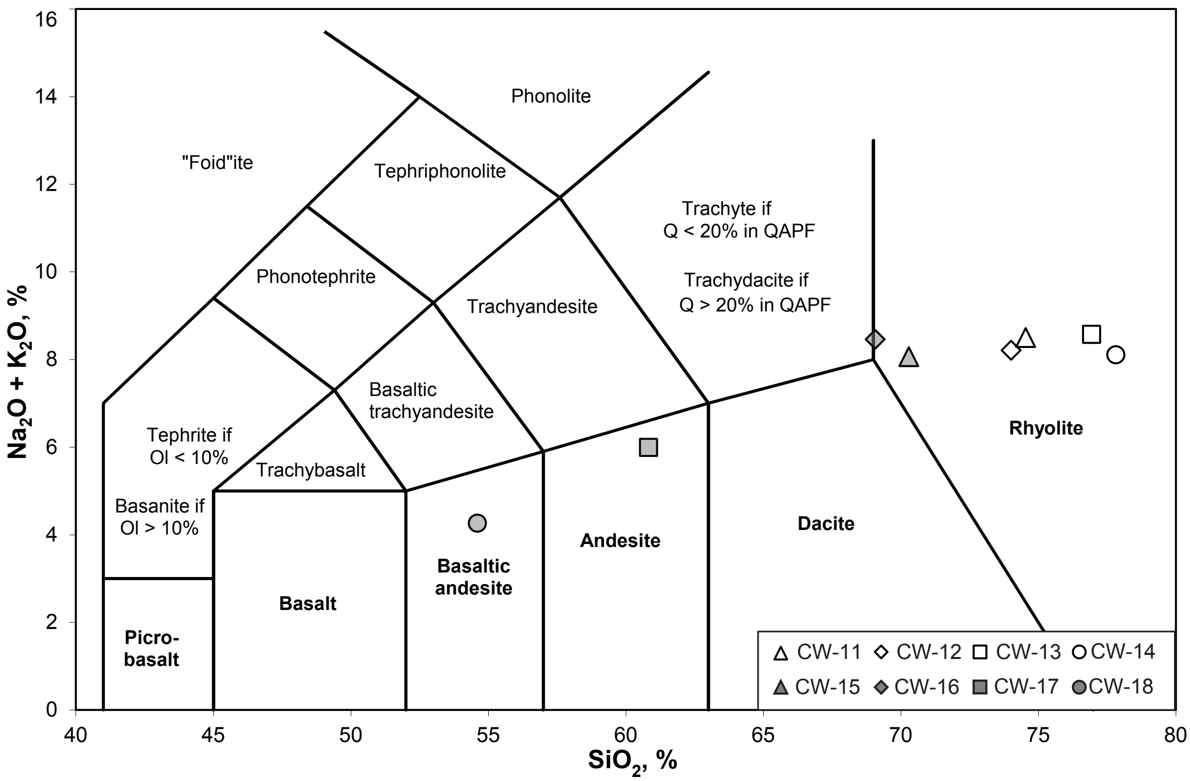

Figure 18. Graph of wt. % total alkalis (K2O + Na2O) vs. wt .% SiO2 for a suite of representative samples, showing the range of compositions in the Chambers Well dike swarm. Dikes primarily plot in the rhyolite field with SiO2 >70%, however, two more mafic dikes that were sampled fall in the andesite and basaltic andesite fields.

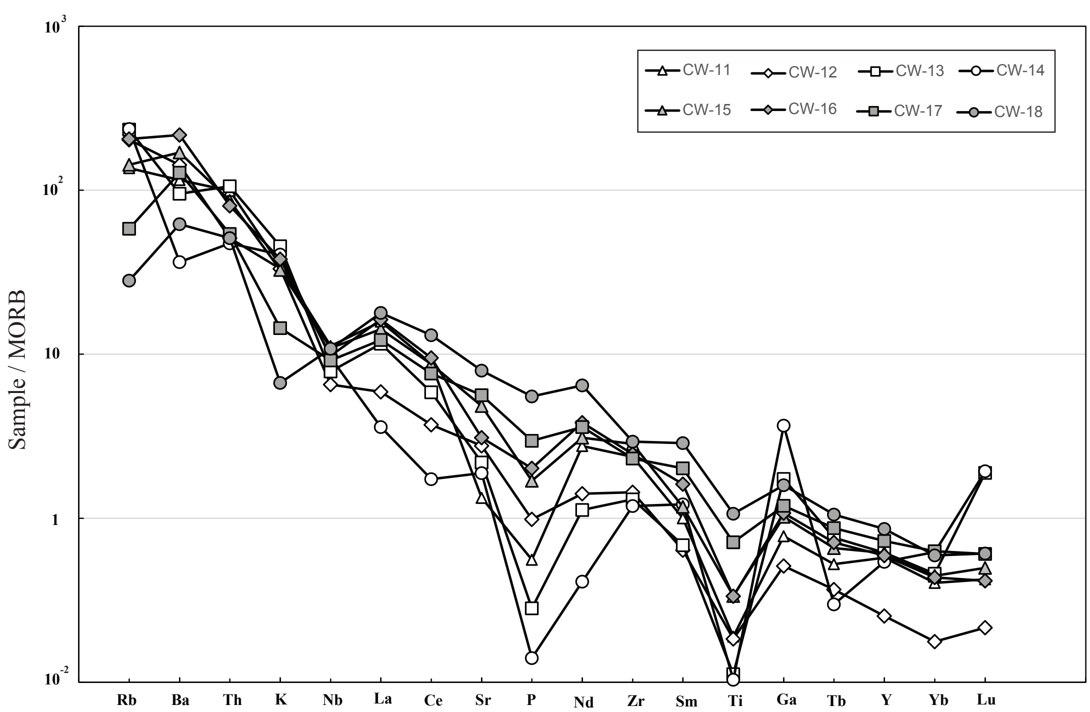

Figure 19. MORB-normalized plot of a series of trace elements, arranged by decreasing incompatibility. All samples are enriched in the highly incompatible elements, and show a decreased enrichment to slight depletion in the more compatible elements (normalized to Pearce and Parkinson, 1993).

contain mainly Miocene zircons, however, within a single sample, these younger zircons commonly do not form a coherent population (Fig. 21). There is no correlation between apparent age and uranium content in the youngest (Miocene) zircons within a single sample, suggesting that the range in zircon ages is not the result of lead loss (Fig. 22). It is apparent, however, that based on cross-cutting relationships established in the field, relatively younger dikes show an increased spread of Miocene-aged zircons (Fig. 23). This is interpreted to represent the combined effects of recycling of zircons from earlier dike/magmatic events and the crystallization of younger zircons with each period of dike formation. Reported dike ages were calculated by omitting slightly older, inherited zircons, and only using the youngest coherent population of zircons from each sample. There is an inherent uncertainty in this method of age calculation, particularly in zirconium-poor rocks, because it relies on the youngest, primary zircons being sampled. This error is amplified by a large statistical uncertainty on the age which is calculated from generally few data points (Fig. 24).

Samples range in age from 18.75-20.1 Ma, and there is no spatial trend in dike ages. The youngest sample from which an age was calculated, also has the highest SiO_2 content, however, at the current resolution there is no clear correlation between age and silica content. Dikes of similar composition and that were assigned to the same map unit, were sampled in various portions of the map area, but yielded ages outside of analytical error of on another. This suggests that dike composition may not be a proxy for age, and instead, dikes of varying compositions were emplaced continuously from 20.12 to 18.75 Ma (Fig. 25). This would imply that there are not consistent relative age relationships between dikes of different compositions, or at least that can be resolved at the current sampling resolution.

Repeated attempts to date diabase dikes (Tmd) were unsuccessful, as samples did not yield any Miocene zircons. Samples were collected from diabase dikes that clearly cross-cut aphyric rhyolite dikes, and therefore must be younger than ~18.75 Ma. The exact age of this younger suite of dikes is unknown.

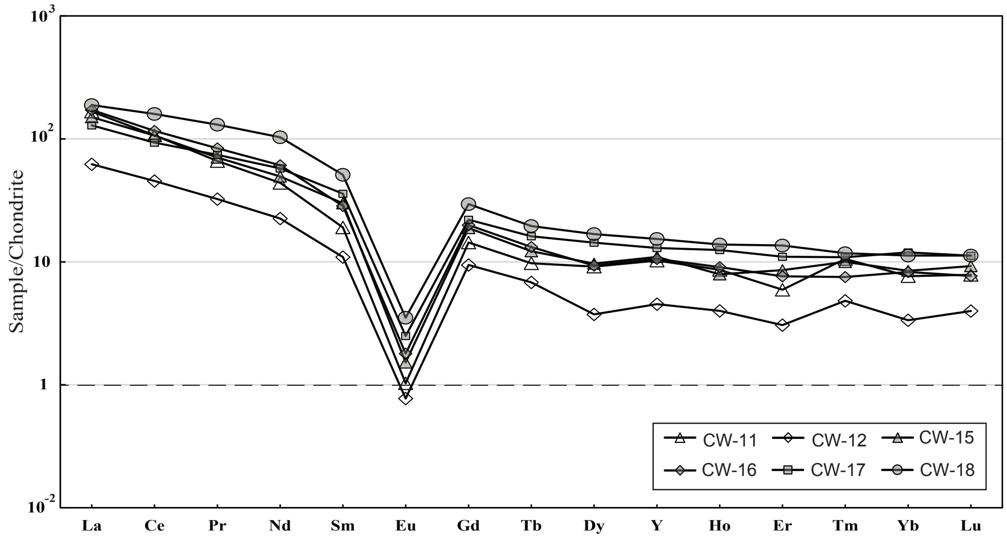

Figure 20. Whole-rock, chondrite normalized, rare earth element (REE) spiderdiagram for six dikes. All samples show a similar REE pattern with a negative slope (La/Yb= 5 to 32) and pronounced Eu anomoly (Normalized to McDonough and Sun, 1995).

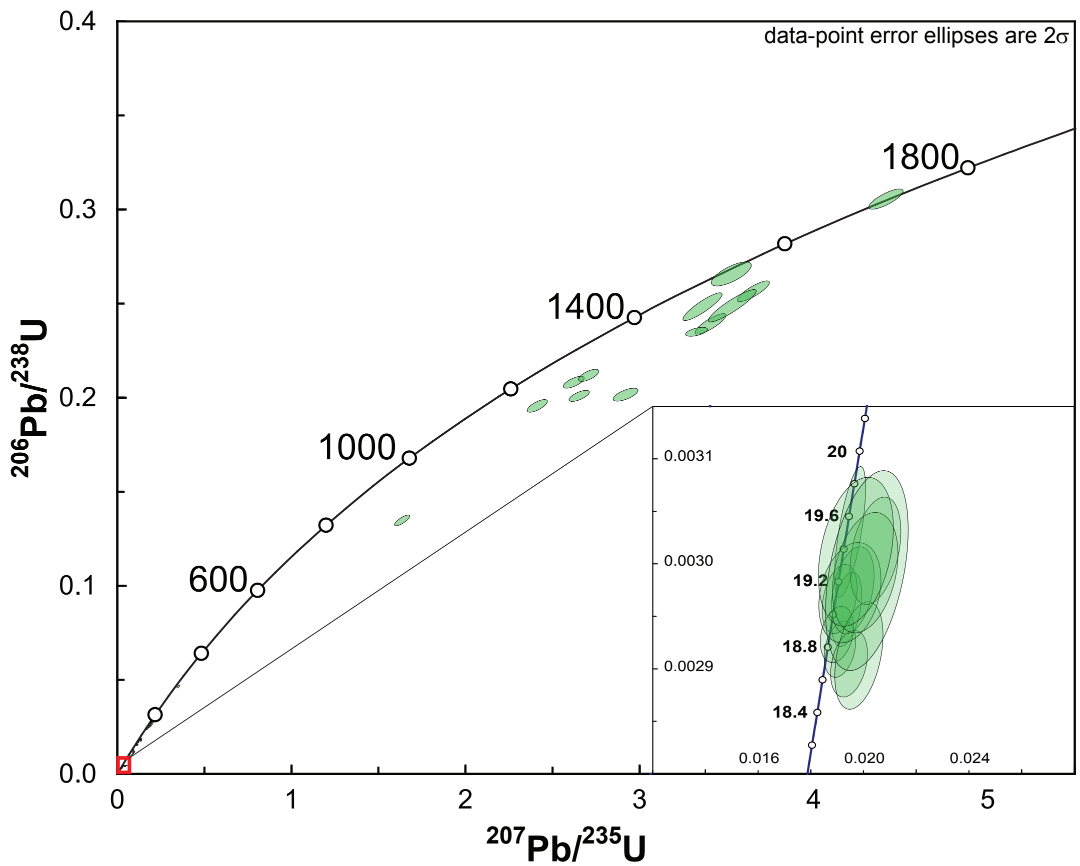

Figure 21. U-Pb concordia diagram showing the range of zircon ages within a single representative rhyolite dike. Most samples contain numerous Proterozoic and Mesozoic zircons, interpreted to have been inherited from the basement rocks that host the dike swarm, and a group of younger Miocence zircons (shown in inset) which record crystallization of the dikes. Ages along concordia are shown in Ma.

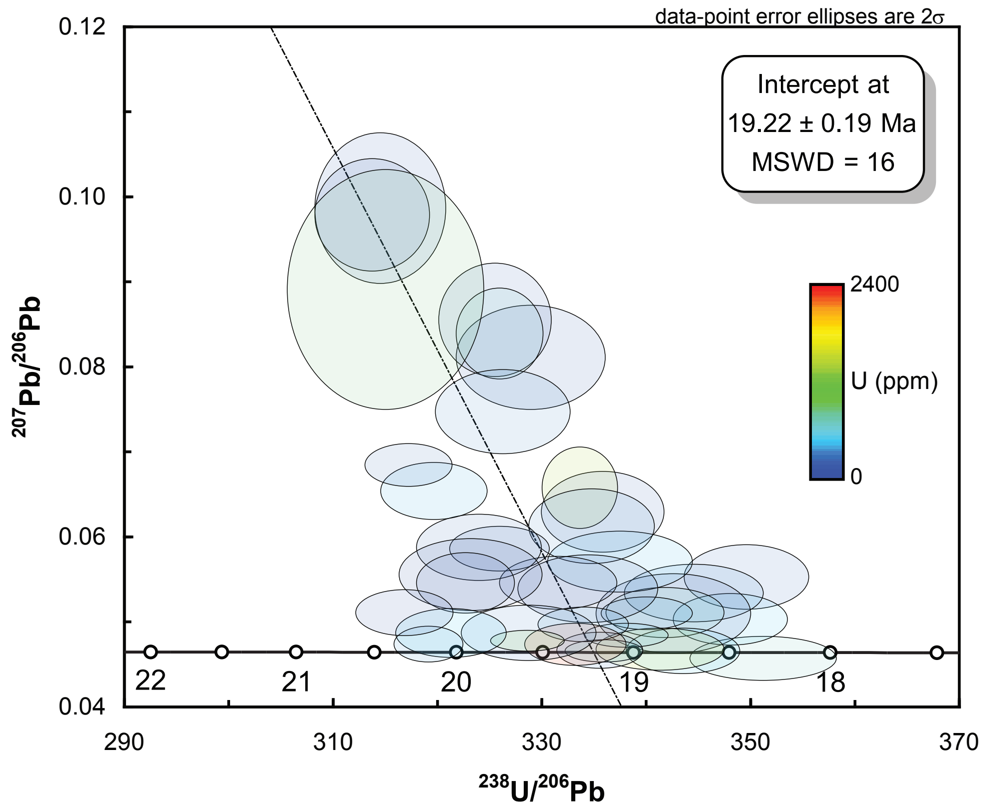

Figure 22. Tera-Wasserburg diagram showing zircon analyses from a representative rhyolite dike. Elipses represent analyses of individual zircons, including a 2σ error, and are colored by approximate uranium content. Zircons do not form a coherent population and the range in apparent ages cannot be explained by lead loss (high uranium content in younger zircons).

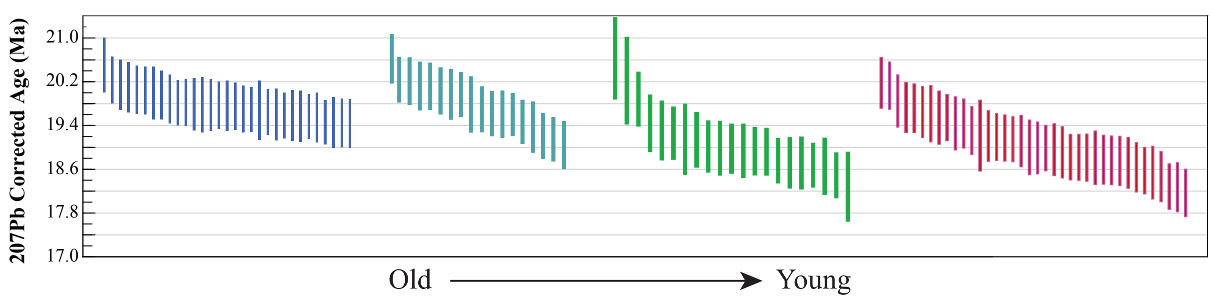

Figure 23. Apparent zircon ages in four samples, for which relative ages are known based on cross cutting relationships. Each bar represents a corrected age from a single analysis ± 2σ. Analyses are grouped and colored by sample, and samples are aranged by relative age. Younger samples show an increased spread in zircon ages. The oldest and youngest zircons within a sample lie outside of analytical error of one another, and cannot represent a single population. The wide range in zircon ages in young samples is attributed to recycling of zircons from older dikes, and therefore, the youngest zircons within a sample record crystallization.

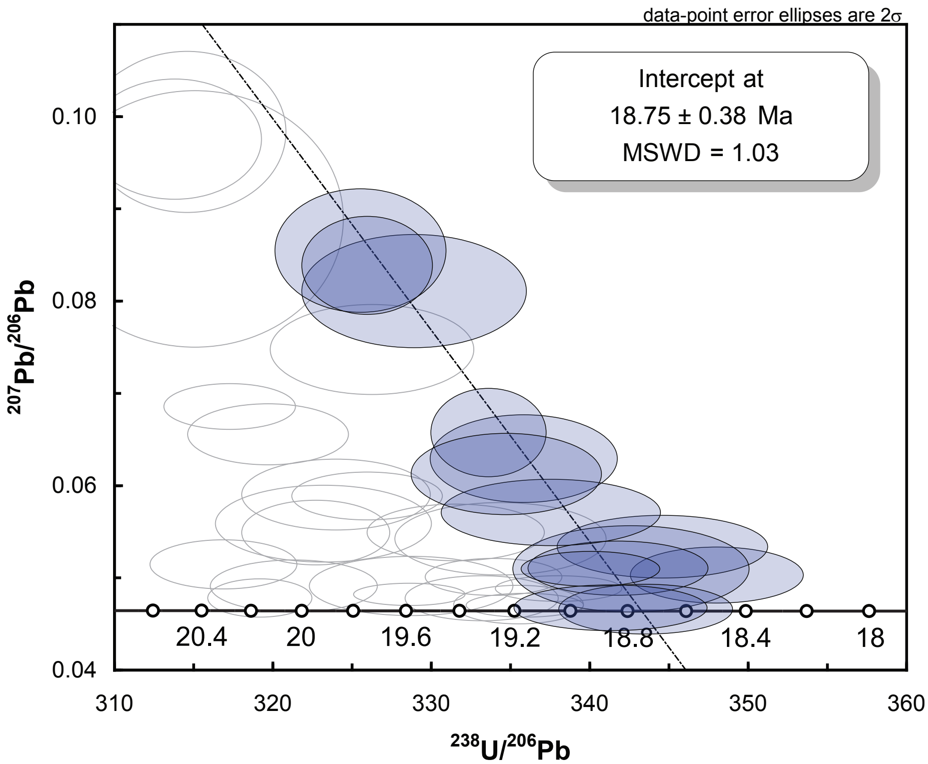

Figure 24. Tera-Wasserburg diagram showing the youngest coherent population of zircons within a sample from a rhyolite dike. The oldest analyses were omitted (light gray ellipses) until a permissible MSWD (≈ 1) was achieved. This method only leaves 14 analyses (filled blue ellipses), from an original 43, that are used in an age calculation, resulting in a large internal uncertainty.

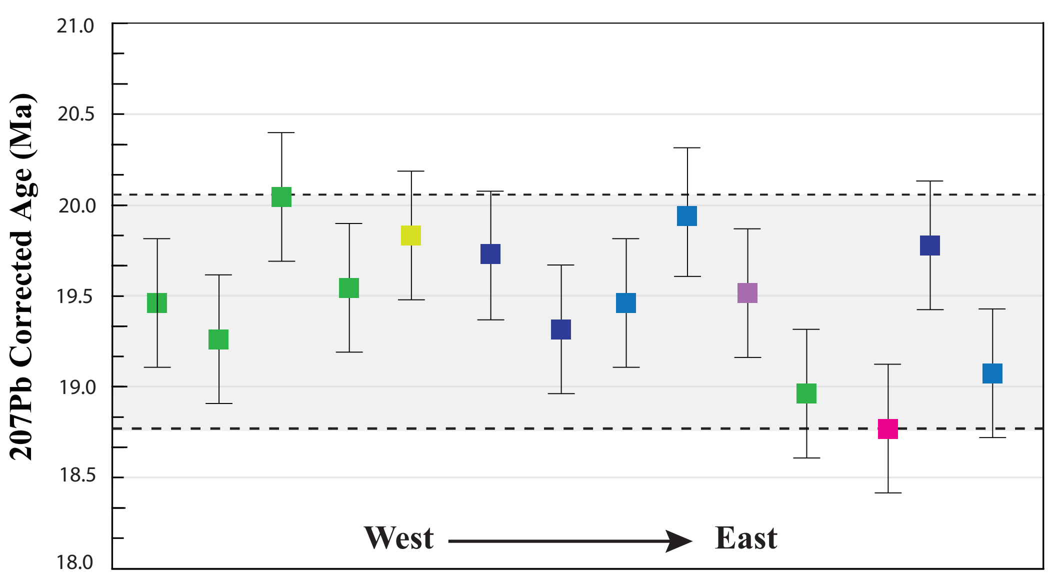

Figure 25. 207Pb Corrected ages of all samples from the Chambers Well dikes. Samples are colored by map unit and arranged schematically by sample location (E-W). Error bars include contributions from internal standard error and external, long-term reproducibility. At the current resolution, dike ages do not vary spatially, and instead span the entire interval from 18.75 to 20.12 Ma. Dikes which were assigned to the same map unit yield varying ages that lie outside of analytical error of one another, suggesting that there were multiple periods of emplacement of dikes with similar compositions.

Additionally, the two ‘upper plate’ dikes that were sampled west of the map area yielded ages that fall within the same age distribution as the Chambers Well dikes (Table 3).

DISCUSSION

Amount of Intrusive Dilation

The dikes in the Chamber Well swarm have sharp, quenched, planar margins and lack any wall rock xenoliths which suggests that they were emplaced primarily through the dilation of extensional fractures and not by wall rock assimilation (Rubin, 1995). The dikes are exceptionally abundant in the portion of the swarm near Chambers Well Rd., and the amount of dike rock far exceeds the amount of wall rock in many locations. Many dikes were intruded along the contacts of other dikes, similar to sheeted dike complexes at mid ocean ridges. Furthermore, many rhyolite dikes contain abundant andesite enclaves, and numerous “hybrid” dikes were observed which were transitional to the designated lithologic map units. Together these observations argue for a large composite magma system that was active in the western Whipple Mountains from approximately 20.12-18.75 Ma. This magma system sourced the Chambers Well dikes, which cumulatively account for roughly 5-7 km of extension that was accommodated through the intrusive dilation of extensional fractures.

An approximately 1 km-thick package of intermediate to felsic lavas is exposed in the western Whipple Mountains and Mopah Range, in the upper plate of the WDF. This volcanic section dips uniformly ~60˚ to the north east, and is unconformably overlain by the gently-dipping Peach Springs Tuff (18.5 Ma) and younger units (Fig. 26) (Gans and Fidler, personal communication). This angular unconformity closely brackets the timing of extensional faulting and tilting within the upper plate of the WDF to between 19.0 and 18.5 Ma. These relationships suggest that from 20.2 to 19.0 Ma, magmatic extension was the primary mechanism by which extension was accommodated, but quickly transitioned to tectonic extension dominated by upper crustal normal faulting and block rotation between 19.0 and 18.5 Ma. The pervasive magmatism from 20.1 to 18.75 Ma may have

Sample ID	Map Unit	Age ± 2σ	MSWD	Sample Location (UTM)			
CW-01	Tfbr	19.72 ± 0.40	1.6	Chambers Well map area	11 S	731571	3795029
CW-02	Tpa	19.15 ± 0.40	2.2	Chambers Well map area	11 S	731571	3795029
CW-04	Tar	18.75 ± 0.38	1.03	Chambers Well map area	11 S	731571	3795029
CW-05	Tchr	18.93 ± 0.39	1.3	Chambers Well map area	11 S	731530	3796092
CW-07	Tkfr	19.51 ± 0.39	1.9	Chambers Well map area	11 S	730971	3796729
CW-21	Tchr	20.12 ± 0.40	2.7	Chambers Well map area	11 S	729728	3793948
KFC-02	Tppd	19.76 ± 0.40	1.3	Chambers Well map area	11 S	730528	3795111
KFC-03	Tfbr	19.85 ± 0.40	1.2	Chambers Well map area	11 S	730613	3795071
KFC-05	Tfbr	19.92 ± 0.40	1.12	Chambers Well map area	11 S	730748	3795092
KFC-06	Tpa	19.47 ± 0.40	1.8	Chambers Well map area	11 S	730814	3795072
KFC-07	Tpa	19.87 ± 0.42	1.9	Chambers Well map area	11 S	730960	3795003
WFW-03	Tchr	19.23 ± 0.39	1.2	"Upper plate" dike	11 S	718855	3799199
WFW-04	Tchr	19.45 ± 0.40	0.99	"Upper plate" dike	11 S	718342	3799194
WFW-06	Tchr	19.55 ± 0.40	1.7	Western footwall	11 S	725686	3797100

Table 3. Summary of U-Pb zircon geochronology. Reported erros include contributions from both the internal standard error and an additional 2% uncertainty to account for the long-term reproducibility of secondary standards at the UCSB LA-ICP-MS facility.

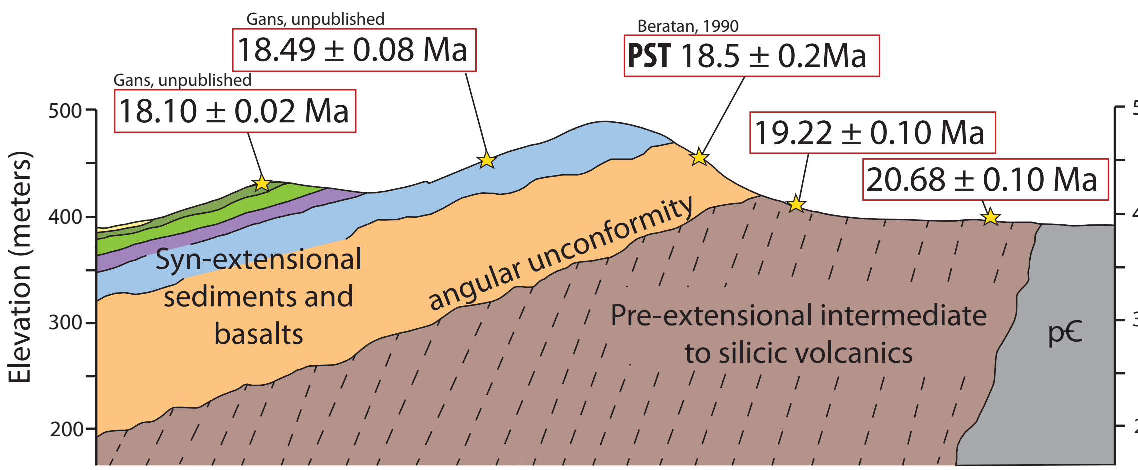

Figure 26. Schematic cross section of the upper plate volcanic stratigraphy of the Western Whipple Mountains and Mopah range. The Chambers Well dikes closely match the ages and compositional ranges of the steeply-dipping “pre-extensional” volcanics, which are unconformably overlain by the gently-dipping Peach Springs Tuff (PST) and a younger, syn/post-extensional mafic “capping sequence” (Fidler, unpublished).

triggered this abrupt transition by thermally weakening the crust. Alternatively, it might instead reflect an abrupt increase in the regional strain rate, such that magmatic inflation could no longer keep pace.

Correlation with Upper Plate Units

We propose that the Chambers Well dikes are the feeders to the thick volcanic section exposed in the adjacent "upper plate" portions of the southwest Whipple Mountains and nearby Mopah Range, roughly 10 km to the west of the Chambers Well map area (Fig. 27). The kilometer-thick accumulation of andesite to rhyolite lava flows and domes is the only volcanic section of similar age in the region that is dominated by felsic lavas, and represents a clear candidate for the eruptive counterparts of the rhyolite-dominated Chambers Well dike swarm. Geochemical analyses of the dikes and representative lava flows demonstrates that they span identical compositional ranges (Fig. 28).

Furthermore, an approximately 8 km^2 exposure of Proterozoic gneisses and amphibolites, similar to the basement rocks in the Chambers Well area was identified in the upper plate of the WDF, ~10km northwest of the map area. The basement rocks are intruded by a number of felsic dikes, which resemble Tchr dikes in the Chambers Well swarm. Mean weighted zircon ages from these dikes are 19.23 ± 0.39 and 19.45 ± 0.40 (MSWD = 1.2 and 0.99, respectively), suggesting that these dikes are in fact members of the Chambers Well dike swarm.

These correlations suggest that the upper plate of the WDF that is exposed in the SW Whipple Mountains and Mopah Range, could not have been transported large distances. While other have proposed that the WDF in the eastern portion of the range has accommodated approximately 40 km of NE-directed slip, our interpretation argues that the western portion of the WDF has not accommodated large amounts, if any, northeast-directed displacement since approximately 20.2 Ma. For this reason, we also question whether the gently-dipping fault separating the Miocene volcanic

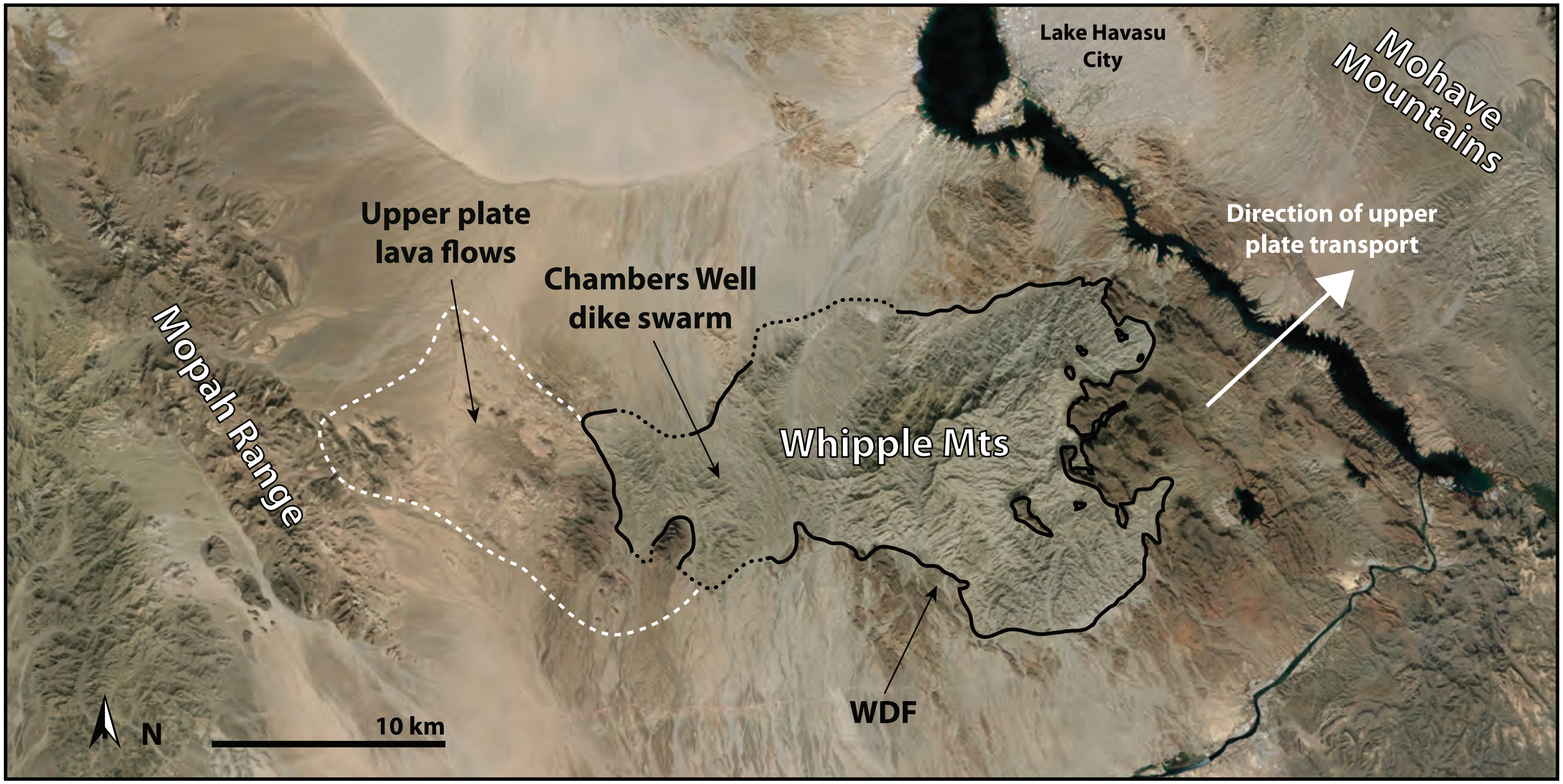

Figure 27. Satellite image of the Whipple Mountains MCC and surrounding ranges, highlighting the locations of the Chambers Well dike swarm and upper plate lava flows which have similar ages and compositions to the dikes. If the Chambers Well dikes were the feeders to this volcanic section, it would imply that there has been very little, if any, NW-directed slip on the western WDF since ~20 Ma (Modified from Google Earth).

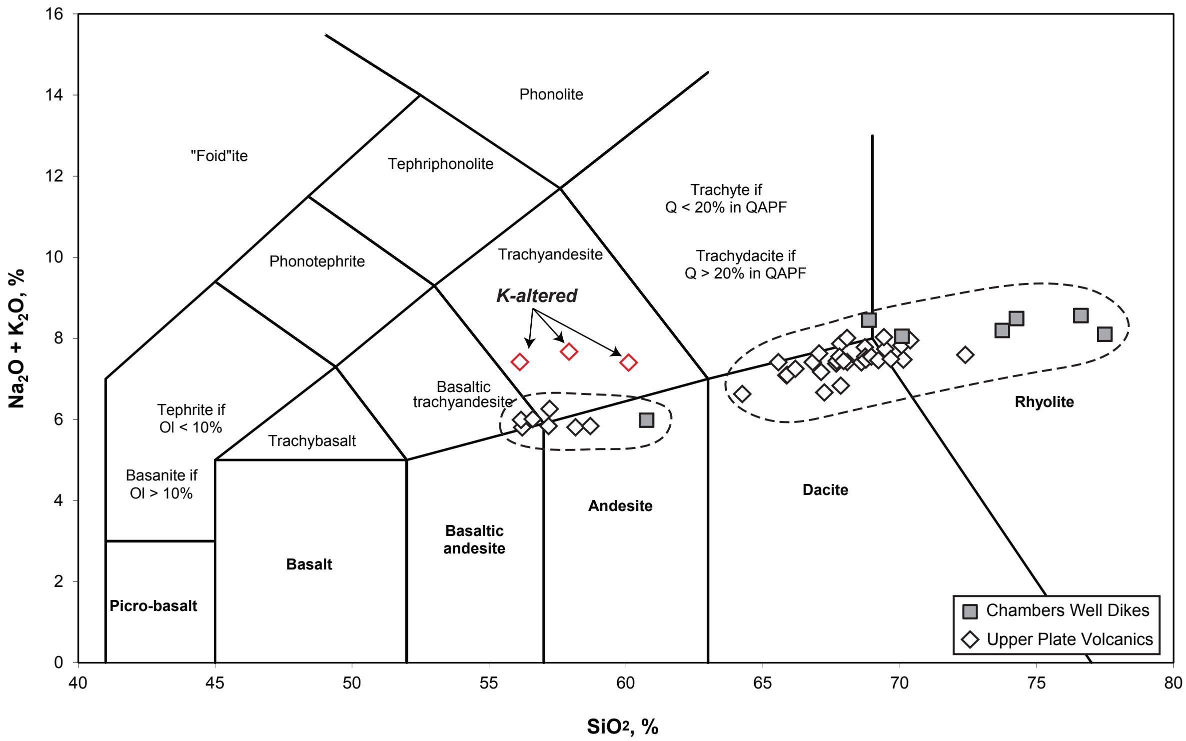

Figure 28. TAS diagram showing the compositional similarities between the Chambers Well dikes and lava flows of similar age in the Mopah Range and Western Whipple Mountains. All of the upper plate samples plot in the high-alkali portions of the andesite, dacite, and rhyolite fields, with the majority of samples clustered near the rhyolite-dacite boundary. Similar to the Chambers Well dikes, andesite lavas form a discrete cluster, separate from the dacites and rhyolites. Three samples from the upper plate volcanic sequence plot in the trachyandesite field, above the other andesite samples, but contain similar SiO2 contents (56-60%). These samples have clear signs of secondary potassic alteration, thus, their magmatic compositions are likely similar to other andesite samples (upper plate data from Gans and Fidler, unpublished).

section in the SW Whipple and Mopah Range from exposures of the "footwall" near the Chambers Well study area is the same structure as the WDF mapped in the eastern portion of the range.

Constraints on the Magnitude and Timing of Footwall Rotation

The fan-shaped geometry of the Chambers Well dike swarm was first noted by Davis *et al.* (1982). They recognized that the dikes dip inward about an axis of sub-vertical dikes, near Chambers Well Road, and speculated that the swarm's geometry may be the result of a N-S trending, linear pluton at depth. In this model, the dikes were emplaced analogously to inward-dipping cone sheets of Anderson (1937). In the Chambers Well dike swarm, however, the fan's axis of symmetry is inclined approximately 53˚ to the SW, as opposed to vertical as in Anderson's model. If the dikes were emplaced radiating from an elongate, compositionally zoned magma body, the asymmetry of the present-day fan suggests that the swarm may have been rotated to the southwest after emplacement of the dikes (Fig. 29). The axis of this fan is oriented approximately 343/53, and is not parallel to the rotation axis suggested by upper plate tilt axes (310˚) and the regional extension direction (040˚) (Gans, personal communication). Therefore, the dip angles of dikes do not account for the total tectonic tilting. Dikes which strike NW, perpendicular to the axis of rotation, are more highly rotated while dikes which strike N-S show less tilting. Assuming that the dikes were emplaced symmetrically about an axis of vertical dikes and that rotation occurred about a horizontal axis, parallel to the strike of upper plate strata and the WDF, ~40˚ of SW rotation is required to restore the axis of symmetry of the dike swarm to vertical. This implies that the WDF initially dipped more steeply to the NE (~40-50˚) and was rotated to its gently-dipping orientation, in agreement with Anderson's theory of faulting (Anderson, 1905).

The dips of hanging wall strata constrain any major tilting to between 18.5 and 19.0 Ma, an interval which also corresponds to the final stages of intrusion in the Chambers Well swarm, with the emplacement of aphyric rhyolite dikes (~18.75 Ma) and a suite of younger diabase dikes (< 18.75 Ma). Nine, steeply-dipping, aphyric rhyolite dikes were mapped in the eastern portion of the dike

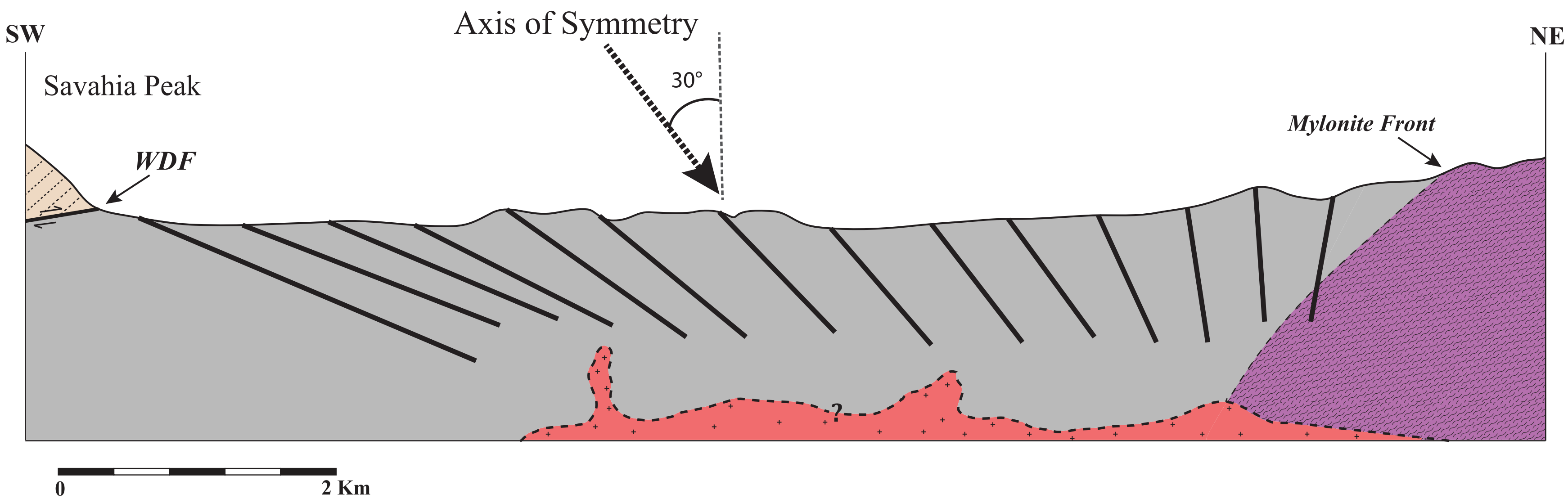

Figure 29. Schematic NE-SW cross section from Savahia Peak to the mylonite front, showing the inward-dipping fan geometry of the dike swarm. The axis of symmetry of the fan of dikes is inclined ~30° to the SW. Assuming that the dikes were emplaced symmetrically about an axis of sub-vertical dikes, similar to the inward-dipping cone sheets of Anderson (1937), this would imply that the dike swarm has been rotated to the SW.

swarm and may document only the final stages of tilting. Diabase dikes, however, must have been emplaced after any major tilting but were intruded along the contacts of pre-existing dikes, leading to a range of orientations (Fig. 30). This explanation for the range of dike orientations in the Chambers Well swarm argues for 40˚ of CCW rotation of the southwestern footwall of the WDF, about a horizontal axis trending 310˚, between 19.0 and 18.5 Ma. Removing this rotation restores the sub-horizontal, western segment of the WDF to an approximately 40˚ dip, in agreement with Andersonian fault mechanics. Additionally, the steeply west-dipping mylonite front is restored to gently dipping (~15˚) (Fig. 31).

CONCLUSIONS

The Chambers Well dike swarm is an impressive suite of basaltic andesite through rhyolite dikes which intruded the lower plate of the Whipple Detachment fault between 20.1 and 18.75 Ma. In the portion of the dike swarm near Chambers Well Road, the amount of dike rock exceeds the amount of wall rock, implying that >100% extension was accommodated by intrusion of the dikes. Applied across the 4km wide map area, the dikes account for >2km of WNW-ESE extension. The Chambers Well dikes closely match the ages and compositional ranges of lava flows exposed locally in SW Whipple Mountains and Mopah Range, and are likely the feeders to this thick volcanic succession. This relationship implies that there has been minimal, if any, northwest-directed slip on the southwestern portion of the WDF since ~ 20Ma. The hundreds of dikes and kilometer-thick volcanic section are evidence of short-lived, but intense magmatism in the SW Whipple Mountains from 20.1 to 18.75 Ma, immediately prior to extensional faulting and tilting of upper plate strata. This voluminous magmatism may have played an active role in the early stages of extension through the thermal weakening of the crust, and was closely followed by extensional faulting and tilting of upper plate strata. Finally, the asymmetric fan-shaped geometry of the Chambers Well dike swarm suggests that the southwestern footwall of the WDF may have been tilted ~40˚ to the SW between 19.0 and 18.5 Ma, implying that the WDF initiated with a much steeper dip (~40-50˚).

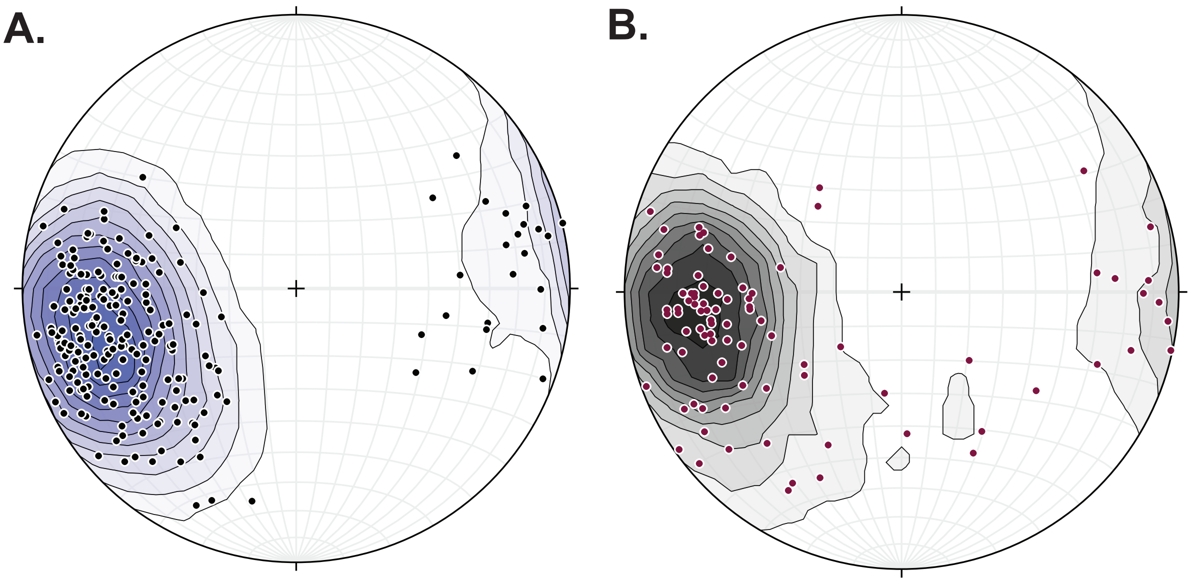

Figure 30. Lower hemisphere stereonet projection of poles to A.) all dikes in the Chambers Well swarm, excluding Tmd dikes (n=225, C.I.= 3σ, signif. level= 3σ) and B.) Tmd dikes (n= 90, C.I. = 2σ, signif. level= 3σ). Tmd dikes are commonly exposed along the margins of other dikes, and their orientations during emplacement were likely controlled by pre-existing dikes. Thus, their orientations generally match those of the rest of the Chambers Well dikes. Tmd dikes, however, also show more variation in orientations, and is likely the result of the dikes intruding locally along other pre-existing weaknesses (foliations, fractures, etc.).

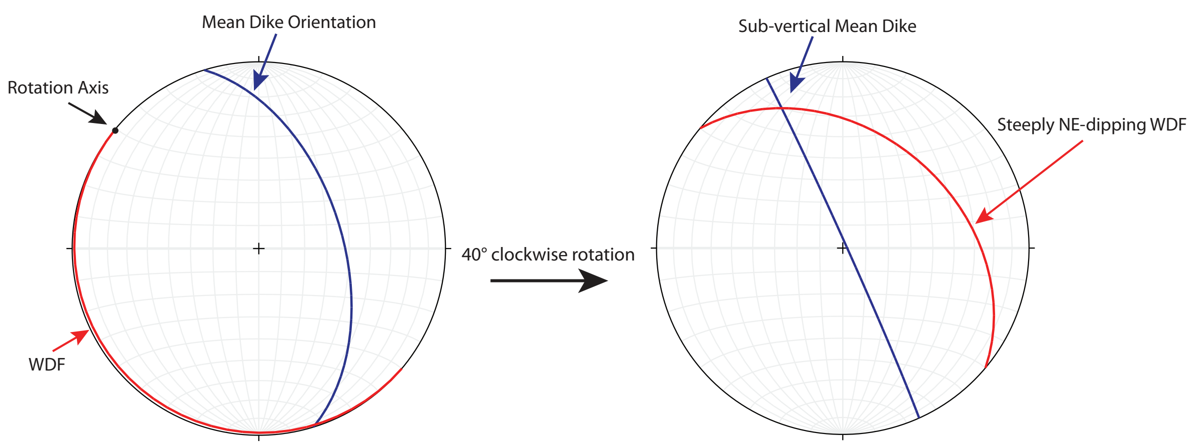

Figure 31. Lower hemisphere stereonet projection showing the restored orientations of the WDF, mean dike orientation, and mylonite front after 40° of clockwise rotation about a horizontal axis, parallel to strike of the WDF (310°). The mean dike orientation is restored to sub vertical, the WDF to steeply NE-dipping, and the mylonite front to sub-horizontal. The restored orientations of the dikes and WDF more closely match the orientations predicted by classical Andersonian rock mechanics, and argues for a sub-horizontal boundary for the upper limit of mylonitization.

REFERENCES

Abers, G.A., Mutter, C.Z., and Fang, J., 1997, Shallow dips of normal faults during rapid extension: Earthquakes in the Woodlark-D'Entrecasteaux rift system, Papua New Guinea. Journal of Geophysical Research v. 102, p. 15,301-15,317.

Anderson, E.M., 1937, The dynamics of the formation of cone-sheets, ring-dykes, and caldron-subsidences. Proceedings of the Royal Society of Edinburgh, v. 56, p. 128-157.

Anderson, E. M., 1905, The dynamics of faulting. Transactions of the Edinburgh Geological Society, v. 8(3), p. 387-402.

Anderson, J.L., and Cullers, R.L., 1990, Middle to upper crustal plutonic construction of a magmatic arc; An example from the Whipple Mountains metamorphic core complex. Geological Society of America Memoir v. 174, p. 47-70.

Coney, P. F., 1980, Cordilleran metamorphic core complexes: An overview, in Crittenden, M. D., Jr.,

Coney, P. F., and Davis, G. H., eds., 1980, Cordilleran metamorphic core complexes. Geological Society of America Memoir v. 153, p. 7–31.

Coney, P.J., and Harms, T.A., 1984, Cordilleran metamorphic core complexes: Cenozoic extensional relics of Mesozoic compression. Geology v. 12, p. 550-554.

Cottle, J.M., Burrows, A.J., Kylander-Clark, A.R.C., Freedman, P.A., and Cohen, R., 2013, Enhanced sensitivity in laser ablation multi-collector inductively coupled plasma mass spectrometry: Journal of Analytical Atomic Spectrometry, v. 28, p. 1700–1706.

Cottle, J.M., Kylander-Clar, A.R.C., and Vrijmoed, J.C., 2012, U-Th/Pb geochronology of detrital zircon and monazite by single shot laser ablation inductively coupled plasma mass spectrometry (SS-LA- ICPMS): Chemical Geology, v. 332–333, p. 136–147.

Davis, G.A. and Lister, G.S., 1988, Detachment faulting in continental extension; perspectives from the southwestern U.S. Cordillera: in Clark, S.P., Jr., et al., eds., Processes in continental lithosphere deformation: Geological Society of America Special Paper 218, p. 133-159

Davis, G.A., Anderson, J.L., Marin, D.L., Krummenacher, D., Frost, E. G., and Armstrong R.L., 1982, Geologic and geochronologic relations in the lower plate of the Whipple detachment fault, Whipple Mountains, southeastern California: a progress report: Mesozoic-Cenozoic tectonic evolution of the Colorado River region, California, Arizona, and Nevada, April 1982, p. 409-412.

Davis, G. A., Anderson, J. L., Frost, E. G., and Shackelford, T. J., 1980, Mylonitization and detachment faulting in the Whipple-Buckskin-Rawhide Mountains terrane, southeastern California and western Arizona, in Crittenden, M. D., Coney, P. J., and Davis, G. H., eds., Cordilleran metamorphic core complexes: Geological Society of America Memoir v. 153, p. 79–129.

DeWitt, E.; Sutter, J.F.; Davis, G.A.; Anderson, J.L., 1986, 40Ar/ 39Ar age-spectrum dating of Miocene mylonitic rocks, Whipple Mountains, southeastern California: Abstracts with Programs, Geological Society of America v.18.6, p. 584.

Dickinson, W.R., Gehrels, G.E., 2003. U–Pb ages of detrital zircons from Permian and Jurassic eolian sandstones of the Colorado Plateau, USA; paleogeographic implications. Sedimentary Geology v. 163 (1–2), p. 29–66.

Howard, K.A, Nielson, J.E., Wilshire, H.G, Nakata, J.K., Goodge, J.W., Reneau, S.L., John, B.E., and Hansen, V.L., 1999, Geologic map of the Mohave Mountains area, Mohave County, western Arizona. US Geological Survey, Miscellaneous Investigations Series, Map I-2308.

Howard, K. A., and John, B. E., 1987, Crustal extension along a rooted system of imbricate low-angle faults; Colorado River extensional corridor, California and Arizona. Geological Society Special Publications v. 28, p. 299-311.

Howard, K.A., Goodge, J.W., and John, B.E., 1982a, Detached crystalline rocks of the Mohave, Buck, and Bill Williams Mountains, western Arizona, in Frost, E.G., and Martin, D.L., eds., Mesozoic-Cenozoic Tectonic Evolution of the Colorado River Region, California, Arizona, and Nevada: San Diego, Calif., Cordilleran Publishers p. 377–390.

Jackson, J. A., and White, N. J., 1989, Normal faulting in the upper continental crust: Journal of Structural Geology v. 11, p. 15-36.

Jackson, J. A., 1987, Active normal faulting and crustal extension, in Coward, M. P., Dewey, J. F., and Hancock, P. L., eds., Continental extensional tectonics: Geological Society of London Special Publication v. 28, p. 3-17.

Jackson, J. A., and McKenzie, D., 1983, The geometrical evolution of normal fault systems: Journal of Structural Geology v. 5, p. 471-482.

Jackson, S.E., Pearson, N.J., Griffen, W.L., and Belousova, E.A., 2004. The application of laser ablation inductively coupled plasma mass spectrometry to in situ U-Pb zircon geochronology. Chemical Geology v. 211, p. 47–69.

Johnson, D.M., Hooper, P.R., and Conrey, R.M., 1999, XRF analysis of rocks and minerals for Major and Trace elements on a single low dilution Li-tetraborate fused bead. JCPDS-International Centre for Diffraction Data.

Leeman, W.P. and Harry, D.L., 1993. A binary source model for extension-related magmatism in the Great Basin, Western North America. Science v. 262, p. 1550-1554.

Ludwig, K.R., 2012, Isoplot/Ex, v.3.75. Berkeley Geochronology Center Special Publication, no. 5.

Nakata, J.K., 1982, Preliminary report on diking events in the Mohave Mountains, Arizona in Frost, E.G. and Martin, D.L., eds., Mesozoic–Cenozoic Tectonic Evolution of the Colorado River Region, California, Arizona, and Nevada: San Diego, Calif., Cordilleran Publishers p. 85–90.

Nielson, J. E., and Beratan, K. K., 1990, Tertiary basin development and tectonic implications, Whipple detachment system, Colorado River extensional corridor, California and Arizona. Journal of Geophysical Research v. 95, p. 599-614.

Paton, C., Hellstom, J., Paul, B., Woodhead, J., and Hergt, J., 2011, Iolite: Freeware for the visualization and processing of mass spectrometric data. Journal of Analytical Atomic Spectrometry v. 26, p. 2508-2518.

Pearce, J.A., Parkinson, I.J, 1993, Trace element models for mantle melting: application to volcanic arc petrogenesis. Geological Society, London Special Publications v. 76, p. 373-403.

Reynolds, S. J., and Spencer, J. E., 1985, Evidence for large-scale transport on the Bullard detachment fault, west-central Arizona. Geology 13(5), p. 353-356.

Rubin, A.M., 1995, Propagation of Magma-Filled Cracks: Annual Review of Earth and Planetary Sciences, v. 23, p. 287-336.

Slama, J., Kosler, J., Condon, D.J., Crowley, J.L., Gerdes, A., Hanchar, J.M., Horstwood, M.S.A. Morris, G.A., Nasdala, L., Norberg, N., Schaltegger, U., Schoene, B., Tubrett, M.N., and Whitehouse, M.J., 2008, Plešovice zircon- A new natural reference material for U-Pb and Hf isotopic microanalysis. Chemical Geology v. 249, p. 1-35.

Spencer, J.E.; Richard, S.M.; Reynolds, S.J.; Miller, R.J.; Shafiqullah, M.; Gilbert, W.G.; and Grubensky, M.J, 1995, Spatial and temporal relationships between mid-Tertiary magmatism and extension in southwestern Arizona. Journal of Geophysical Research v. 100, p. 10321-10351.

Stacey, J.S., and Kramers, J.D., 1975, Approximation of terrestrial lead isotope evolution by a two-stage model: Earth and Planetary Science Letters, v. 26, p. 207-221.

Wernicke, B. P., Christiansen, R. L., England, P. C., and Sonder, L. J., 1987, Tectonomagmatic evolution of Cenozoic extension in the North American cordillera. Geological Society Special Publications, v. 28, p. 203-221

Wiedenbeck, M., Allé, P., Corfu, F., Griffin, W.L., Meier, M., Oberli, F., von Quadt, A., Roddick, J.C. and Spiegel, W., 1995, Three natural zircon standards for U-Th-Pb, Lu-Hf, trace element and REE analyses. Geostandards Newsletter, v. 19, p. 1-23.

Appendix A: Whole-Rock Geochemistry

	CW-11	CW-12	CW-13	CW-14	CW-15	CW-16	CW-17	CW-18
SiO2	74.54	74.01	76.93	77.81	70.29	69.07	60.82	54.59
TiO2	0.24	0.23	0.14	0.13	0.43	0.42	0.91	1.35
Al2O3	13.66	14.17	12.57	12.34	15.06	15.54	15.75	14.91
Fe2O3	1.43	1.26	0.65	0.55	2.60	2.78	6.40	8.05
MnO	0.01	0.02	0.00	0.01	0.03	0.05	0.07	0.10
MgO	0.49	0.46	0.19	0.16	0.96	1.11	4.23	7.96
CaO	0.92	1.38	0.69	0.71	2.17	2.14	5.36	8.06
Na2O	3.97	3.89	2.66	2.84	3.82	3.52	4.12	3.40
K2O	4.53	4.32	5.91	5.27	4.24	4.94	1.87	0.87
P2O5	0.04	0.07	0.02	0.01	0.12	0.14	0.21	0.40
Rb	76.43	113.61	131.06	132.48	80.13	114.94	32.58	15.73
Sc	2.50	2.56	6.30	0.00	3.50	4.19	9.68	11.09
V	50.50	59.50	45.00	14.00	163.00	72.30	346.00	1027.00
Ni	6.90	7.10	35.00	14.00	47.40	18.10	387.00	22000.00
Ga	16.09	21.30	14.22	13.15	17.24	19.67	19.35	18.87
Cu	11.06	10.14	8.13	11.12	11.16	37.28	28.51	13.63
Zn	9.05	24.35	0.00	4.05	48.69	42.46	40.73	47.18
Cr	12.90	5.10	5.00	13.00	7.90	28.60	84.76	212.50
Sr	119.67	248.52	197.10	169.90	435.14	278.55	507.07	715.07
Y	16.09	7.10	17.27	15.17	17.24	16.57	20.36	24.12
Zr	174.98	106.51	96.52	87.98	209.96	182.25	171.06	217.04
Nb	26.15	15.22	18.29	22.25	25.36	22.78	21.38	25.16
Cs	0.27	0.74	1.40	0.08	1.28	0.43	0.22	0.25
Ba	727.00	897.00	600.00	230.00	1071.00	1368.00	805.00	391.70
La	39.50	14.73	29.00	9.00	35.60	40.70	30.53	44.65
Ce	65.70	27.90	44.00	13.00	65.20	71.20	57.14	97.86
Pr	6.12	3.01	3.50	0.90	6.55	7.77	6.89	12.12
Nd	20.10	10.30	8.20	3.00	22.60	27.90	26.26	47.16
Sm	2.63	1.68	1.80	3.20	3.09	4.24	5.30	7.56
Eu	0.58	0.44	0.92	0.92	0.86	1.01	1.41	1.98
Gd	2.86	1.88	6.40	13.50	3.75	3.96	4.38	5.86
Tb	0.35	0.25	0.51	0.20	0.44	0.48	0.58	0.71
Dy	2.25	0.92	3.20	2.80	2.38	2.29	3.52	4.13
Ho	0.47	0.22	1.40	0.60	0.43	0.50	0.68	0.76
Er	0.95	0.49	2.50	0.80	1.37	1.22	1.76	2.17
Tm	0.26	0.12	0.43	0.24	0.25	0.19	0.27	0.29
Yb	1.23	0.54	1.40	1.90	1.36	1.33	1.92	1.81
Lu	0.19	0.10	0.86	0.88	0.23	0.19	0.28	0.28
Hf	3.86	3.44	2.80	3.80	5.00	4.80	4.31	5.21
Ta	10.23	11.91	29.00	4.40	13.81	14.07	12.41	8.26
Pb	7.77	13.83	20.00	0.60	18.20	11.64	4.44	1.40
Th	11.91	6.13	12.70	5.70	10.33	9.63	6.50	6.12
U	2.02	2.86	3.10	0.54	1.99	1.41	1.28	0.79

Appendix B: U-Pb Zircon Data (LA-ICP-MS)

					MEASURED ISOTOPIC RATIOS						APPARENT AGE	
Spot	Pb (ppm)	Th (ppm)	U (ppm)	U/Th	$^{207}Pb/^{206}Pb$	2σ %	$^{206}Pb/^{238}U$	2σ %	$^{206}Pb/^{238}U$ Age	2σ abs	$^{207}Pb/^{206}Pb$ Corrected Age	2σ abs
CW-01 zircon (spot size = 24 μm, shot frequency = 4 Hz, shot count = 100, laser energy = 3 mJ at 75%)												
spot 1	2.33	272	335	1.27	0.0485	0.0015	0.002975	0.000049	19.15	0.32	19.10	0.32
spot 2	6.2	726	435.2	0.5965	0.0485	0.0014	0.003027	0.000043	19.48	0.28	19.43	0.28
spot 3	2.19	274	169	0.658	0.0457	0.0025	0.003024	0.00004	19.46	0.26	19.48	0.27
spot 4	6.99	816	482	0.564	0.0487	0.0013	0.003036	0.000044	19.54	0.28	19.49	0.29
spot 5	11.02	1370	659	0.4886	0.0464	0.001	0.003034	0.000022	19.53	0.14	19.53	0.15
spot 6	2.918	343.7	304.5	0.8866	0.0463	0.0014	0.003049	0.000029	19.62	0.19	19.63	0.19
spot 7	3.77	442	296.2	0.682	0.0485	0.0018	0.00306	0.000042	19.69	0.27	19.64	0.27
spot 8	9.58	1145	591	0.5106	0.0468	0.001	0.003056	0.000023	19.67	0.15	19.66	0.15
spot 9	22.6	2650	925	0.3449	0.04838	0.00086	0.003063	0.000043	19.71	0.28	19.67	0.28
spot 10	1.78	208	208	1.011	0.0474	0.0017	0.003062	0.000045	19.71	0.29	19.68	0.29
spot 11	3.67	447	263.7	0.5901	0.0471	0.0018	0.003061	0.000045	19.7	0.29	19.69	0.29
spot 12	2.26	253	165.4	0.671	0.0558	0.003	0.003099	0.000048	19.95	0.31	19.71	0.32
spot 13	2.971	342.4	282.5	0.8384	0.0516	0.0018	0.003092	0.000029	19.9	0.19	19.77	0.19
spot 14	4.775	524.4	247.1	0.46	0.0694	0.0027	0.003167	0.000044	20.38	0.28	19.79	0.29
spot 15	29.17	3410	1127	0.3212	0.04921	0.00078	0.003089	0.000036	19.88	0.23	19.81	0.23
spot 16	12.5	1480	554	0.405	0.0524	0.002	0.003104	0.000056	19.98	0.36	19.83	0.36
spot 17	6.6	781	431.1	0.55	0.0459	0.0011	0.003081	0.000026	19.83	0.17	19.84	0.17
spot 18	1.15	129	99.9	0.822	0.0479	0.0033	0.003091	0.000048	19.9	0.31	19.86	0.32
spot 19	4.993	572.5	342.7	0.596	0.0464	0.0013	0.003088	0.000033	19.87	0.21	19.88	0.22
spot 20	10.9	1320	457	0.554	0.0472	0.0013	0.003092	0.000031	19.9	0.2	19.88	0.20
spot 21	25.36	3017	1048	0.349	0.04797	0.0008	0.003097	0.000043	19.93	0.28	19.89	0.28
spot 22	3.26	382	271.6	0.734	0.0478	0.0017	0.003098	0.00003	19.94	0.19	19.91	0.20
spot 23	3.06	356	255	0.7273	0.0482	0.0016	0.003108	0.000036	20.01	0.23	19.96	0.24
spot 24	1.205	135.9	146.5	1.087	0.0481	0.0026	0.003111	0.000048	20.02	0.31	19.98	0.32
spot 25	5.78	698	431	0.6171	0.0459	0.001	0.003103	0.000026	19.97	0.17	19.99	0.17
spot 26	2.48	292	178.4	0.6167	0.0475	0.0021	0.003115	0.000039	20.05	0.25	20.02	0.26
spot 27	1.356	158.3	172.8	1.106	0.0457	0.002	0.003112	0.000065	20.03	0.42	20.05	0.42
spot 28	4.73	541	321	0.5903	0.0489	0.0014	0.003147	0.000032	20.26	0.21	20.19	0.21

Spot	Pb (ppm)	Th (ppm)	U (ppm)	U/Th	MEASURED ISOTOPIC RATIOS $^{207}Pb/^{206}Pb$	2σ %	$^{206}Pb/^{238}U$	2σ %	APPARENT AGE $^{206}Pb/^{238}U$ Age	2σ abs	$^{207}Pb/^{206}Pb$ Corrected Age	2σ abs
CW-01 zircon (Cont.)												
spot 29	2.41	299	180	0.781	0.0444	0.0023	0.003133	0.00004	20.17	0.26	20.22	0.27
spot 30	1.576	184.6	208.8	1.173	0.0454	0.0019	0.003137	0.000038	20.19	0.24	20.22	0.25
spot 31	3.79	427	269	0.6265	0.0494	0.0014	0.003155	0.000035	20.31	0.22	20.23	0.23
spot 32	10.66	762	382	0.5047	0.1679	0.0074	0.003717	0.000047	23.92	0.3	20.25	0.36
spot 33	2.749	308.7	206.2	0.6712	0.0467	0.0015	0.003171	0.000027	20.41	0.17	20.40	0.18
spot 34	2.966	292.6	210.9	0.707	0.0575	0.0019	0.003275	0.00005	21.08	0.32	20.78	0.32
spot 35	154.5	215.7	472	2.3	0.10404	0.00031	0.2825	0.0035	1603	18	1592.98	20.24
CW-02 zircon (spot size = 24 μm, shot frequency = 4 Hz, shot count = 100, laser energy = 4 mJ at 75%)												
spot 1	19.99	2188	650	0.2962	0.0607	0.0024	0.003092	0.000024	19.9	0.15	19.54	0.16
spot 2	6.66	780.5	350.6	0.4485	0.048	0.0023	0.003131	0.000036	20.15	0.23	20.11	0.24
spot 3	48.12	5530	1387	0.2515	0.0506	0.0018	0.003142	0.00004	20.22	0.25	20.12	0.26
spot 4	13.06	1565	506	0.3255	0.0505	0.0013	0.003157	0.000038	20.32	0.25	20.21	0.25
spot 5	5.3	619	704	1.148	0.0491	0.0016	0.003156	0.00003	20.31	0.19	20.24	0.20
spot 6	3.195	367.1	296.6	0.8024	0.0461	0.0023	0.003209	0.000039	20.65	0.25	20.66	0.26
spot 7	2.099	259.7	158.2	0.625	0.0542	0.0024	0.002972	0.000047	19.13	0.3	18.94	0.31
spot 8	20.73	2770	1062	0.394	0.0467	0.00074	0.00295	0.000036	18.99	0.23	18.98	0.23
spot 9	2.514	318.7	251.1	0.8147	0.0475	0.0019	0.002969	0.00004	19.11	0.26	19.08	0.26
spot 10	16.29	2116	783.9	0.3829	0.0492	0.001	0.003014	0.000032	19.4	0.21	19.33	0.21
spot 11	4.78	397	232.3	0.6072	0.1293	0.0032	0.003359	0.000053	21.62	0.34	19.35	0.33
spot 12	4.318	540	194.1	0.3719	0.0464	0.0024	0.003044	0.000045	19.6	0.29	19.59	0.30
spot 13	3.607	446.6	325.2	0.7487	0.0462	0.0013	0.003048	0.000037	19.62	0.24	19.62	0.24
spot 14	11.16	1322	667	0.5145	0.04608	0.00081	0.003068	0.000041	19.75	0.27	19.76	0.27
spot 15	1.998	166.8	135.4	0.8259	0.1025	0.0051	0.003313	0.000059	21.32	0.38	19.81	0.38
spot 16	2.763	324.5	272.8	0.8612	0.0497	0.0018	0.003099	0.00004	19.94	0.26	19.86	0.26
spot 17	14.14	1789	794	0.4542	0.04647	0.00082	0.003106	0.000031	19.99	0.2	19.99	0.20
spot 18	1.665	203.9	143.5	0.7165	0.0484	0.003	0.003117	0.000049	20.06	0.32	20.01	0.32
spot 19	6.86	166.3	150.6	0.9039	0.0486	0.001	0.01593	0.00018	101.9	1.1	101.81	1.16
spot 20	7.01	159	170.9	1.127	0.04847	0.00087	0.01626	0.00023	104	1.5	103.93	1.48
spot 21	13.25	28.76	49.57	1.78	0.3154	0.0031	0.03326	0.00051	210.9	3.2	140.36	3.11

					MEASURED ISOTOPIC RATIOS						**APPARENT AGE**	
Spot	**Pb (ppm)**	**Th (ppm)**	**U (ppm)**	**U/Th**	**$^{207}Pb/^{206}Pb$**	**2σ %**	**$^{206}Pb/^{238}U$**	**2σ %**	**$^{206}Pb/^{238}U$ Age**	**2σ abs**	**$^{207}Pb/^{206}Pb$ Corrected Age**	**2σ abs**
CW-04 zircon (spot size = 24 μm, shot frequency = 4 Hz, shot count = 100, laser energy = 4 mJ at 75%)												
spot 17	5.801	776	267.3	0.3594	0.0551	0.0021	0.00286	0.00004	18.41	0.26	18.21	0.26
spot 18	5.32	721	683	1.013	0.0455	0.001	0.002847	0.000047	18.32	0.3	18.35	0.30
spot 19	6.59	862	462.4	0.5577	0.0501	0.0014	0.002873	0.000037	18.49	0.24	18.41	0.24
spot 20	3.91	493	326	0.6979	0.0532	0.0017	0.002902	0.000046	18.68	0.3	18.52	0.30
spot 21	1.071	133.1	137.3	1.008	0.0508	0.0032	0.002919	0.000052	18.79	0.33	18.69	0.34
spot 22	3.93	457	156	0.3561	0.081	0.0038	0.003041	0.000054	19.57	0.35	18.72	0.35
spot 23	16.67	1959	682.6	0.3401	0.0509	0.0012	0.002926	0.00004	18.84	0.26	18.73	0.26
spot 24	9.53	1239	464.4	0.399	0.0464	0.0011	0.002911	0.000038	18.74	0.25	18.74	0.25
spot 25	4.33	504.4	229.2	0.4577	0.0628	0.0029	0.002978	0.000043	19.17	0.28	18.77	0.28
spot 1	4.35	447.7	222.3	0.491	0.0854	0.0042	0.003073	0.000042	19.78	0.27	18.81	0.28
spot 2	9.12	1081	397	0.3665	0.0569	0.0018	0.002963	0.00005	19.07	0.32	18.82	0.32
spot 3	19.99	2188	650	0.2962	0.0838	0.0043	0.003069	0.000032	19.76	0.21	18.82	0.22
spot 4	6.66	780.5	350.6	0.4485	0.0508	0.0015	0.002941	0.000031	18.93	0.2	18.83	0.20
spot 5	48.12	5530	1387	0.2515	0.0656	0.0039	0.002998	0.000027	19.3	0.17	18.83	0.19
spot 6	39.78	5015	1497	0.3006	0.04656	0.0007	0.00293	0.000043	18.86	0.27	18.86	0.28
spot 7	6	768	315.5	0.428	0.0611	0.0026	0.002988	0.000044	19.23	0.28	18.88	0.29
spot 8	13.06	1565	506	0.3255	0.0482	0.0011	0.002958	0.000029	19.04	0.19	19.00	0.19
spot 9	5.33	554.5	320.8	0.566	0.0746	0.0027	0.003066	0.00005	19.74	0.32	19.03	0.32
spot 10	2.524	329.3	191	0.6117	0.0537	0.0024	0.002991	0.000049	19.25	0.31	19.08	0.32
spot 11	7.91	913	239.2	0.2652	0.0986	0.006	0.003181	0.000052	20.47	0.33	19.12	0.35
spot 12	5.3	619	704	1.148	0.0464	0.001	0.002977	0.000027	19.16	0.17	19.16	0.18
spot 13	3.195	367.1	296.6	0.8024	0.0465	0.0017	0.002981	0.00003	19.19	0.19	19.19	0.20
spot 14	4.2	411	222.2	0.5638	0.0978	0.0037	0.003189	0.000046	20.52	0.3	19.19	0.30
spot 15	8.65	1021.9	339.8	0.3329	0.0495	0.0016	0.002995	0.000032	19.28	0.21	19.20	0.21
spot 16	3.301	375.1	153.1	0.4087	0.0544	0.0025	0.003017	0.000042	19.42	0.27	19.22	0.27
spot 17	138.8	17700	2259	0.1336	0.04713	0.00056	0.003002	0.000036	19.32	0.23	19.31	0.23
spot 18	23.83	2746	843	0.3234	0.089	0.011	0.003176	0.000078	20.44	0.5	19.34	0.56
spot 19	4.76	524.2	230.1	0.4422	0.0584	0.0021	0.003069	0.000037	19.75	0.24	19.45	0.24
spot 20	5.42	593	303	0.54	0.0485	0.0018	0.003043	0.000049	19.58	0.32	19.54	0.32
spot 21	29.34	3294	944	0.286	0.04759	0.00092	0.003044	0.000027	19.59	0.18	19.56	0.18
spot 22	3.798	420	258.7	0.6306	0.0586	0.0021	0.003088	0.000047	19.88	0.3	19.57	0.30
spot 23	16	1702	388	0.228	0.0652	0.0027	0.00313	0.000041	20.14	0.26	19.67	0.27
spot 24	1.725	165.6	141.8	0.8332	0.0554	0.0026	0.003096	0.000054	19.92	0.35	19.70	0.35

					MEASURED ISOTOPIC RATIOS						APPARENT AGE	
Spot	**Pb (ppm)**	**Th (ppm)**	**U (ppm)**	**U/Th**	**$^{207}Pb/^{206}Pb$**	**2σ %**	**$^{206}Pb/^{238}U$**	**2σ %**	**$^{206}Pb/^{238}U$ Age**	**2σ abs**	**$^{207}Pb/^{206}Pb$ Corrected Age**	**2σ abs**
CW-04 zircon (Cont.)												
spot 25	5.19	513	252.9	0.4967	0.0683	0.002	0.003154	0.000034	20.3	0.22	19.74	0.22
spot 26	5.39	612	156	0.2627	0.0544	0.0029	0.0031	0.000037	19.95	0.24	19.75	0.25
spot 27	16.85	1961	437.1	0.2186	0.0485	0.0013	0.003114	0.000042	20.04	0.27	19.99	0.27
spot 28	7.38	787	338	0.4276	0.0472	0.0017	0.003135	0.000027	20.18	0.17	20.16	0.18
spot 29	3.83	394	167.1	0.4239	0.0509	0.0022	0.003158	0.000038	20.33	0.25	20.21	0.25
spot 30	7.3	144.9	154.7	1.113	0.04965	0.00082	0.01907	0.00033	121.8	2.1	121.59	2.10
spot 31	6.84	122.8	152.6	1.348	0.05059	0.00098	0.02098	0.00055	133.8	3.5	133.53	3.49
spot 32	40.7	552	826	1.455	0.04958	0.00029	0.02563	0.0003	163.1	1.9	163.09	1.91
spot 33	15.5	29.14	78.9	2.71	0.07788	0.00036	0.1976	0.0017	1162.2	9	1163.50	9.78
spot 34	158.3	235.9	560	2.477	0.10418	0.00022	0.2163	0.0048	1262	25	1227.41	26.76
CW-05 zircon (spot size = 24 µm, shot frequency = 4 Hz, shot count = 100, laser energy = 4 mJ at 75%)												
spot 1	2.533	256.1	167.2	0.6259	0.0488	0.0028	0.002993	0.000078	19.27	0.5	19.21	0.51
spot 2	1.871	199.6	134	0.6518	0.0495	0.0028	0.00292	0.000052	18.79	0.33	18.72	0.34
spot 3	2.063	202.9	133.3	0.6419	0.0487	0.0023	0.002991	0.000047	19.26	0.3	19.20	0.31
spot 4	5.29	89	83.7	0.99	0.04797	0.00085	0.01685	0.00052	107.7	3.3	107.74	3.31
spot 5	88.7	9560	2211	0.231	0.04675	0.00049	0.002953	0.000046	19.01	0.29	19.00	0.30
spot 6	11.54	158.3	589	3.662	0.04964	0.00055	0.02284	0.00057	145.5	3.6	145.45	3.61
spot 7	28.06	379	729.3	1.926	0.04948	0.00042	0.02462	0.00036	156.8	2.2	156.73	2.28
spot 8	16.48	121.7	352.2	2.857	0.05376	0.00037	0.04523	0.00061	285.1	3.7	284.54	3.81
spot 9	17.34	214.6	182.6	0.8412	0.05054	0.00068	0.02575	0.00044	163.9	2.8	163.65	2.78
spot 10	5.05	534.2	243.2	0.4529	0.0493	0.0017	0.003012	0.000042	19.39	0.27	19.32	0.27
spot 11	24.92	330.2	262.7	0.7888	0.04982	0.0005	0.02468	0.00035	157.2	2.2	157.04	2.22
spot 12	6.21	141.2	2440	17.49	0.04882	0.00029	0.01423	0.00031	91.1	2	90.97	1.98
spot 13	10.06	205.8	471.9	2.318	0.04817	0.00036	0.01571	0.00023	100.5	1.5	100.47	1.47
spot 14	17.1	23.2	102.8	4.6	0.09834	0.00056	0.2477	0.006	1425	31	1411.16	33.55
spot 15	90	123	211.5	2.9	0.10356	0.00033	0.2557	0.0046	1467	23	1445.58	25.72
spot 16	1.37	22.3	285.7	13.8	0.04946	0.00082	0.01687	0.00063	107.9	4	107.67	4.00
spot 17	7.2	118	1900	21	0.04837	0.00027	0.01705	0.00041	109	2.6	108.96	2.61
spot 18	32.65	3556	1265	0.3638	0.04667	0.00068	0.00303	0.000051	19.51	0.33	19.50	0.33
spot 19	5.44	66	189	2.918	0.05136	0.00082	0.02529	0.00089	161	5.6	160.58	5.61
spot 20	8.08	117.3	234.8	2.03	0.05019	0.00053	0.02395	0.00042	152.6	2.6	152.36	2.66

					MEASURED ISOTOPIC RATIOS						APPARENT AGE	
Spot	Pb (ppm)	Th (ppm)	U (ppm)	U/Th	$^{207}Pb/^{206}Pb$	2σ %	$^{206}Pb/^{238}U$	2σ %	$^{206}Pb/^{238}U$ Age	2σ abs	$^{207}Pb/^{206}Pb$ Corrected Age	2σ abs
CW-05 zircon (cont.)												
spot 21	8.65	113.7	321.7	2.891	0.0494	0.0006	0.02582	0.00083	164.3	5.2	164.32	5.24
spot 22	15.81	209.2	196.1	0.958	0.04918	0.0006	0.02559	0.00034	162.9	2.1	162.92	2.16
spot 23	7.51	98	118.2	1.221	0.049	0.0011	0.02518	0.00057	160.3	3.6	160.36	3.61
spot 24	0.625	67.5	76.3	1.155	0.0448	0.0042	0.003204	0.000092	20.62	0.59	20.66	0.60
spot 25	1.98	169.9	112.1	0.667	0.091	0.014	0.003336	0.00009	21.47	0.58	20.26	0.67
spot 26	129.7	1679	995	0.603	0.04963	0.00032	0.02652	0.0005	168.7	3.1	168.69	3.16
spot 27	21.3	283.3	174.1	0.6279	0.04857	0.00061	0.02517	0.00039	160.2	2.5	160.39	2.48
spot 28	154	183.7	207.1	1.143	0.10515	0.00022	0.3047	0.0044	1714	22	1714.26	25.12
spot 29	113.6	187.5	196.3	1.07	0.10352	0.00042	0.2384	0.0043	1380	22	1350.23	24.00
spot 30	0.676	56.8	74	1.321	0.0455	0.0033	0.003779	0.000069	24.32	0.44	24.35	0.46
spot 31	13.12	379.1	822.7	2.164	0.04748	0.00039	0.01157	0.00014	74.16	0.88	74.16	0.90
spot 32	27.65	758.7	855	1.1261	0.04762	0.00034	0.01264	0.00022	81	1.4	80.97	1.41
spot 33	22	557	684	1.297	0.05587	0.00082	0.01281	0.00025	82.1	1.6	81.20	1.58
spot 34	10.28	223	505.5	2.261	0.04873	0.00052	0.01556	0.0002	99.5	1.3	99.44	1.28
spot 35	76.6	1061	1034	0.98	0.04964	0.00023	0.02463	0.00036	156.9	2.2	156.76	2.28
spot 36	24.9	312.4	222.8	0.7131	0.05097	0.00059	0.02699	0.00038	171.7	2.4	171.36	2.41
spot 37	59.15	407.9	1010	2.507	0.05395	0.0002	0.04768	0.00071	300.3	4.3	299.65	4.42
spot 38	16.44	103.2	389.7	3.8	0.05301	0.00032	0.05117	0.00057	321.7	3.5	321.63	3.56
spot 39	99.6	331	536	1.648	0.06661	0.00055	0.0892	0.002	551	12	545.24	11.98
spot 40	17.76	63.71	69.67	1.109	0.0602	0.00061	0.0991	0.0014	609.2	7.9	609.10	8.45
spot 41	37.82	56.9	1152	20.2	0.10281	0.00024	0.2346	0.0031	1360	16	1330.54	17.48
spot 42	100.3	152.5	135.9	0.8953	0.08917	0.00026	0.2378	0.0045	1375	23	1372.57	25.50
spot 43	56.9	85.9	159.7	1.849	0.08845	0.00027	0.2378	0.0033	1377	17	1373.85	18.84
spot 44	71.86	108.3	111.7	1.0383	0.08944	0.00032	0.2404	0.0029	1389	15	1386.70	16.63
spot 45	4.903	6.93	21.84	3.27	0.08871	0.00065	0.2413	0.0047	1393	24	1393.08	26.67
spot 46	201.5	276.5	760	2.781	0.09572	0.00026	0.2457	0.0029	1416	15	1404.89	16.56
spot 47	70.8	98.9	1077	11.09	0.10347	0.00019	0.2575	0.003	1476	16	1455.70	17.06
spot 48	96.3	130.9	590	4.527	0.10395	0.00025	0.2666	0.0039	1523	20	1505.05	21.98
spot 49	73.3	82.6	1152	14.37	0.1095	0.00069	0.272	0.011	1548	57	1523.53	60.61
spot 50	122.7	167.2	564	3.77	0.10408	0.00085	0.2712	0.0042	1546	21	1530.24	23.70
spot 51	135.1	164.8	446.1	2.712	0.10636	0.0003	0.282	0.0043	1601	22	1585.25	24.24
spot 52	77.9	95.8	438	4.56	0.10763	0.00021	0.2891	0.0042	1636	21	1621.81	23.74
spot 53	60.17	74.67	156.9	2.115	0.10443	0.00025	0.2891	0.0031	1637	15	1628.83	17.86

					MEASURED ISOTOPIC RATIOS				APPARENT AGE			
Spot	Pb (ppm)	Th (ppm)	U (ppm)	U/Th	$^{207}Pb/^{206}Pb$	2σ %	$^{206}Pb/^{238}U$	2σ %	$^{206}Pb/^{238}U$ Age	2σ abs	$^{207}Pb/^{206}Pb$ Corrected Age	2σ abs
CW-05 zircon (cont.)												
spot 54	365	447	305	0.704	0.10495	0.00019	0.2902	0.0043	1645	21	1633.81	24.37
spot 55	36.65	46.59	109.6	2.363	0.10333	0.00028	0.2896	0.0042	1639	21	1634.04	23.86
spot 56	234.9	246.2	435	1.772	0.10464	0.00017	0.2912	0.0037	1647	19	1640.06	21.12
spot 57	71.5	85.5	150.8	1.78	0.10586	0.00032	0.2953	0.0042	1667	21	1660.16	23.87
spot 58	67.1	82.6	140.9	1.681	0.10055	0.00036	0.2959	0.0044	1670	22	1675.48	25.13
spot 59	44.58	56.8	84.2	1.49	0.10312	0.00036	0.3012	0.0048	1696	24	1699.35	27.33
spot 60	93.4	115.2	172.6	1.519	0.10523	0.00043	0.3032	0.0037	1709	19	1705.68	21.28
spot 61	150.9	186.8	395.1	2.125	0.10581	0.00019	0.3042	0.0042	1712	21	1709.92	23.99
spot 62	213.1	181.2	156.3	0.8672	0.16866	0.00062	0.4373	0.0052	2338	23	2266.13	32.08
CW-06 zircon (spot size = 24 µm, shot frequency = 4 Hz, shot count = 100, laser energy = 4 mJ at 75%)												
spot 1	7.97	929	398	0.4216	0.0475	0.0023	0.0022	0.00077	14.2	4.9	14.15	4.95
spot 2	2.347	208	191.2	0.929	0.0768	0.0062	0.00275	0.00041	17.7	2.6	17.02	2.54
spot 3	7.91	944	696	0.743	0.0486	0.0012	0.002904	0.000026	18.69	0.17	18.64	0.17
spot 4	10.78	1286	379.7	0.2946	0.0494	0.0016	0.002912	0.000042	18.75	0.27	18.67	0.27
spot 5	16.07	1937	623	0.3202	0.0475	0.001	0.002918	0.000022	18.79	0.14	18.76	0.15
spot 6	17.75	2144	657.1	0.2977	0.047	0.0011	0.002932	0.000022	18.87	0.14	18.86	0.15
spot 7	13.73	1620	747	0.4591	0.04754	0.00087	0.002956	0.000029	19.03	0.19	19.00	0.19
spot 8	7.9	911	530	0.566	0.0467	0.0011	0.002966	0.000027	19.09	0.17	19.08	0.18
spot 9	2.23	95.8	814	10.2	0.0689	0.0023	0.003053	0.000048	19.65	0.31	19.09	0.31
spot 10	4.08	486	212.9	0.4387	0.0476	0.0022	0.002972	0.000039	19.13	0.25	19.10	0.26
spot 11	10.92	1263	470	0.3684	0.0478	0.0014	0.002974	0.000034	19.14	0.22	19.11	0.22
spot 12	1.125	115	168.5	1.54	0.0475	0.0026	0.003011	0.000058	19.38	0.37	19.35	0.38
spot 13	2.202	239	190.9	0.807	0.0513	0.003	0.003097	0.000045	19.94	0.29	19.81	0.30
spot 14	4.03	103.7	433.5	4.14	0.0552	0.0018	0.0089	0.0014	56.8	8.7	56.54	8.87
spot 15	0.052	2.1	27.3	3.8	0.0554	0.0036	0.01044	0.00027	67	1.7	66.27	1.74
spot 16	1.023	44.1	237.4	5.47	0.04808	0.00077	0.01035	0.00017	66.4	1.1	66.32	1.09
spot 17	2.994	96.9	199.3	1.982	0.0474	0.001	0.010645	0.000086	68.26	0.55	68.26	0.56
spot 18	1.202	34.9	865	24.48	0.04796	0.00041	0.011138	0.000082	71.41	0.52	71.36	0.53
spot 19	0.961	28.06	155.7	5.57	0.048	0.0011	0.01161	0.00016	74.4	1	74.36	1.03
spot 20	3.574	84.1	150	1.783	0.0475	0.001	0.01474	0.00014	94.35	0.92	94.37	0.91
spot 21	6.983	158.9	343.8	2.17	0.04822	0.00067	0.01563	0.00021	99.9	1.3	99.95	1.34

Spot	Pb (ppm)	Th (ppm)	U (ppm)	U/Th	MEASURED ISOTOPIC RATIOS $^{207}Pb/^{206}Pb$	2σ %	$^{206}Pb/^{238}U$	2σ %	$^{206}Pb/^{238}U$ Age	2σ abs	APPARENT AGE $^{207}Pb/^{206}Pb$ Corrected Age	2σ abs
CW-06 zircon (Cont.)												
spot 22	10.8	210	189	0.938	0.0511	0.0019	0.01648	0.00028	105.4	1.8	104.98	1.80
spot 23	15.12	212.7	94.8	0.454	0.04958	0.00089	0.02538	0.00036	161.5	2.3	161.51	2.29
spot 24	7.749	104.3	248.5	2.374	0.04991	0.00059	0.02636	0.00021	167.7	1.3	167.62	1.35
spot 25	158.4	322	397.8	1.288	0.08839	0.00027	0.1336	0.0023	808	13	785.65	13.25
spot 26	143.5	272.2	488	1.811	0.08956	0.00041	0.1948	0.0028	1147	15	1130.42	15.97
spot 27	533	856	1323	1.546	0.10514	0.00079	0.2009	0.0027	1180	14	1141.17	15.24
spot 28	34.56	54.45	903.5	16.65	0.09598	0.00029	0.2001	0.0025	1176	13	1150.55	14.23
spot 29	722	1296	738	0.5733	0.09144	0.00022	0.2075	0.0026	1215	14	1198.83	14.84
spot 30	83.45	150	182.3	1.2183	0.09282	0.00032	0.2111	0.0026	1234	14	1216.80	14.84
spot 31	65.8	101.6	276	2.594	0.10301	0.0003	0.2341	0.002	1356	10	1327.43	11.62
spot 32	91.8	205	543	2.75	0.10328	0.00025	0.248	0.0071	1427	37	1403.61	39.37
spot 33	52.2	75	315	4	0.0965	0.0013	0.2649	0.0052	1514	27	1510.54	29.43
CW-07 zircon (spot size = 24 µm, shot frequency = 4 Hz, shot count = 100, laser energy = 3 mJ at 75%)												
spot 1	10.6	1336.3	806.8	0.5973	0.0483	0.0012	0.002958	0.000011	19.039	0.071	18.99	0.08
spot 2	3.713	458	307.7	0.6649	0.0518	0.0025	0.003026	0.000021	19.48	0.13	19.34	0.15
spot 3	3.537	423.3	253.5	0.5898	0.0495	0.0023	0.003035	0.000015	19.54	0.1	19.46	0.11
spot 4	4.32	519	426	0.8064	0.0486	0.0015	0.003037	0.000016	19.55	0.1	19.49	0.11
spot 5	3.118	380	338	0.8749	0.0501	0.002	0.003043	0.000021	19.59	0.13	19.50	0.14
spot 6	25.5	3030	1109	0.359	0.04782	0.00084	0.0030396	0.0000087	19.565	0.056	19.53	0.06
spot 7	16.62	2001	828	0.4087	0.0474	0.00071	0.003044	0.000015	19.595	0.097	19.57	0.10
spot 8	20.46	2465	1030	0.4112	0.04805	0.00091	0.003066	0.000015	19.733	0.098	19.69	0.10
spot 9	4.37	540	433	0.825	0.0483	0.0016	0.003069	0.000051	19.75	0.33	19.71	0.33
spot 10	18.6	2157	775.9	0.3556	0.04796	0.00092	0.00307	0.000016	19.76	0.1	19.72	0.11
spot 11	2.87	347	299	0.872	0.0487	0.002	0.003077	0.000021	19.81	0.13	19.75	0.14
spot 12	16.92	2002	1049	0.514	0.0469	0.00081	0.003073	0.000013	19.779	0.083	19.77	0.09
spot 13	8.126	983	456.2	0.4594	0.0484	0.0014	0.003083	0.000019	19.84	0.12	19.79	0.13
spot 14	7.393	883	559	0.6227	0.0482	0.0015	0.003084	0.00002	19.85	0.13	19.81	0.13
spot 15	5.49	532	334	0.6167	0.0803	0.0022	0.003215	0.000018	20.69	0.12	19.81	0.13
spot 16	14.45	1677	727	0.4277	0.0477	0.0011	0.00309	0.000016	19.89	0.1	19.86	0.11
spot 17	2.932	342.2	195.8	0.5656	0.0509	0.0017	0.003104	0.000034	19.98	0.22	19.87	0.22
spot 18	13.7	1620	837	0.5159	0.04706	0.00081	0.003091	0.000012	19.895	0.08	19.88	0.08

					MEASURED ISOTOPIC RATIOS						APPARENT AGE	
Spot	**Pb (ppm)**	**Th (ppm)**	**U (ppm)**	**U/Th**	**$^{207}Pb/^{206}Pb$**	**2σ %**	**$^{206}Pb/^{238}U$**	**2σ %**	**$^{206}Pb/^{238}U$ Age**	**2σ abs**	**$^{207}Pb/^{206}Pb$ Corrected Age**	**2σ abs**
					CW-07 zircon (Cont.)							
spot 19	9.39	1105	731.8	0.6519	0.0481	0.00084	0.003097	0.000011	19.934	0.074	19.89	0.08
spot 20	18.27	2156	757	0.3471	0.047	0.0012	0.003093	0.000011	19.908	0.07	19.89	0.08
spot 21	10.65	1284.6	550.1	0.4212	0.0479	0.0013	0.0031	0.000013	19.955	0.082	19.92	0.09
spot 22	12.23	1484	777	0.5169	0.04854	0.00088	0.003107	0.000012	19.998	0.074	19.94	0.08
spot 23	2.04	239	168.8	0.715	0.0489	0.003	0.00311	0.000041	20.02	0.27	19.95	0.27
spot 24	4.337	498.5	437.8	0.865	0.0499	0.0015	0.003118	0.000016	20.07	0.11	19.98	0.11
spot 25	12.22	1431	780	0.5375	0.04803	0.00058	0.003112	0.000016	20.03	0.11	19.99	0.10
spot 26	6.41	743	516	0.686	0.0486	0.001	0.003115	0.000017	20.05	0.11	19.99	0.11
spot 27	4.25	509	366.9	0.716	0.0487	0.0015	0.003116	0.000026	20.06	0.17	20.00	0.17
spot 28	11.67	1347	476.4	0.3491	0.0471	0.0014	0.003115	0.000023	20.05	0.14	20.03	0.15
spot 29	15.86	1902	753	0.3895	0.0477	0.001	0.003124	0.000021	20.1	0.14	20.07	0.14
spot 30	5.83	683	416.4	0.599	0.049	0.0017	0.003135	0.000016	20.17	0.11	20.11	0.11
spot 31	28.8	3320	1234	0.3671	0.04743	0.00075	0.003131	0.000013	20.149	0.085	20.13	0.09
spot 32	4.66	520	445	0.8351	0.0472	0.0013	0.003136	0.000016	20.19	0.11	20.16	0.11
spot 33	3.34	392	219	0.547	0.047	0.0021	0.003145	0.000029	20.24	0.19	20.23	0.19
spot 34	8.33	955	535	0.5519	0.0489	0.0013	0.003198	0.00002	20.58	0.13	20.52	0.13
spot 35	1.38	156	117	0.746	0.056	0.0039	0.003232	0.000038	20.8	0.24	20.55	0.26
spot 36	1.778	173	425	2.35	0.0486	0.0015	0.003678	0.000074	23.67	0.47	23.60	0.48
					CW-21 zircon (spot size = 24 μm, shot frequency = 4 Hz, shot count = 100, laser energy = 3 mJ at 75%)							
spot 1	23.06	2780	908	0.3291	0.0543	0.0025	0.003003	0.000019	19.33	0.12	19.14	0.14
spot 2	42.83	4647	1812	0.3863	0.0535	0.0026	0.003107	0.000019	20	0.12	19.82	0.14
spot 3	18.62	2030	1077	0.5231	0.04981	0.00098	0.003106	0.000014	19.994	0.087	19.91	0.09
spot 4	9.62	1084	707	0.645	0.0483	0.0013	0.003115	0.000015	20.047	0.099	20.00	0.10
spot 5	3.596	390.4	317.5	0.807	0.045	0.002	0.003105	0.00002	19.98	0.13	20.02	0.14
spot 6	8.82	970.6	463	0.474	0.0497	0.0015	0.003132	0.000016	20.16	0.1	20.08	0.11
spot 7	9.37	1026	640	0.616	0.04786	0.00094	0.003129	0.000019	20.14	0.13	20.10	0.12
spot 8	3.3	348	234.5	0.663	0.0489	0.0022	0.003139	0.000021	20.21	0.13	20.14	0.15
spot 9	5.11	555	406	0.7258	0.0447	0.0018	0.003123	0.000025	20.1	0.16	20.14	0.17
spot 10	0.85	89	103	1.218	0.0539	0.0057	0.003161	0.000046	20.34	0.3	20.15	0.33
spot 11	10.13	1119	593	0.5289	0.0508	0.0013	0.003152	0.000017	20.29	0.11	20.18	0.11
spot 12	3.27	349.6	244.8	0.699	0.0485	0.0028	0.003143	0.00003	20.23	0.19	20.18	0.21

Spot	Pb (ppm)	Th (ppm)	U (ppm)	U/Th	MEASURED ISOTOPIC RATIOS $^{207}Pb/^{206}Pb$	2σ %	$^{206}Pb/^{238}U$	2σ %	APPARENT AGE $^{206}Pb/^{238}U$ Age	2σ abs	$^{207}Pb/^{206}Pb$ Corrected Age	2σ abs
CW-21 zircon (Cont.)												
spot 13	8.12	871.7	583	0.667	0.0465	0.0012	0.003138	0.00002	20.2	0.13	20.20	0.13
spot 14	6.83	692	576.3	0.834	0.056	0.0023	0.00318	0.00002	20.46	0.13	20.22	0.14
spot 15	94.6	10370	2104	0.201	0.0512	0.0015	0.003161	0.000024	20.34	0.16	20.22	0.16
spot 16	3.997	412.8	370.2	0.897	0.0514	0.002	0.003165	0.000023	20.37	0.15	20.24	0.16
spot 17	13.49	1435	732	0.5065	0.0472	0.001	0.003153	0.000017	20.29	0.11	20.27	0.11
spot 18	3.25	339	315	0.916	0.0476	0.0021	0.003159	0.000025	20.33	0.16	20.30	0.17
spot 19	11.95	1263	595	0.4587	0.0479	0.0014	0.003163	0.00002	20.36	0.13	20.32	0.13
spot 20	4.04	438	447	1.007	0.0474	0.0017	0.003166	0.000025	20.38	0.16	20.35	0.17
spot 21	2.939	303.8	289.7	0.945	0.051	0.0014	0.003183	0.000026	20.48	0.17	20.37	0.17
spot 22	2.78	285	237.4	0.849	0.0477	0.0019	0.003182	0.000035	20.48	0.22	20.45	0.23
spot 23	6.389	598	358	0.5911	0.0766	0.0054	0.003305	0.000029	21.27	0.18	20.46	0.23
spot 24	5.28	571	334	0.5777	0.0499	0.0013	0.003198	0.000027	20.58	0.17	20.49	0.18
spot 25	2.899	298.9	261.9	0.864	0.0487	0.0021	0.003203	0.000034	20.62	0.22	20.56	0.23
spot 26	3.68	375	291	0.791	0.0549	0.0028	0.003234	0.000019	20.81	0.13	20.59	0.14
spot 27	2.99	248	233	0.934	0.0743	0.008	0.003378	0.000052	21.74	0.34	20.97	0.39
WFW-01 zircon (spot size = 24 µm, shot frequency = 4 Hz, shot count = 100, laser energy = 3 mJ at 75%)												
spot 1	-0.742266	800.2	770	0.962	0.7396	0.0018	-5.74E-05	0.00000069	-0.3702	0.0044	-0.05	0.00
spot 2	-0.7418	303.8	1130	3.76	0.7383	0.0013	-4.31E-05	0.0000044	-0.278	0.028	-0.03	0.00
spot 3	0.744	66.57	68.8	1.033	0.0503	0.0066	0.003263	0.000051	21	0.33	20.90	0.37
spot 4	0.724	66.8	73.1	1.08	0.0477	0.0068	0.003317	0.000049	21.35	0.32	21.31	0.36
spot 5	0.357	9.71	8.12	0.834	0.073	0.015	0.0116	0.00042	74.4	2.6	71.96	2.95
spot 6	0.84	22.66	12.91	0.574	0.0596	0.0085	0.01145	0.00027	73.4	1.7	72.27	1.87
spot 7	8.9	22.9	69.5	3.01	0.3192	0.0085	0.01742	0.00015	111.36	0.94	73.23	1.43
spot 8	8.77	7.7	46.4	5.99	0.396	0.02	0.02139	0.00094	136.4	5.9	76.57	4.86
spot 9	8.055	5.89	39.3	6.56	0.413	0.019	0.0225	0.0011	143.3	6.7	77.43	5.17
spot 10	19.68	472	720.2	1.519	0.04834	0.00039	0.01327	0.00022	85	1.4	84.91	1.40
spot 11	23.5	282	488	1.86	0.05023	0.00045	0.02717	0.00037	172.8	2.3	172.66	2.34
spot 12	33.9	357.9	652	1.81	0.0503	0.00036	0.03015	0.00019	191.5	1.2	191.40	1.20
spot 13	162.3	733	630	0.869	0.0579	0.00025	0.07337	0.00032	456.4	1.9	455.40	1.98
spot 14	245.9	314.4	196.7	0.625	0.09976	0.00032	0.2634	0.0011	1507.2	5.4	1495.68	6.46
spot 15	170.8	184.1	413	2.208	0.1072	0.00043	0.2996	0.0011	1689.2	5.4	1681.06	6.67

					MEASURED ISOTOPIC RATIOS						APPARENT AGE	
Spot	**Pb (ppm)**	**Th (ppm)**	**U (ppm)**	**U/Th**	**$^{207}Pb/^{206}Pb$**	**2σ %**	**$^{206}Pb/^{238}U$**	**2σ %**	**$^{206}Pb/^{238}U$ Age**	**2σ abs**	**$^{207}Pb/^{206}Pb$ Corrected Age**	**2σ abs**
WFW-01 zircon (Cont.)												
spot 16	160.2	175	378.5	2.21	0.10826	0.00033	0.30051	0.00078	1693.8	3.9	1683.70	5.05
spot 17	105.7	105.6	277	2.669	0.10433	0.00029	0.3008	0.0035	1695	17	1694.33	19.74
spot 18	155.9	170.1	419.9	2.48	0.10682	0.00022	0.3057	0.0011	1719.5	5.4	1715.95	6.65
WFW-04 zircon (spot size = 24 µm, shot frequency = 4 Hz, shot count = 100, laser energy = 3 mJ at 75%)												
spot 1	0.864	70.3	45.9	0.6451	0.119	0.028	0.0033	0.00011	21.23	0.68	19.29	0.99
spot 2	2.43	274.8	171.6	0.616	0.0555	0.0027	0.003032	0.000029	19.52	0.18	19.29	0.22
spot 3	5.23	623	334	0.5335	0.0479	0.0016	0.003019	0.000023	19.43	0.15	19.40	0.18
spot 4	1.066	129.5	98	0.761	0.0515	0.0036	0.003037	0.000043	19.55	0.28	19.42	0.30
spot 5	4.26	509	280.6	0.545	0.0483	0.0036	0.003028	0.000032	19.49	0.21	19.44	0.24
spot 6	3.03	367	205	0.5479	0.0469	0.0029	0.003032	0.000024	19.52	0.15	19.50	0.20
spot 7	1.077	131.6	179.2	1.357	0.0466	0.0027	0.003057	0.000035	19.67	0.23	19.67	0.25
spot 8	0.451	17.08	45.79	2.658	0.0481	0.0046	0.00981	0.00011	62.95	0.73	62.87	0.85
spot 9	0.351	12.7	35.3	2.8	0.0534	0.0062	0.01021	0.00015	65.51	0.98	64.98	1.13
spot 10	0.936	31.53	109.7	3.433	0.0493	0.0018	0.01056	0.0001	67.7	0.65	67.55	0.74
spot 11	4.56	153.1	233	1.528	0.047	0.0013	0.011161	0.000067	71.55	0.43	71.59	0.57
spot 12	0.204	6.27	96.1	14.8	0.0488	0.0024	0.01126	0.0001	72.17	0.65	72.06	0.76
spot 13	5.66	146.3	995	6.79	0.0485	0.00044	0.014971	0.000075	95.79	0.48	95.73	0.68
spot 14	1.587	37.8	2295	61.6	0.04947	0.00032	0.016094	0.000086	102.92	0.54	102.74	0.75
spot 15	22.6	500	1323	2.647	0.04823	0.00033	0.016073	0.000058	102.79	0.37	102.77	0.63
WFW-06 zircon (spot size = 24 µm, shot frequency = 4 Hz, shot count = 100, laser energy = 3 mJ at 75%)												
spot 1	5.89	720	200	0.291	0.0563	0.0045	0.00292	0.00003	18.79	0.19	18.56	0.24
spot 2	3.96	466	165	0.362	0.0551	0.0056	0.00301	0.000041	19.37	0.26	19.16	0.31
spot 3	5.44	614	198	0.3046	0.0678	0.0053	0.003065	0.000044	19.73	0.28	19.20	0.32
spot 4	1.86	215.4	108	0.4862	0.0473	0.0034	0.00301	0.00004	19.38	0.26	19.35	0.29
spot 5	49.2	5870	1061	0.1802	0.0481	0.00095	0.003018	0.000013	19.429	0.082	19.38	0.13
spot 6	0.905	81.6	56.4	0.6938	0.098	0.013	0.003222	0.000071	20.74	0.45	19.39	0.55
spot 7	2.809	306.7	129.5	0.4217	0.0646	0.0082	0.003084	0.000051	19.85	0.33	19.39	0.39
spot 8	4.06	464	166	0.35	0.0614	0.0038	0.003074	0.00004	19.78	0.26	19.41	0.29
spot 9	2.023	235.5	98	0.4118	0.0459	0.0067	0.003014	0.000037	19.4	0.24	19.41	0.31

					MEASURED ISOTOPIC RATIOS						APPARENT AGE	
Spot	Pb (ppm)	Th (ppm)	U (ppm)	U/Th	$^{207}Pb/^{206}Pb$	2σ %	$^{206}Pb/^{238}U$	2σ %	$^{206}Pb/^{238}U$ Age	2σ abs	$^{207}Pb/^{206}Pb$ Corrected Age	2σ abs
WFW-06 zircon (Cont.)												
spot 10	4.34	496.1	153.6	0.301	0.0652	0.0046	0.003094	0.000036	19.92	0.23	19.44	0.27
spot 11	26.57	3308	661	0.1968	0.0516	0.0018	0.0030524	0.0000099	19.647	0.064	19.52	0.12
spot 12	7.36	860	241	0.285	0.0506	0.0046	0.003053	0.000031	19.65	0.2	19.55	0.25
spot 13	21.08	2517	493	0.1903	0.0468	0.0016	0.003041	0.000025	19.58	0.16	19.56	0.19
spot 14	14.33	1690	823	0.488	0.0501	0.0012	0.00306	0.000017	19.69	0.11	19.60	0.15
spot 15	23.8	2792	537	0.1905	0.0552	0.003	0.003081	0.000022	19.83	0.14	19.61	0.19
spot 16	14.97	1743	405.2	0.2333	0.0569	0.0046	0.003089	0.000021	19.88	0.13	19.62	0.20
spot 17	28.57	3576	773	0.2118	0.0505	0.0016	0.003065	0.000015	19.726	0.094	19.63	0.14
spot 18	12.06	1370	701.3	0.508	0.054	0.0017	0.003081	0.000017	19.83	0.11	19.64	0.15
spot 19	14	1724	436.3	0.2575	0.0519	0.0021	0.003074	0.000017	19.79	0.11	19.65	0.16
spot 20	1.025	110.5	75.2	0.666	0.0605	0.0072	0.00312	0.000068	20.08	0.44	19.72	0.48
spot 21	28.76	3310	724.1	0.2151	0.054	0.0015	0.003095	0.000021	19.92	0.14	19.73	0.17
spot 22	1.37	140	70.9	0.521	0.067	0.011	0.003155	0.000054	20.3	0.35	19.78	0.45
spot 23	1.448	131.5	79.1	0.595	0.086	0.013	0.003235	0.000072	20.82	0.47	19.78	0.57
spot 24	1.76	181	172	0.931	0.0584	0.0055	0.00314	0.000043	20.21	0.28	19.90	0.32
spot 25	1.94	183.2	109.7	0.597	0.081	0.011	0.003248	0.000061	20.9	0.39	19.99	0.48
spot 26	18.17	2080	479.8	0.2305	0.0547	0.0038	0.003154	0.000022	20.3	0.14	20.09	0.20
spot 27	5.01	548	313	0.571	0.0558	0.0031	0.003168	0.000038	20.39	0.24	20.15	0.27
KFC-02 zircon (spot size = 24 µm, shot frequency = 4 Hz, shot count = 100, laser energy = 3 mJ at 75%)												
spot 1	13.24	1465	582	0.3916	0.0478	0.0011	0.003041	0.000028	19.57	0.18	19.54	0.18
spot 2	11.73	1137	409.8	0.3591	0.084	0.011	0.003192	0.00005	20.55	0.32	19.57	0.42
spot 3	1.022	108.4	107.5	0.986	0.0531	0.0031	0.00307	0.000048	19.76	0.31	19.59	0.32
spot 4	24.31	2645	1211	0.4562	0.04702	0.00083	0.003048	0.000034	19.62	0.22	19.60	0.22
spot 5	12.78	1403	644.4	0.4594	0.0469	0.0011	0.003049	0.000032	19.62	0.21	19.61	0.21
spot 6	8.45	921	462	0.5007	0.0487	0.0014	0.003056	0.000032	19.67	0.2	19.61	0.21
spot 7	9.84	1074	529.7	0.489	0.0474	0.0013	0.003054	0.000033	19.66	0.21	19.63	0.21
spot 8	2.162	219.9	125.5	0.5667	0.0556	0.0044	0.003094	0.00005	19.91	0.32	19.68	0.34
spot 9	4.71	527	234.7	0.4444	0.0461	0.002	0.003057	0.000038	19.67	0.25	19.68	0.25
spot 10	6.81	748	539	0.7107	0.0476	0.0013	0.003063	0.000031	19.71	0.2	19.69	0.20
spot 11	15.99	1794	911	0.4999	0.04812	0.00091	0.003077	0.000025	19.8	0.16	19.76	0.16
spot 12	17.46	1906	779.4	0.4067	0.0537	0.0013	0.003103	0.000025	19.97	0.16	19.79	0.16

					MEASURED ISOTOPIC RATIOS				APPARENT AGE			
Spot	Pb (ppm)	Th (ppm)	U (ppm)	U/Th	$^{207}Pb/^{206}Pb$	2σ %	$^{206}Pb/^{238}U$	2σ %	$^{206}Pb/^{238}U$ Age	2σ abs	$^{207}Pb/^{206}Pb$ Corrected Age	2σ abs
					KFC-02 zircon (Cont.)							
spot 13	9.39	1009	648	0.635	0.0469	0.0012	0.003081	0.000037	19.83	0.24	19.82	0.24
spot 14	6.64	706	512.1	0.719	0.0485	0.0015	0.003091	0.000036	19.89	0.23	19.84	0.23
spot 15	18.58	2028	611.8	0.3041	0.0477	0.0012	0.003089	0.000031	19.88	0.2	19.85	0.20
spot 16	15.01	1690	873	0.538	0.0481	0.001	0.003092	0.000031	19.9	0.2	19.86	0.20
spot 17	2.79	135.6	119	0.8625	0.1899	0.009	0.003772	0.00006	24.27	0.39	19.87	0.42
spot 18	10.03	1054	767	0.7217	0.0524	0.0016	0.003113	0.000034	20.04	0.22	19.89	0.22
spot 19	18.03	1962	904	0.4604	0.04789	0.00088	0.003096	0.00003	19.93	0.19	19.89	0.19
spot 20	3.33	357	317	0.896	0.0473	0.0018	0.003094	0.000049	19.91	0.31	19.89	0.32
spot 21	4.23	399	185.1	0.4588	0.0865	0.0086	0.003265	0.000049	21.01	0.32	19.95	0.38
spot 22	4.264	454.9	293	0.6264	0.0473	0.0018	0.003103	0.000036	19.97	0.23	19.95	0.24
spot 23	3.5	376	362	0.948	0.0482	0.0016	0.003108	0.00004	20	0.26	19.96	0.26
spot 24	14.24	1549	709	0.4573	0.0473	0.0011	0.00311	0.000043	20.02	0.27	20.00	0.28
spot 25	9.57	990	641	0.661	0.0516	0.0012	0.003134	0.000036	20.17	0.23	20.04	0.23
spot 26	10.13	1078	662	0.6122	0.048	0.0011	0.003124	0.000036	20.11	0.23	20.07	0.23
spot 27	6.03	622	483	0.7771	0.0469	0.0013	0.003127	0.000036	20.12	0.23	20.11	0.23
spot 28	7.04	743	556	0.7483	0.048	0.0011	0.003139	0.000032	20.2	0.21	20.16	0.21
spot 29	45.54	5030	1836	0.3644	0.04855	0.0006	0.003148	0.000025	20.26	0.16	20.21	0.16
spot 30	5.369	554.3	358.5	0.646	0.0482	0.0013	0.003148	0.000038	20.26	0.24	20.22	0.25
spot 31	2.105	218.7	187.2	0.8448	0.0516	0.0022	0.003167	0.000032	20.39	0.21	20.25	0.21
spot 32	6.34	682	430.4	0.639	0.0469	0.0014	0.003153	0.000039	20.3	0.25	20.28	0.25
spot 33	16.26	1699	726	0.4179	0.0476	0.001	0.003157	0.000033	20.32	0.21	20.29	0.21
spot 34	3.64	367	274	0.765	0.0503	0.0021	0.003172	0.000047	20.42	0.3	20.32	0.31
spot 35	5.93	621	485	0.7829	0.0466	0.0011	0.003159	0.000032	20.33	0.21	20.33	0.21
spot 36	6.44	672	519	0.7662	0.0496	0.0014	0.003174	0.000029	20.43	0.19	20.35	0.19
spot 37	6.527	648.5	469	0.724	0.0563	0.0015	0.003203	0.000037	20.62	0.24	20.36	0.24
spot 38	13.46	1402	731	0.5223	0.0481	0.00098	0.003187	0.00003	20.51	0.19	20.47	0.19
spot 39	1.532	142	97.1	0.6649	0.054	0.0035	0.003245	0.000051	20.88	0.33	20.69	0.34
spot 40	4.22	414	298	0.704	0.0531	0.0019	0.003292	0.000036	21.19	0.23	21.01	0.24
spot 41	1.91	186	188	0.9934	0.0508	0.0026	0.003286	0.000036	21.15	0.23	21.03	0.24
spot 42	7.5	100	125	1.241	0.339	0.058	0.00699	0.00093	44.8	5.9	28.33	5.00

Spot	Pb (ppm)	Th (ppm)	U (ppm)	U/Th	MEASURED ISOTOPIC RATIOS $^{207}Pb/^{206}Pb$	2σ %	$^{206}Pb/^{238}U$	2σ %	$^{206}Pb/^{238}U$ Age	2σ abs	APPARENT AGE $^{207}Pb/^{206}Pb$ Corrected Age	2σ abs
KFC-03 zircon (spot size = 24µm, shot frequency = 4 Hz, shot count = 100, laser energy = 3 mJ at 75%)												
spot 1	-0.28252	352.5	1964	5.51	0.6592	0.0016	-8.43E-06	0.00000023	-0.0544	0.0015	-0.01	0.00
spot 2	3.501	374	210.1	0.555	0.053	0.0029	0.003057	0.000046	19.68	0.3	19.51	0.30
spot 3	4.258	453.8	442.9	0.9775	0.0487	0.0013	0.003044	0.000038	19.59	0.25	19.54	0.25
spot 4	3.644	398.6	388.8	0.972	0.0462	0.0014	0.003047	0.00005	19.61	0.32	19.62	0.32
spot 5	5.204	548.5	322.1	0.595	0.0487	0.0016	0.003059	0.000053	19.69	0.34	19.63	0.34
spot 6	2.089	198.5	205.9	1.0449	0.0646	0.0042	0.003133	0.000062	20.17	0.4	19.70	0.40
spot 7	8.95	964	586	0.6114	0.0487	0.0012	0.003072	0.000048	19.77	0.31	19.72	0.31
spot 8	2.007	207	202.4	0.9806	0.0497	0.0024	0.003076	0.000062	19.8	0.4	19.72	0.40
spot 9	1.675	165.1	176.4	1.0624	0.0528	0.0025	0.003089	0.000049	19.88	0.31	19.72	0.32
spot 10	5.036	525	311.4	0.5946	0.0494	0.0018	0.003079	0.000045	19.82	0.29	19.74	0.29
spot 11	1.583	164.5	117.5	0.7214	0.0526	0.0038	0.003101	0.000054	19.96	0.35	19.80	0.36
spot 12	3.23	333	213	0.6407	0.0493	0.0022	0.003089	0.000055	19.88	0.35	19.81	0.36
spot 13	5.02	506	325.6	0.6523	0.0546	0.002	0.00311	0.000048	20.02	0.31	19.81	0.31
spot 14	3.17	346	175	0.523	0.0492	0.0031	0.003095	0.00005	19.92	0.32	19.85	0.33
spot 15	2.146	224.2	219.2	0.9759	0.0485	0.0023	0.003094	0.000044	19.92	0.28	19.86	0.29
spot 16	3.55	362	309	0.8431	0.0479	0.0019	0.003094	0.000053	19.92	0.34	19.88	0.34
spot 17	1.713	177.3	166	0.9275	0.0511	0.003	0.003107	0.000054	20	0.34	19.88	0.35
spot 18	4.272	460.4	350.9	0.7619	0.0506	0.0015	0.003112	0.000051	20.03	0.33	19.92	0.33
spot 19	2.67	265	183	0.6903	0.0517	0.0026	0.003125	0.000067	20.11	0.43	19.98	0.43
spot 20	2.299	236.3	214.1	0.894	0.0493	0.0029	0.003118	0.000043	20.07	0.27	20.00	0.29
spot 21	2.09	214.2	217.2	1.0115	0.0508	0.0023	0.003124	0.000049	20.11	0.32	20.00	0.32
spot 22	3.155	321.7	293.7	0.912	0.0485	0.0017	0.003118	0.000038	20.07	0.25	20.02	0.25
spot 23	11.42	1183	458	0.3906	0.0502	0.0016	0.003128	0.000041	20.14	0.27	20.04	0.27
spot 24	4.6	489	373.8	0.801	0.0483	0.0016	0.003123	0.000041	20.1	0.26	20.05	0.27
spot 25	0.986	96.8	101.5	1.052	0.0525	0.0042	0.003141	0.000057	20.21	0.37	20.06	0.38
spot 26	6.83	619	293.5	0.4793	0.086	0.014	0.003283	0.000091	21.13	0.58	20.07	0.67
spot 27	27.1	2912	1072	0.376	0.04776	0.00092	0.003125	0.000047	20.11	0.3	20.08	0.30
spot 28	2.304	239.9	172	0.7105	0.0483	0.0032	0.003133	0.000069	20.16	0.44	20.12	0.45
spot 29	1.439	146.4	108.3	0.7404	0.051	0.0041	0.003167	0.000058	20.38	0.38	20.27	0.39
spot 30	1.064	99.4	100.7	1.0242	0.0559	0.0046	0.003189	0.000059	20.52	0.38	20.28	0.39
spot 31	3.32	200.3	183.3	0.9141	0.125	0.011	0.0035	0.000081	22.52	0.52	20.29	0.56
spot 32	2.97	270	209	0.787	0.0653	0.0026	0.003239	0.00006	20.85	0.39	20.35	0.38
spot 33	1.418	134.9	129.3	0.9543	0.0491	0.0037	0.003179	0.000055	20.46	0.36	20.39	0.37

					MEASURED ISOTOPIC RATIOS						APPARENT AGE	
Spot	Pb (ppm)	Th (ppm)	U (ppm)	U/Th	$^{207}Pb/^{206}Pb$	2σ %	$^{206}Pb/^{238}U$	2σ %	$^{206}Pb/^{238}U$ Age	2σ abs	$^{207}Pb/^{206}Pb$ Corrected Age	2σ abs
					KFC-03 zircon (Cont.)							
spot 34	3.42	328	203	0.6106	0.0536	0.0026	0.003246	0.000054	20.89	0.35	20.70	0.35
spot 35	7.37	64.5	78.3	1.194	0.478	0.012	0.00741	0.00025	47.6	1.6	21.66	1.03
					KFC-05 zircon (spot size = 24 µm, shot frequency = 4 Hz, shot count = 100, laser energy = 3 mJ at 75%)							
spot 1	5.32	593	331.6	0.577	0.049	0.0017	0.003035	0.000036	19.54	0.23	19.47	0.23
spot 2	17.89	2008	936	0.4643	0.04679	0.00084	0.00303	0.000034	19.5	0.22	19.49	0.22
spot 3	10.08	1100	618	0.58	0.0523	0.0018	0.003078	0.000038	19.81	0.25	19.66	0.25
spot 4	6.644	738.8	307	0.4151	0.0476	0.0018	0.00306	0.000046	19.7	0.29	19.67	0.30
spot 5	2.675	273.1	206.4	0.7533	0.0568	0.0022	0.003099	0.000042	19.94	0.27	19.69	0.27
spot 6	3.5	377	186.4	0.5004	0.0499	0.0025	0.003084	0.000051	19.85	0.33	19.76	0.33
spot 7	11.32	1253	652	0.5216	0.048	0.0011	0.003088	0.000039	19.87	0.25	19.84	0.25
spot 8	4.74	481	420	0.8649	0.0594	0.0028	0.003139	0.000043	20.2	0.28	19.87	0.28
spot 9	2.498	268.9	162.6	0.5977	0.0494	0.0025	0.003116	0.000055	20.05	0.35	19.98	0.36
spot 10	5.22	559	392	0.7057	0.0488	0.0012	0.003114	0.000044	20.04	0.28	19.98	0.28
spot 11	3.76	401	261.1	0.6478	0.0503	0.0019	0.00312	0.000043	20.08	0.27	19.98	0.28
spot 12	4.48	429	267	0.6188	0.0759	0.0031	0.003226	0.000045	20.76	0.29	19.99	0.29
spot 13	2.516	269.1	188.2	0.719	0.0477	0.0024	0.003111	0.000047	20.02	0.3	19.99	0.31
spot 14	6.65	719	450	0.644	0.0479	0.0016	0.003112	0.000046	20.03	0.3	19.99	0.30
spot 15	4.183	441.7	270.5	0.6177	0.0534	0.0022	0.003142	0.000045	20.23	0.29	20.04	0.29
spot 16	3.06	321	207.1	0.643	0.0468	0.0023	0.003119	0.000045	20.08	0.29	20.07	0.30
spot 17	5.28	563	416	0.7357	0.0495	0.0015	0.00313	0.00004	20.15	0.26	20.07	0.26
spot 18	34.38	3820	1184	0.3135	0.04808	0.00079	0.003125	0.000043	20.11	0.28	20.07	0.28
spot 19	6.1	590	251	0.65	0.0498	0.0024	0.003137	0.000052	20.19	0.33	20.10	0.34
spot 20	0.992	104.2	110.5	1.059	0.0514	0.0036	0.003147	0.000047	20.25	0.3	20.13	0.31
spot 21	5.336	567.8	336.6	0.594	0.049	0.0016	0.00314	0.000038	20.21	0.24	20.14	0.25
spot 22	5.24	563	311.7	0.5547	0.0479	0.002	0.00314	0.00004	20.21	0.26	20.17	0.26
spot 23	3.25	356	233.6	0.671	0.0471	0.0021	0.003139	0.000051	20.21	0.33	20.19	0.33
spot 24	1.612	162.4	162.9	1.037	0.0541	0.003	0.003177	0.000045	20.45	0.29	20.25	0.30
spot 25	1.225	129.6	86.7	0.6616	0.047	0.0041	0.003149	0.000054	20.26	0.35	20.25	0.36
spot 26	1.451	146.9	151.3	1.0213	0.0536	0.0028	0.003186	0.000049	20.5	0.32	20.32	0.32
spot 27	0.659	63.2	69.3	1.087	0.0568	0.0062	0.003203	0.000063	20.62	0.4	20.35	0.43
spot 28	1.559	169.4	161.6	0.943	0.0485	0.0023	0.00317	0.00004	20.4	0.26	20.35	0.26

					MEASURED ISOTOPIC RATIOS						APPARENT AGE	
Spot	Pb (ppm)	Th (ppm)	U (ppm)	U/Th	$^{207}Pb/^{206}Pb$	2σ %	$^{206}Pb/^{238}U$	2σ %	$^{206}Pb/^{238}U$ Age	2σ abs	$^{207}Pb/^{206}Pb$ Corrected Age	2σ abs
KFC-05 zircon (Cont.)												
spot 29	3.85	404	268	0.6618	0.0493	0.002	0.003174	0.000044	20.43	0.28	20.35	0.29
spot 30	0.921	93.6	62.7	0.686	0.0481	0.0049	0.003173	0.00007	20.42	0.45	20.38	0.47
spot 31	18.65	2015	608	0.29905	0.0479	0.0012	0.003173	0.000039	20.42	0.25	20.38	0.25
spot 32	0.578	55	51.6	0.938	0.0621	0.0086	0.003237	0.000063	20.83	0.4	20.42	0.46
spot 33	1.853	189.5	159.2	0.838	0.0493	0.0026	0.003185	0.000045	20.5	0.29	20.43	0.30
spot 34	1.527	155.7	157.9	1.034	0.051	0.0024	0.003195	0.000049	20.56	0.31	20.44	0.32
spot 35	3.123	332.9	260.7	0.7895	0.0487	0.0021	0.003186	0.000039	20.51	0.25	20.45	0.26
spot 36	2.88	266.2	225.5	0.844	0.0587	0.0078	0.003253	0.000085	20.93	0.54	20.61	0.58
spot 37	2.06	214	190	0.8919	0.0508	0.0023	0.003225	0.000039	20.75	0.25	20.64	0.26
spot 38	16.98	1735	562	0.3237	0.0523	0.0014	0.003237	0.000041	20.83	0.27	20.68	0.26
spot 39	6.72	674.7	382.6	0.5661	0.0484	0.0013	0.003242	0.000037	20.87	0.24	20.81	0.24
spot 40	2.35	183	189	1.0246	0.066	0.01	0.00335	0.00013	21.56	0.82	21.03	0.86
spot 41	7.09	699	332	0.4803	0.0482	0.0016	0.003284	0.000044	21.13	0.28	21.09	0.29
spot 42	53.9	62.5	939	18.2	0.1046	0.00063	0.2871	0.0057	1626	28	1617.34	31.72
KFC-06 zircon (spot size = 24 µm, shot frequency = 4 Hz, shot count = 100, laser energy = 3 mJ at 75%)												
spot 1	-0.30647	793.3	1898	2.414	0.25041	0.00072	-2.47E-05	0.00000021	-0.1593	0.0013	-0.12	0.00
spot 2	-0.27248	685	2740	4.16	-0.10694	0.00044	0.0000412	0.0000021	0.266	0.014	0.32	0.02
spot 3	0.227	23.6	38.5	1.633	0.058	0.01	0.002784	0.000079	17.92	0.51	17.66	0.55
spot 4	3.701	400.4	217.6	0.5503	0.052	0.0023	0.003007	0.000054	19.35	0.35	19.22	0.35
spot 5	13.53	1513	691	0.4521	0.0499	0.0011	0.003015	0.000033	19.41	0.21	19.32	0.21
spot 6	4.75	514	353.5	0.6965	0.0523	0.0017	0.003038	0.000047	19.56	0.3	19.41	0.30
spot 7	4.31	257.2	174.3	0.6856	0.165	0.011	0.003553	0.000074	22.86	0.48	19.44	0.51
spot 8	1.477	158.3	139.3	0.8768	0.0552	0.0033	0.003055	0.000053	19.66	0.34	19.45	0.35
spot 9	5.69	636	430	0.6703	0.0475	0.0014	0.003027	0.000036	19.48	0.23	19.46	0.23
spot 10	2.107	229.2	202.8	0.8751	0.0475	0.0024	0.003057	0.000039	19.68	0.25	19.65	0.26
spot 11	1.352	141.3	150.4	1.0596	0.0507	0.0032	0.003117	0.000061	20.06	0.39	19.95	0.40
spot 12	4.39	489	378.8	0.7821	0.0486	0.0014	0.003129	0.000038	20.14	0.25	20.08	0.25
spot 13	3.839	371.8	213.4	0.5721	0.0501	0.0023	0.003182	0.000038	20.48	0.24	20.39	0.25
spot 14	2.63	33.82	39.5	1.152	0.39	0.045	0.00563	0.00053	36.2	3.4	20.49	2.82
spot 15	41.1	4200	1276	0.3033	0.0621	0.0023	0.003287	0.00004	21.16	0.25	20.74	0.26
spot 16	5.09	521	351	0.775	0.0482	0.0018	0.003432	0.000061	22.09	0.39	22.04	0.39

Spot	Pb (ppm)	Th (ppm)	U (ppm)	U/Th	MEASURED ISOTOPIC RATIOS $^{207}Pb/^{206}Pb$	2σ %	$^{206}Pb/^{238}U$	2σ %	$^{206}Pb/^{238}U$ Age	2σ abs	APPARENT AGE $^{207}Pb/^{206}Pb$ Corrected Age	2σ abs
KFC-06 zircon (Cont.)												
spot 17	104.2	438.2	433	0.989	0.0706	0.0013	0.07413	0.00084	461	5	452.67	5.08
spot 18	11.31	17.96	136	7.62	0.08933	0.00044	0.2267	0.0032	1317	17	1309.93	17.99
spot 19	3.475	6.1	37.74	7.41	0.09058	0.00065	0.2384	0.0035	1378	18	1373.41	19.67
spot 20	2.44	3.33	30.6	12.1	0.08893	0.00088	0.2395	0.0039	1386	21	1382.56	21.99
spot 21	88.5	122.2	59.49	0.493	0.09965	0.00098	0.2668	0.0035	1524	18	1514.81	19.58
spot 22	81.6	112.4	86	0.75	0.10067	0.00073	0.2906	0.0064	1644	32	1645.49	35.88
spot 23	50.23	64.4	238.2	3.69	0.10498	0.00024	0.2963	0.0031	1672	15	1667.72	17.30
spot 24	102.5	130.7	241.9	1.8545	0.10385	0.00026	0.2985	0.0032	1684	16	1682.57	17.90
spot 25	106.9	133.5	364.2	2.758	0.10423	0.00025	0.2987	0.003	1685	15	1682.82	16.78
spot 26	111.1	139.4	254	1.855	0.10484	0.00025	0.3009	0.0044	1695	22	1693.72	24.60
spot 27	42	51.7	109.5	2.119	0.10388	0.00038	0.3026	0.0033	1706	17	1705.45	18.51
spot 28	167.5	105.2	114.6	1.0704	0.26264	0.00058	0.6551	0.0079	3247	31	3210.88	101.36
KFC-07 zircon (spot size = 24 μm, shot frequency = 4 Hz, shot count = 100, laser energy = 3 mJ at 75%)												
spot 1	1.505	851.3	2131	2.479	0.0583	0.0027	0.000461	0.0000067	2.971	0.043	2.93	0.04
spot 2	0.855	557	1692	3.032	0.0515	0.0017	0.0004594	0.0000071	2.961	0.046	2.94	0.05
spot 3	6.59	3980	4710	1.175	0.0643	0.0025	0.0004704	0.0000081	3.032	0.052	2.96	0.05
spot 4	1.009	671.7	2243	3.313	0.0482	0.0017	0.0004621	0.0000072	2.978	0.046	2.97	0.05
spot 5	0.712	452	1170	2.52	0.0515	0.0032	0.0004659	0.0000078	3.002	0.05	2.98	0.05
spot 6	2.57	789	1216	1.61	0.116	0.012	0.000528	0.000015	3.403	0.094	3.10	0.10
spot 7	5.355	3482	4267	1.212	0.0492	0.0012	0.0004953	0.0000066	3.192	0.043	3.18	0.04
spot 8	4.55	1939	2691	1.363	0.0693	0.0039	0.000532	0.000011	3.428	0.073	3.33	0.07
spot 9	0.351	163.5	366.5	2.232	0.0505	0.0047	0.000604	0.000012	3.89	0.079	3.87	0.08
spot 10	16.23	1465	694.2	0.4687	0.0981	0.0082	0.003213	0.000064	20.68	0.41	19.33	0.44
spot 11	17.05	1857	684	0.3661	0.04797	0.00098	0.003038	0.000046	19.56	0.3	19.52	0.30
spot 12	1.375	145.9	169	1.145	0.0494	0.003	0.003061	0.000053	19.7	0.34	19.63	0.35
spot 13	1.973	205.2	199.2	0.9574	0.0485	0.0024	0.00307	0.000048	19.76	0.31	19.71	0.31
spot 14	9.1	947	427	0.449	0.0478	0.0011	0.003087	0.000045	19.87	0.29	19.83	0.29
spot 15	26.93	2774	1151	0.415	0.0523	0.0011	0.003122	0.000037	20.1	0.24	19.95	0.24
spot 16	2.105	199.2	161.3	0.7939	0.0572	0.0032	0.003144	0.000063	20.24	0.41	19.96	0.41
spot 17	6.04	616	369	0.591	0.0487	0.0013	0.003118	0.000057	20.07	0.36	20.01	0.37
spot 18	2.194	223.2	221.9	0.9827	0.0491	0.0023	0.003122	0.000044	20.09	0.28	20.03	0.29

					MEASURED ISOTOPIC RATIOS				APPARENT AGE			
Spot	**Pb (ppm)**	**Th (ppm)**	**U (ppm)**	**U/Th**	**$^{207}Pb/^{206}Pb$**	**2σ %**	**$^{206}Pb/^{238}U$**	**2σ %**	**$^{206}Pb/^{238}U$ Age**	**2σ abs**	**$^{207}Pb/^{206}Pb$ Corrected Age**	**2σ abs**
KFC-07 zircon (Cont.)												
spot 19	2.254	228.9	171.5	0.7347	0.051	0.0024	0.003134	0.000072	20.17	0.46	20.06	0.46
spot 20	2.631	267.8	277.2	1.0323	0.0502	0.0018	0.003132	0.000046	20.16	0.3	20.06	0.30
spot 21	23.7	2418	793	0.3209	0.0469	0.0011	0.00312	0.000045	20.08	0.29	20.07	0.29
spot 22	6.86	663	470.8	0.716	0.0519	0.0017	0.003162	0.00005	20.35	0.32	20.21	0.32
spot 23	2.631	259.8	179.7	0.6831	0.0572	0.0034	0.003196	0.000054	20.57	0.35	20.29	0.35
spot 24	4.346	438.5	273.7	0.6173	0.05	0.0022	0.003175	0.000047	20.44	0.3	20.34	0.31
spot 25	5.26	441.4	322.5	0.726	0.062	0.012	0.00324	0.00016	20.9	1	20.44	1.06
spot 26	2.94	268	196.6	0.742	0.0476	0.0022	0.00325	0.000054	20.92	0.35	20.89	0.35